REMOVAL OF PERFLUOROALKYL SUBSTANCES (PFAS) FROM WATER USING MODIFIED BIOCHAR ADSORBENTS PRODUCED FROM CANOLA STRAW

A Thesis Submitted to the
College of Graduate and Postdoctoral Studies
In Partial Fulfillment of the Requirements
For the Degree of Master of Science
In the Chemical and Biological Engineering
University of Saskatchewan
Saskatoon

By

MALIHE AFROOZ

Permission to Use

In presenting this thesis in partial fulfillment of the requirements for a Postgraduate degree from the University of Saskatchewan, I agree that the Libraries of this University may make it freely available for inspection. I further agree that permission for copying of this thesis/dissertation in any manner, in whole or in part, for scholarly purposes may be granted by Professor Jafar Soltan and Professor Kerry N. McPhedran who supervised my thesis work. It is understood that any copying or publication or use of this thesis or parts for financial gain shall not be allowed without my written permission. It is also understood that due recognition shall be given to me and to the University of Saskatchewan in any scholarly use which may be made of any material in my thesis.

Requests for permission to copy or to make other use of material in this thesis in whole or parts shall be addressed to:

Head of the Department of Chemical and Biological Engineering

57 Campus Drive

University of Saskatchewan

Saskatoon, Saskatchewan S7N 5A9

Canada

OR

Dean

College of Graduate and Postdoctoral Studies

University of Saskatchewan

116 Thorvaldson Building, 110 Science Place

Saskatoon, Saskatchewan S7N 5C9

Canada

Abstract

Perfluorooctanoic acid (PFOA) is a persistent organic pollutant commonly found in water sources, causing severe health and environmental concerns. In this research, microwave-activated biochar adsorbents derived from canola straw were modified by chemical activators (H_3PO_4 and $ZnCl_2$) to improve the PFOA removal from water. In order to obtain optimal microwave-assisted pyrolysis (MWP) conditions, different biochar adsorbents were synthesized by altering the activator molarity, microwave heating time, and microwave power. This was done utilizing a central composite design (CCD) coupled with a response surface methodology (RSM). Based on the analysis of H_3PO_4-treated biochar (PBC) and $ZnCl_2$-treated biochar (ZnBC), it was found that chemical treatment of biochar under optimum MWP conditions (irradiation time of 6 min and microwave power of 600 W) enhanced the chemical functional groups, porosity, and surface area of canola-based biochar. In this condition, removal efficiencies of PFOA by PBC and ZnBC reached 368 μg/g (92%) and 336 μg/g (84%) at equilibrium and 25 °C, respectively. These amounts were significantly higher than untreated biochar (UBC), with a low removal efficiency of only 25 μg/g (5%), and raw canola straw (RCS), which exhibited a very low removal efficiency of 5 μg/g (1%).

Chemical treatment increased the PFOA adsorption by improving the interactions between PFOA and the modified biochar. Chemical analyses were conducted to identify the elemental composition of PBC and ZnBC. Furthermore, FT-IR and XPS results confirmed the addition of new chemical functional groups to the biochar surface during chemical treatment and pyrolysis. The results of a kinetic study showed that PBC and ZnBC are involved in chemisorption to remove PFOA. A Freundlich isotherm model best fitted the data for PFOA adsorption on modified adsorbents, suggesting heterogeneous multilayer adsorption is more likely to occur. Various background salts were examined, and the results demonstrated that salting-out and divalent bridges can enhance PFOA adsorption. Further investigation explored that the modified biochar adsorbents showed excellent performances over a pH range of 3 to 9. This study strongly suggests that the modified biochar adsorbents, produced through a straightforward method from readily available agricultural waste, present a sustainable and eco-friendly adsorbent for PFOA removal from water.

Acknowledgements

I extend my deepest gratitude to my esteemed supervisors, Prof. Jafar Soltan, and Prof. Kerry N. McPhedran, for their unwavering support throughout this research. Their generous sharing of knowledge and experience and patience in correcting my mistakes have been invaluable. Frankly, without their guidance, this thesis would not have come to fruition.

I am also thankful for the valuable insights from my Graduate Advisory Committee member, Prof. Catherine Niu. Her guidance and advice have significantly enriched the quality of this work.

I want to express my sincere appreciation to the Saskatchewan Structure Sciences Center (SSSC) staff for their invaluable assistance and cooperation in conducting the analyses, which have been instrumental in advancing my research. I sincerely thank Mr. Ken Thomas for his technical assistance and contribution to developing LC-MS/MS analysis. His expertise has played a vital role in enhancing the robustness of this research.

I express my deepest gratitude to my parents, Ali Mohammad and Masoumeh, whose guidance and unwavering love have accompanied me in my pursuits throughout my life. In particular, I would like to thank my inspirational father for his constant love for encouraging me to pursue my dreams. Furthermore, many thanks go to my lovely brother, Morteza, for his unwavering support throughout my journey.

Lastly, my heartfelt appreciation goes to my friends who supported me and made many unforgettable memories during this period.

Dedication

To my father, the inspirational and unwavering beacon in my life's journey. His wisdom, kindness, and unconditional love and support have shaped the compassionate, resilient individual navigating the complexities of life.

Table of Contents

List of Tables

List of Figures

NOMENCLATURE (symbols)

PleTerm	Defenition
A_e	Adsorption efficiency
a_Y	Yan model constant
a_{YN}	Yoon- Nelson model constant
b_Y	Yan model constant
b_{YN}	Yoon- Nelson model constant
C_0	Initial concentrations of the solute (µg/L)
C_e	Equilibrium concentration of the solute (µg/L)
K_c	Thermodynamic equilibrium constant
K_F	Adsorption affinity ((µg/g)(L/µg)1/n)
K_L	Langmuir adsorption energy (L/µg)
K_T	Equilibrium constant (L/µg)
M	Mass of adsorbent (g)
q_e	Adsorption capacity (µg/g) at equilibrium
q_m	Maximum capacity of adsorption per unit of adsorbent (µg/g)
q_t	Adsorption capacity (µg/g) at time (h)
R	Universal gas constant (J/mol K),
T	Temperature (K)
t	Time (min)
t_b	Breakthrough point (min)
t_e	Exhaustion point (min)

V	Flow rate (mL/min)
ΔG^0	Gibbs free energy change
ΔH^0	Enthalpy change
ΔS^0	Breakthrough point (min)
τ	Time to 50% breakthrough (min)

NOMENCLATURE (abbreviations)

PleTerm	Defenition
AC	Activated carbon
BET	Brunauer–Emmett–Teller
CCD	Central composite design
CP	Conventional pyrolysis
EDX	Energy-dispersive X-ray spectroscopy
EPA	United state environmental protection agency
FT-IR	Fourier transform infrared
GHG	Average greenhouse gas emission
MAC	Maximum acceptable concentration
MWP	Microwave-assisted pyrolysis
PBC	H_3PO_4-treated biochar
PFAS	Per- and poly-fluoroalkyl substances
PFCA	Perfluoroalkyl carboxylic acid
PFOA	Perfluorooctanoic acid
PFOS	Perfluorooctane sulfonate acid
PFSA	Perfluoroalkyl sulfonic acid
POP	Persistent organic pollutants
PZC	Point of zero charge
RCS	Raw canola straw
RSM	Response surface methodology
SEM	Scanning electron microscopy
TEM	Transmission electron microscopy

UBC	Untreated biochar
XPS	X-ray photoelectron spectroscopy
XRD	X-ray diffraction
ZnBC	$ZnCl_2$-treated biochar

Chapter 1.

Introduction and Thesis Outline

1.1. Introduction

Known as man-made organofluorine chemical compounds, per- and poly-fluoroalkyl substances (PFAS) have been synthesized since 1940. However, the use of PFAS in industrial applications and consumer products dates back to the 1950s [1]. Nowadays, various compounds of PFAS are widely used in textiles, paper, food packaging, leather, fire retardants, fabrics, non-stick pots and pans, carpets, waterproof clothing, waxes, paints, cleaning agents, and many industrial applications, namely surfactants, semiconductors, and photolithography. The most common sources of PFAS compounds have been presented in Figure 1.1 [2]. Chemical and thermal stability, acid-base resistance, water repellency, and surface activity make these compounds excellent for numerous applications. Before their toxicity was discovered, PFAS compounds were believed to be environmentally inert, but since 2010, they have been recognized as emerging contaminants and persistent organic pollutants (POPs).

The release of PFAS into the environment can pollute soil and groundwater resources. With the increase in the prevalence of PFAS, they have been detected in various aquatic media, such as groundwater, surface water, seawater, rain, snow, etc., among which these compounds mostly contaminate groundwater and surface water [3]. Infiltration of contaminated water from agricultural areas, landfills, firefighting training sites, and sewage systems are the primary sources of groundwater and surface water contamination with PFAS [4]. The concentrations of PFAS in groundwater and surface water are about hundreds of μg/L [5]. Hence, many societies have a public health concern due to their bioaccumulation in the food chain and environmental persistence. It has been demonstrated that PFAS accumulation in aquatic environments can lead to adverse immunological effects and severe disruptions of reproductive, liver, and neurological systems. Further, it can cause prostate and pancreatic cancers, increase diabetes and cholesterol risks, and lead to immunotoxicological effects in children [6]. Consuming seafood previously exposed to contaminated water or drinking contaminated water can result in human exposure to PFAS. Due to the serious concerns regarding the presence of PFAS in the environment and

ecosystems, it is imperative to use simple and cost-effective methods to reduce or eliminate PFAS in water and wastewater.

PFAS have been detected in freshwater sites throughout the world, and low concentrations of PFAS (between pg/L and µg/L) have been detected in aquatic environments. While over 3,000 PFAS compounds are used worldwide, only a few hundred PFAS compounds have been identified and used in Canada. Canadian standards do not allow some of these chemicals, like perfluorooctane sulfonate (PFOS) and perfluorooctanoic acid (PFOA), to be manufactured in this country [7]. According to Guidelines for Canadian Drinking Water Quality, the maximum acceptable concentrations (MAC) for PFOA and PFOS are 0.2 µg/L and 0.6 µg/L, respectively. Since 2016, the United States Environmental Protection Agency (EPA) has issued health advisory levels for drinking water of about 100 to 7,000 ng/L for C4–C7 PFASs and nearly 70 ng/L for PFOS and PFOA [5].

Figure 1.1. Main common sources of PFAS compounds (adapted fromYadav et al. [2])

1.2. Organization of thesis

There are five chapters in this master's thesis, which follows the College of Graduate and Postdoctoral Studies guidelines. A brief introduction to the subject matter is provided in Chapter 1. Chapter 2 presents a comprehensive literature review on PFAS compounds and their removal by various methods. Chapter 3 presents the experimental procedures, including the materials and techniques used to synthesize and characterize the adsorbents to explore their physical and chemical properties. Additionally, a detailed description of analysis methods for PFOA adsorption to understand the adsorption mechanism and research objectives are provided.

Chapter 4 focuses on the analysis of results obtained from various characterization techniques, namely Fourier-transform infrared (FT-IR), Raman spectroscopy, scanning electron microscopy (SEM), energy dispersive X-ray (EDX), X-ray diffraction (XRD), Brunauer-Emmett-Teller (BET) analysis, and X-ray photoelectron spectroscopy (XPS). This Chapter investigates the PFOA adsorption onto PBC and ZnBC adsorbents synthesized under the obtained optimal conditions. In addition, the impact of critical factors (pH, ionic strength, and co-existing ions) and equilibrium, isotherm, kinetics, and thermodynamic parameters to find the adsorption mechanism is assessed. In conclusion, Chapter 5 summarizes the leading research results based on the findings presented in the preceding chapters. In addition, it provides recommendations for future research directions, highlighting areas that could be further explored and improved. References include listing all sources cited in each Chapter, organized by the appropriate citation style.

Chapter 2.

Literature Review

2.1. PFAS chemistry and classification

PFAS molecules are made up of a hydrophobic alkyl chain where hydrogen atoms have been partially (poly-) or fully (per-) substituted by fluorine atoms attached to a carbon chain with a hydrophilic group (usually a sulphonic, carboxylic, or phosphoric acid) at the end (Figure 2.1) [8,9]. Since PFAS compounds have acidic functional groups, they are usually found in aquatic environments as anion forms. However, they can also form cationic and zwitterionic species. Different PFAS compounds exhibit different properties due to their structural variations in chain length, branching within the chain, and functional headgroups. Covalent bonds between carbon and fluorine contribute to the thermal stability of PFAS compounds. Furthermore, PFAS chemicals exhibit lipophobic and hydrophobic properties due to the low polarizability of fluorine atoms. As a result of the chemical functional groups attached to fluoroalkyl chains, PFAS have high chemical stability. A PFAS compound becomes more chemically inert by replacing hydrogen with fluorine and increasing the carbon chain length. Hydrophilic functional groups lead to the high solubility and mobility of PFAS in water [10].

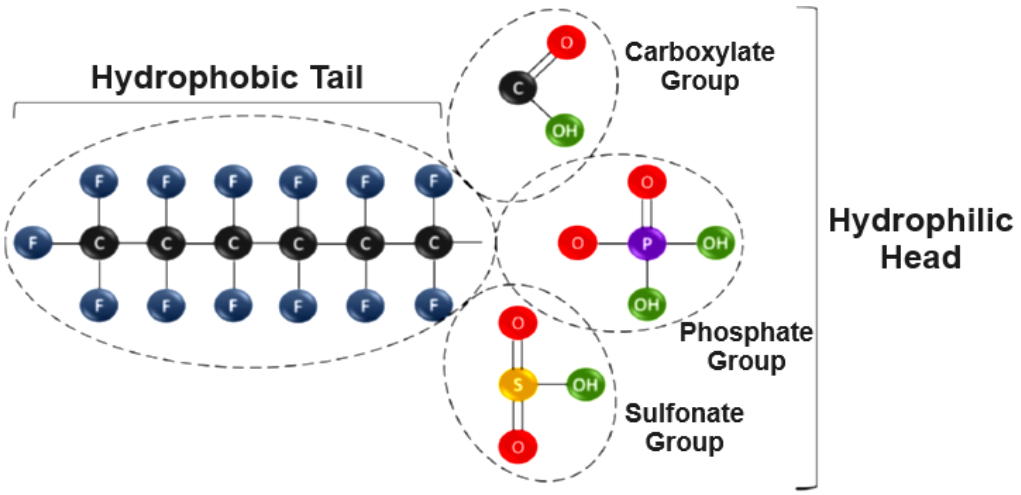

Figure 2.1. General chemical structure of perfluorinated PFAS substances (adapted from Panieri et al. [8])

The well-recognized PFAS classification system compiled by Buck et al. identifies two broad subcategories of PFAS: nonpolymeric and polymeric (Figure 2.2) [1]. PFAS can be further divided into heterogeneous groups, as shown in Table 2.1. PFASs are also classified based on the length of their carbon chains, namely short-chain (with carbon chain lengths below C8) and long-chain (with carbon chain lengths above C8), and the long-chain PFASs are more toxic than short-chain compounds [11,12]. The long-chain PFAS compounds like PFOS and PFOA and their salts are widely used in different industries. Additionally, according to their functional groups, PFASs are usually categorized into two main types: perfluoroalkyl sulfonic acids (PFSAs), and perfluoroalkyl carboxylic acids (PFCAs) [12]. However, some PFAS substances may contain other functional groups like phosphoric acid and sulfonamide. As carbon-chain length increases, the possibility for biomagnification and bioaccumulation of PFAS in biota increases. Furthermore, PFSAs are more likely to be bioaccumulated than PFCAs [4]. PFOA, with a chemical formula of $CF_3(CF_2)_6COOH$, is not a natural chemical and has been in the environment since World War II. The use of PFOA dates back many decades, but concern about its toxicity was raised in the early 2000s, and it was classified as a likely carcinogen by the USEPA in 2009 [13].

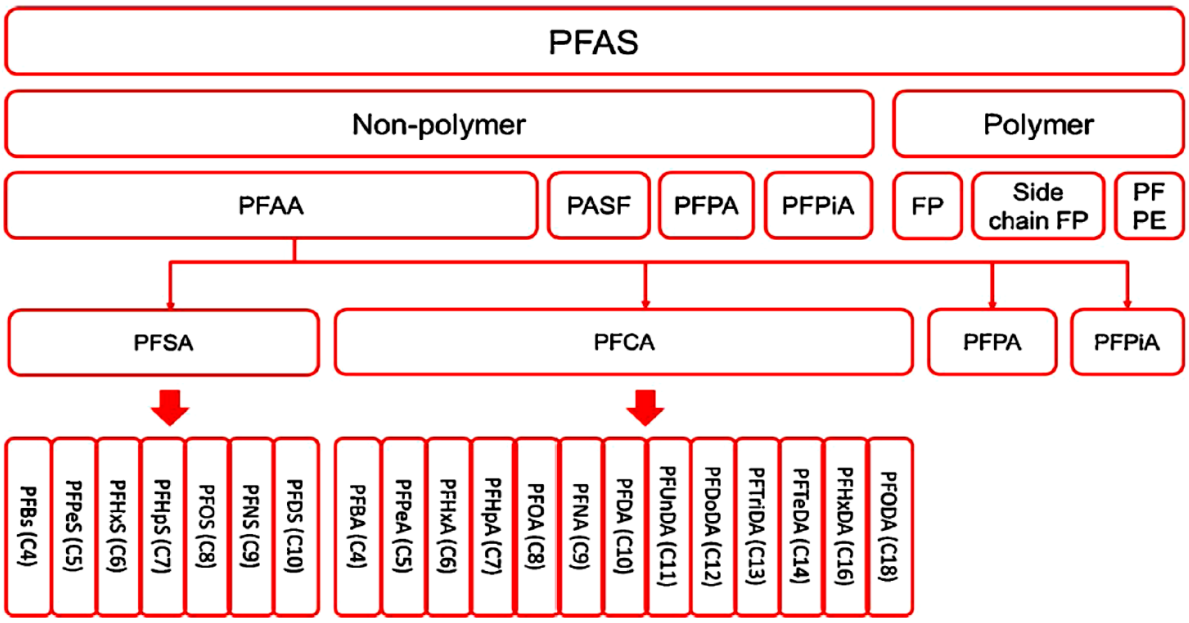

Figure 2.2. Polymeric and non-polymeric classification of PFAS (adapted from Buck et al. [1])

Table 2.1. PFAS categories and their subgroups (adapted from Panieri et al. [8])

Non-Polymeric PFAS			
Perfluorinated PFAS		**Polyfluorinated PFAS**	
Subgroup	**Example**	**Subgroup**	**Example**
Perfluoroalkyl acids (PFAAs)	PFBS, PFHXS, PFOS	Fluorotelomer compounds (FT)	6:2 FTO,8:2 FTI
Perfluoroalkane sulfonic acids & sulfonates (PFSAs)	PFOSI	Perfluoroalkane sulfonamido compounds (Me/Et/Bu-FASAs)	MeFOSA, FOSE
Perfluoroalkane sulfonic acids (PFSIAs)	PFBA, PFHXA, PFOA	Miscellaneous	4,8-Dioxa-3H-perfluorononanoate
Perfluorocarboxylic acids & carboxylates (PFCAs)	C8-PFPA		
Perfluoroalky1 phosphonic acids (PFPAs)	C8/C8-PFPiA		
Perfluoroalky1 phosphinic acids (PFPIAs)			
Perfluoroalkyl ether acids (PFEAs)	GenX, Adona, F-53B		
Perfluoroalkane sulfonamides (FASA)	FOSA		
Perfluoroalkane sulfonyl fluorides (PASFs)	PBSF, POSF		
Perfluoroalkyl iodides (PFAIs)	PFHxI		
Perfluoroalkanoyl fluorides (PAFs)	POF		
Perfluoroalkyl aldehydes (PFALs)	PFNAL		
Polymeric PFAS			
Subgroup	**Example**		
Fluoropolymers	PVDF, FEP, PFA, ETFE, PTFE (Teflon)		
Side-chain fluorinated polymers	Fluorinated/urethane/acrylate/methacrylate/oxetane polymers		
Perfluoropolyethers (PFPEs)	PFPE-BP, Fluorolink-PFPE		

In recent years, PFOA has attracted the most attention because of its high persistence, toxicity, and bioaccumulation. For example, in 2010, the presence of PFAS in European groundwater was investigated, and PFOA accounted for 48% of the PFAS compounds detected [14].

2.2. PFAS removal techniques

Analysis and remediation of PFAS are highly challenging and time-consuming due to their low MAC. Several technologies are currently available for removing PFAS from aqueous media, categorized as destructive and non-destructive (separation) techniques. Destructive methods for PFAS chemicals include electrochemical, thermal, sonochemical, and plasma treatments, among which electrochemical, sonolysis, and plasma treatments are more effective at decomposing PFAS chemicals in the laboratory [13,15]. A strong bond between carbon and fluorine atoms in the PFAS structure makes it difficult to destroy PFAS in practice, and therefore, most of these

techniques have been used on a limited basis. The long treatment times and high energy requirements of these technologies make them challenging to scale up.

Three main methods are applied for the separation of PFAS: coagulation-flocculation, membrane filtration, and adsorption. As a pretreatment step in wastewater treatment, coagulation-flocculation remove suspended and dissolved solids. Despite this, conventional coagulants cannot efficiently remove PFAS from aqueous solutions; they are only used as a pre-treatment step for separating the organic matter from water. Therefore, other separation technologies like adsorption are used to enhance the removal of PFAS [16]. Since semi-permeable membranes have smaller pores than PFAS molecules, the membrane filtration method can separate PFAS molecules. Studies have shown that nanofiltration (NF) and reverse osmosis (RO) are effective membrane techniques for removing PFAS. However, the high energy demands of these two techniques make them very costly to employ at large scales. In addition, as a result of these processes, concentrated waste streams containing high levels of PFAS contaminants are produced, and managing these wastes is a costly and challenging process [12]. In comparison, PFAS compounds with different physicochemical properties can be removed from water using the adsorption method. Furthermore, the adsorption technique treats water containing various levels of PFAS. According to several studies, adsorption is an effective method for removing organic compounds from water [17,18].

2.2.1. Adsorption process

Chemical and/or physical adsorption can remove PFAS compounds from contaminated water by adhering them to an adsorbent surface. Adsorption of PFAS molecules on polar and apolar adsorbents occurs through electrostatic and hydrophobic interactions with the charged functional groups and the nonpolar tail in PFAS molecules [19]. A PFAS molecule typically exists in an anionic form in aquatic environments, resulting in an electrostatic attraction between its anionic chemical functional groups and the positive sites on the surface of the adsorbents. Hydrophobic surfaces of the adsorbents and the perfluoroalkyl tails of PFAS have hydrophobic interactions during adsorption.

PFAS can be effectively eliminated from contaminated waters by using carbon-based adsorbents. Activated carbon (AC) is widely used as a commercial adsorbent to remove PFAS from wastewater. Two techniques of adsorption treatment are more common in water treatment:

AC followed by incineration and advanced ion exchange (AIX) [18,20]. As well as serving as adsorbents, ion exchange resins possess ion exchange capabilities. Positively charged resin sites can bind negatively charged heads of PFAS molecules, and hydrophobic tails of PFAS molecules are adsorbed on the hydrophobic backbones and/or crosslinks of resins. Since resins are expensive, their regeneration and reuse after exhaustion with contaminants may be of the utmost importance; however, common chemicals for the desorption of contaminants (methanol and NaCl) may not be effective for some PFAS contaminants [17].

2.3. Biochar: a green adsorbent for PFAS

In a green adsorption process, low-cost biomaterials derived from natural and agricultural sources (such as canola straw), including residues, byproducts, and agricultural wastes, are utilized as adsorbents, which are inexpensive, abundant, environmentally friendly, and easy to produce. Biochar is a low-cost carbon residue synthesized by pyrolyzing biomass materials under different anaerobic conditions. Generally, biochar is produced economically because raw materials are widely available, and activation processes are not required [21]. Adsorbents based on low-cost and engineered biochar can be used for large-scale water treatment instead of AC. A cheap, readily available, and easily recovered alternative adsorbent can significantly reduce operation costs. In 2017, the average energy demand and the average greenhouse gas (GHG) emissions for biochar production were almost 6.1 MJ/kg and 0.9 kg CO_2/kg, respectively, while these amounts for AC production were 97 MJ/kg and 6.6 kg CO_2/kg [22].

The pores and surface functional groups on biochar surfaces play a crucial role in interacting with their surroundings. Biochar adsorption behaviour is related to the feedstock composition and pyrolysis conditions. The release of volatile components from the carbon matrix and the loss of water during pyrolysis lead to the formation of pores in the biochar structure and the development of pores in the carbon matrix. PFAS adsorption is significantly affected by the pyrolytic temperature of biochar. When biochar is pyrolyzed at low temperatures, electrostatic interactions with adsorbates increase because of many ionic groups on its surface. At high temperatures, pyrolysis, decarbonylation, and decarboxylation occur, leading to the loss of polar chemical functional groups in biochar, so it interacts through hydrophobic components with contaminants [23].

Biochar can absorb PFAS from the environment, including water and soil. For example, a study conducted by Abdel-Fattah et al. demonstrated that biochar can adsorb heavy metals [24].

Dechene et al. examined the adsorption of polar organic contaminants and pesticides onto soil amended with biochar [25]. Kupryianchyk et al. reported how PFAS binds to biochar and paved the way for further investigation of biochar's potential use in in-situ PFAS remediation [26]. A few studies have compared PFAS adsorption by different biochar adsorbent [4, 29-33]. However, these studies have not included detailed comparisons between biochar prepared under different chemical treatment and pyrolysis conditions.

A variety of biomass sources have been investigated for the utilization of biochar in ongoing experimental research. According to Guo and Huo, research was underway on biochar made from corn straw at various operating temperatures (250, 400, 550, and 700°C). In particular, higher pyrolytic temperatures produce biochar with a greater surface area and a greater degree of aromaticity. Moreover, the research demonstrates that biochar produced at higher temperatures exhibits enhanced hydrophobicity, facilitating the adsorption of PFAS [27]. Various chemical treatments, including acid or alkali treatment, nanoparticle coating, and metal and salt impregnation, have been demonstrated to enhance microporosity [28].

2.4. PFAS and biochar interactions

Due to the amphiphilic properties of PFAS compounds, it is challenging to understand their adsorption by biochar. Factors like the types of PFAS compounds present, the properties of biochar, and the environmental conditions influence the interaction between PFAS compounds and biochar materials. Since PFAS molecules have hydrophilic and hydrophobic properties, they adsorb on biochar adsorbents through several mechanisms (Figures 2.3 and 2.4). These include electrostatic attractions, covalent bonds, intramolecular interactions (such as hydrogen bonds), fluorophilic interactions, hydrophobic interactions, and PFAS aggregation.

It is not possible to attribute PFAS adsorption to one or two unique mechanisms. However, the prevalence of each mechanism in the adsorption process can vary based on the type of biochar and the type of PFAS. There may be a difference in the dominant mechanism in each case of adsorption. This highlights the complexity and specificity of the interactions between biochar and PFAS during the adsorption process compared to other contaminants. There has been a strong correlation between PFAS adsorption capacity and the surface area of the adsorbent [34].

Electrostatic interactions occur when molecules with opposite charges attract or when bodies with the same charge repel each other (Figures 2.4a and b) [29]. A PFAS can be attracted

to surfaces with a net positive charge due to the negative charge held by the ionic forms of functional groups or electron pairs of atoms. Due to the strong electronegativity of fluorine atoms, PFAS molecules have an exterior charge that is net negative with a positive region along the carbon backbone (Figure 2.3). Due to these properties, PFASs can interact electrostatically with charged surfaces of biochar [29]. However, these interactions are primarily mediated by charged hydrophilic functional groups. PFAS can be repelled or attracted by surface functional groups based on their charge [35]. Hydroxyl groups can form weak dipole-dipole interactions. Adsorbed PFAS molecules may increase the net surface negative charge as they propel other PFAS molecules away from the surface of the adsorbent, preventing the adsorption or effective distribution of PFAS adsorbate. A hydrophobic CF_2 moiety repels water and prevents hydrogen bonding with functional groups [36]. The functional groups of PFAS could act as proton acceptors for the surface functional groups of biochar (-COOH). At neutral pH, the OH moiety of phenol groups on the biochar can form hydrogen bonds with fluorine atoms.

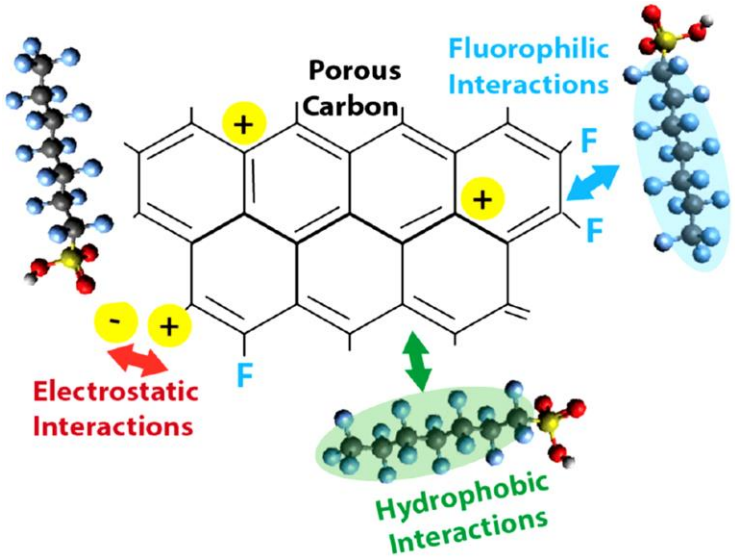

Figure 2.3. Different interactions between biochar structure and PFAS molecule (adapted from Saha et al. [34])

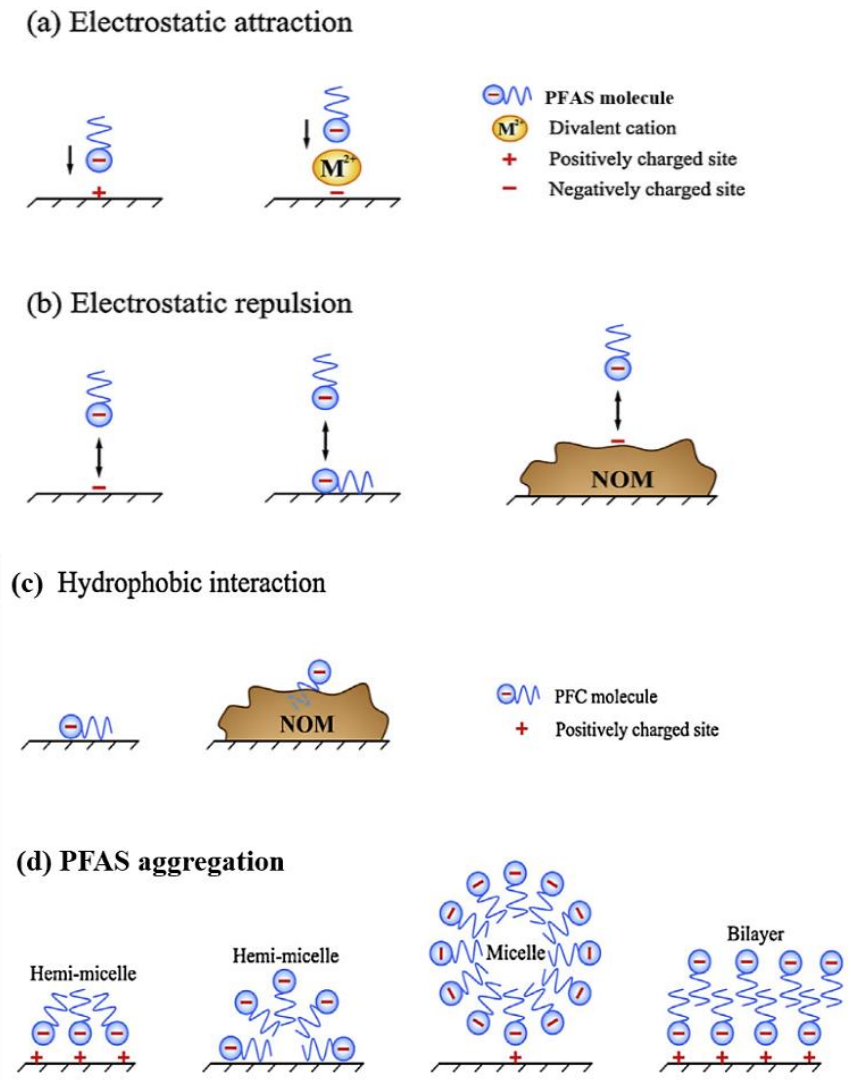

Figure 2.4. Schematic diagram for electrostatic attraction (a), electrostatic repulsion (b), hydrophobic interaction (c), and self-aggregations (d) in PFAS adsorption process (adapted from Du et al. [29])

A complex interaction between PFAS molecules and biochar electronic double layers may influence the mode and rate of adsorption. The adsorption of PFAS onto biochar can be caused by their hydrophobic nature and the resultant partitioning into hydrophobic sites of biochar. Porosity, hydrophobicity, and degree of carbonization of the biochar determine how well it binds PFAS [37].

Hydrophobic adsorption can be divided into partitioning and surface (Figure 2.4c). Partitioning relates to interactions where PFAS hydrophobic tails ($(CF_2)_n$ moiety) are attracted to

and seated in the amorphous hydrophobic organic matter. The hydrophobicity of the tails of PFAS is responsible for their surface adsorption [29].The aggregation of PFAS forms micelles, hemi-micelles, and bilayers (Figure 2.4d). These structures resemble fluids and have hydrophobic interiors and hydrophilic exteriors. As a result of water electrostatically repelling PFAS at this interface, PFAS spontaneously binds to surfaces. There is a tendency for PFAS to adhere to hydrophobic surfaces, including other PFAS, resulting in their congregating. The hydrophobic tails of PFAS molecules tend to cluster together, while the hydrophilic parts are oriented outward. As a result of this arrangement, they can interact with the surrounding aqueous phase by van der Waals forces while excluding water from their interior. Consequently, the hydrogen bond network around the cluster is disrupted, resulting in a dry interface [36]. PFAS molecules can also form bilayers under certain conditions, especially when accumulating on an electrically charged surface. Even though these clusters are called hemi-micelles, they are considered monolayers. The phenomenon has been well documented in the literature and observed in several studies over the years [38].

2.5. Biochar production

Biochar is produced from biomass during thermal decomposition under an oxygen-limited environment to prevent combustion. The degradation process during pyrolysis involves the depolymerization of different biopolymers and the carbonization of the biomass to recalcitrant forms via dehydration, decarboxylation, demethylation, aromatization, condensation, and other chemical reactions [39]. In the pyrolysis process, the required heat is supplied by direct or indirect heating from hot solids, hot gases, or oxidation reactions. In numerous studies, microwave-assisted pyrolysis (MWP) has been considered as an alternative to conventional pyrolysis (CP) primarily because it is selective, volumetric, uniform, fast heating, and increases energy efficiency, which accelerates the reaction rate [31,32]. By providing instant on/off control, microwave heating increases the yield and improves the product quality. Heating rates in MWP range from 0.1 °C/s to >1000 °C/s, which significantly impacts production yields. Moreover, this method is environmentally friendly because it minimizes the emission of pollutants and hazardous products. The biochar produced by MWP has higher quality, surface area, and pore volume with clean and uniform micropores than the biochar produced by

conventional heating methods. Therefore, MWP can produce porous biochar, which is suitable for adsorption applications [40].

2.6. Pyrolysis conditions

The decomposition temperature for hemicellulose is between 220 and 315 °C, while for lignin and cellulose, the range is 315 to 400 °C. The pyrolysis conditions greatly influence the physicochemical properties of biochar, and organic fractions decompose and transform into new compounds at various temperature ranges [42]. In general, pyrolysis is divided into three categories based on the reactor's heating rate, temperature, and residence time of vapours: slow, fast, and flash pyrolysis. Pyrolysis temperature is the most significant factor in determining the biochar surface functional groups and surface area. Furthermore, it determines biochar porosity by degassing volatiles and cracking during shrinkage. Biochar contains a wide range of pores, from micropores (less than 2 nm) to macropores (greater than 50 nm). When biochar is produced at higher pyrolysis temperatures, it usually loses most of its surface functional groups but has a higher surface area. Moreover, at higher temperatures, biochar tends to be more similar to graphite in terms of structure and composition, while at lower temperatures, products are more similar to their original ingredients [42].

2.7. Modification of biochar

There are many methods available for modifying biochar to improve its adsorption effectiveness. The modification methods of biochar serve four primary purposes: 1) increasing the volume and surface area, 2) creating surface charges, 3) creating or increasing the surface chemical functional groups, and 4) magnetizing the biochar to be recycled and recovered more efficiently (Figure 2.5). One treatment can improve two or more properties simultaneously; for example, some chemical treatment increases both oxygen-containing functional groups and specific surface area [43]. Chemical activation is the most common way for biochar treatment because more well-developed microporous biochar with a higher surface area is produced by this method.

Chemical modification methods include alkalinity modification, acid modification, carbonaceous material modification, and modification using metal salts or oxidizing agents. The biochar can be pre-treated before or after pyrolysis by various chemical activators (acids, bases,

and salts). To optimize porosity development, reagent dosage, activation time, and activation temperature should all be optimized for this treatment [44].

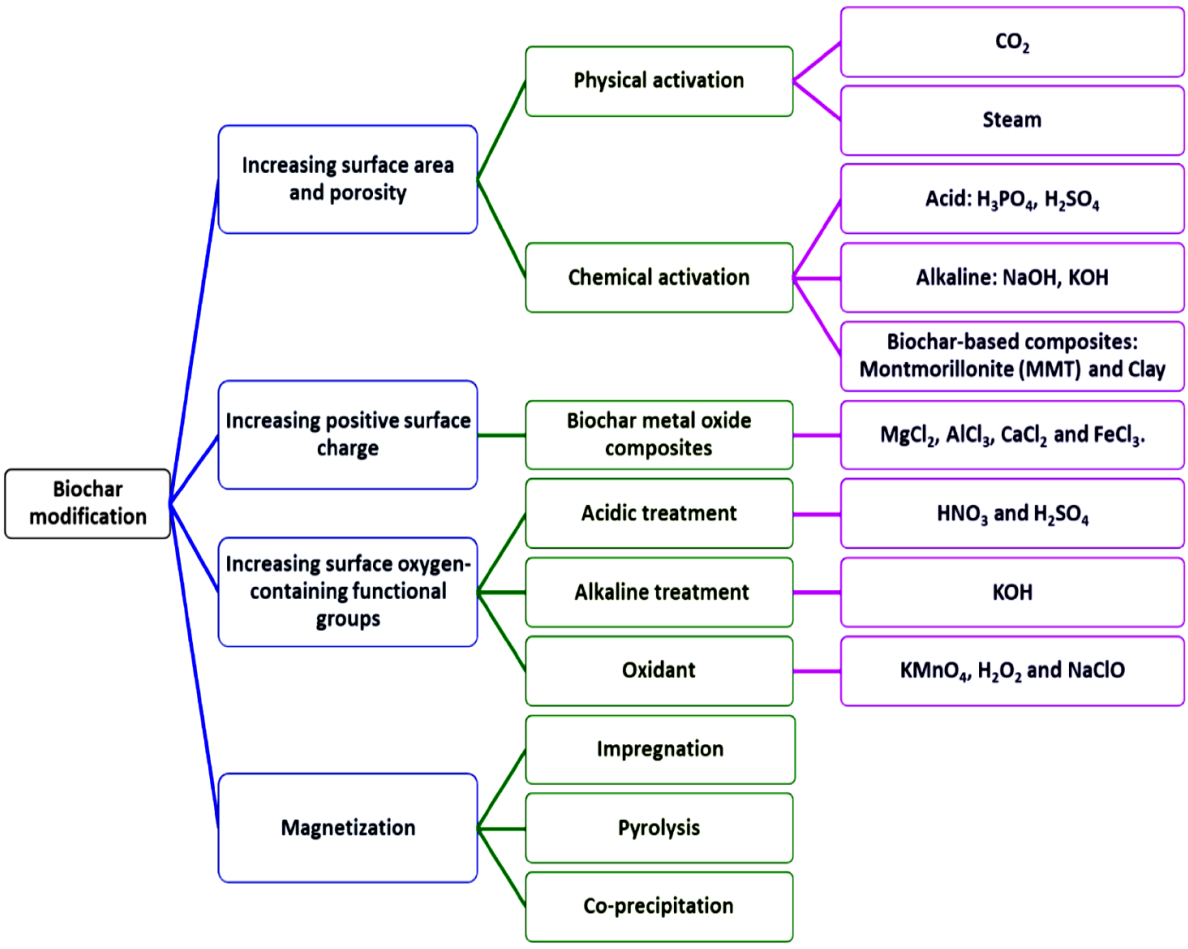

Figure 2.5. Biochar modification methods and their classification (adapted from Zeghioud et al. [45])

H_3PO_4: Among the most popular acid activators, H_3PO_4 can introduce both P-containing chemical functional groups and micropores into biochar. On the other hand, H_3PO_4 also acts as a dehydration agent during crosslinking reactions, including condensation and cyclization, which lead to the formation of pores. Additionally, organic phosphate esters are produced by the reaction of biomass alcohol groups with phosphate radicals, which prevents the collapse of micropores and protects the carbon skeleton [44]. Based on Chu et al. (2018) findings, biochar produced from pine sawdust treated with H_3PO_4 had a total pore volume and surface area of 0.87 cm^3/g and 1,627 m^2/g, respectively, following the introduction of P-containing chemical

functional groups, while these amounts are to 0.18 cm^3/g and 411 m^2/g for untreated pine sawdust [46].

$ZnCl_2$: The Lewis acid nature of $ZnCl_2$ makes it an excellent salt activator for biochar. Due to its intense dehydration, biomass compounds can decompose at a lower temperature, enhancing biochar production yield. In addition, $ZnCl_2$ penetrates lignocellulosic biomass due to its dissolving action on cellulose, which produces pores in the biomass. Moreover, due to its high boiling point, $ZnCl_2$ remains liquid during carbonization. So, the activation temperature is lower than its boiling point, acting as a skeleton to support the carbon structure. After removing $ZnCl_2$, the porous structure of the produced biochar is preserved [44]. According to a Wang and Liu (2017) study, biochar produced by a $ZnCl_2$ activator had a total pore volume and high surface area of 0.54 cm^3/g and 832 m^2/g, respectively, with a biochar yield production >30% [47]. Recently, a mixture of $FeCl_3$ and $ZnCl_2$ was developed as an activator and attracted considerable attention due to its ability to activate and graphitize biochar simultaneously. In 2017, Tian et al. used $ZnCl_2$ and $FeCl_3$ to produce a graphitic structure biochar derived from inner shaddock skin with a large volume porous structure (1.68 cm^3/g) and a high surface area (2,513 m^2/g) [48].

2.8. Generalized models and equations for PFASs and biochar adsorbents

Adsorbents are typically evaluated through batch and fixed-bed experiments to determine their effectiveness in removing pollutants. This section explains the most common and important models used to describe the PFAS adsorption process on carbon-based adsorbents.

2.8.1. Kinetic models

Understanding adsorption kinetics is essential to optimizing the adsorption process. Equilibrium in the adsorption process describes the condition in which the adsorbate concentration in the liquid phase remains constant. By understanding the adsorption rate, the selection of suitable adsorbents and the design of more efficient adsorption systems can be facilitated [29]. Additionally, kinetics are crucial in accurately determining the required contact time between an adsorbent and its corresponding adsorbate. In addition to providing insights into fundamental adsorption mechanisms, studying adsorption kinetics can provide insight into interactions between molecules and adsorbent surfaces, the role that diffusion plays, and the dynamics of interactions between adsorbate and adsorbent. As a result of this knowledge, a better

understanding of surface science and interfacial phenomena will be obtained. The most common kinetic models used for PFAS compounds are reviewed in the following.

A pseudo-first-order kinetic model is illustrated in Eq. 2.1, proposing a linear relationship between the amount of PFAS absorbed and the PFAS concentration in the solution. PFAS concentration at t (h) is represented by C_t (µg/L), C_0 is the PFAS concentration at t = 0 (µg/L), q_t is the mass PFAS absorbed per unit biochar (µg/g) at time t (h), q_e is the mass PFAS absorbed per unit biochar at equilibrium (µg/g), and k_{pfo} is the first order rate constant (h) [49].

$$q_t = q_e(1 - \exp(-k_{pfo}t)) \quad \text{Eq. 2.1}$$

Eq. 2.2 can fit data to the pseudo-second-order model. This model assumes that the rate-limiting step is chemical adsorption or chemisorption. The rate is exponentially related to the concentration of PFAS in the solution, indicating an excess of one reactant in the solution (sorption sites). For second-order adsorption, k_{pso} is the adsorption rate constant (g/(µg h)) [49].

$$\frac{t}{q_t} = \frac{1}{k_{pso}{q_e}^2} + \left(\frac{1}{q_e}\right) \quad \text{Eq. 2.2}$$

An intra-particle diffusion model can be used to determine three stages of adsorption (Eq. 2.3). In the model, the k_p (µg/(g $h^{0.5}$)) represents the rate constant for stage I. In stage I, the adsorbate molecules approach the adsorbent material and initiate adsorption. Adsorbent molecules penetrate the internal pores of the adsorbent material during stage II, representing intra-particle diffusion. During this stage, the adsorbate moves within the material's structure. Stage III is characterized by equilibrium, showing the completion of the adsorption process with a constant concentration of adsorbate. The intercept of stage I may be used to derive C, a constant related to resistance to boundary layer mass transfer. The presence of larger C values suggests that boundary layers are thicker and more influential [50].

$$q_t = k_p t^{0.5} + C \quad \text{Eq. 2.3}$$

The Elovich model has been used to describe the adsorption of liquid-solid systems and is usually expressed as Eq. 2.4 [51]. It has been successfully used to model the adsorption of inorganic and organic pollutants on various adsorbents. In this equation, a is the initial adsorption rate (µg/g min), and b is the desorption constant (g/µg).

$$q_t = \frac{1}{b}\ln(1 + abt)$$ Eq. 2.4

2.8.2. Isotherm models

The following isotherm models are used to study a relationship between the amount of contaminant adsorbed on the surface of the biochar and the concentration remaining in the solution. In the isotherm equations, q_e represents the equilibrium adsorption capacity (µg/g), C_o corresponds to the initial concentration of PFAS in the solution (µg/L), and C_e corresponds to the remaining concentration of PFAS in the solution (µg/L) at equilibrium for a given mass of adsorbent M (g). The following equation (Eq. 2.5) was used to calculate the PFOA adsorption capacity on various adsorbents [52]:

$$q_e(\mu g/g) = \frac{(C_0 - C_e)}{M} \times V$$ Eq. 2.5

A_e is the adsorption efficiency and is usually used to compare different adsorbent performances. It is determined using Eq. 2.6 [53]:

$$A_e(\%) = \frac{(C_0 - C_e)}{C_0} \times 100$$ Eq. 2.6

According to the Langmuir isotherm model (Eq. 2.7), adsorption involves a single adsorbate attached to homogeneous sites on a flat surface. The model assumes that each site can accommodate only one molecule, and when all active sites are occupied, a monolayer is formed, preventing further adsorption. The attached molecule remains fixed without any subsequent interaction with the solution or the surface [45,46]. According to Eq. 2.7, q_m represents the maximum capacity of sorbate adsorption per unit of biochar (measured in grams). Langmuir adsorption energy is indicated by K_L (expressed as L/µg).

$$q_e = \frac{K_L\, q_m C_e}{1 + K_L C_e}$$ Eq. 2.7

The Freundlich isotherm (Eq. 2.8) indicates accommodating multilayered adsorption phenomena. This isotherm model explains the exponential distribution of active sites, surface heterogeneity, and their energies. K_F ((µg/g)(L/µg)1/n) describes the adsorption affinity, with higher values indicating higher affinity. Additionally, 1/n serves as a constant related to adsorption intensity. Notably, when this value is between 0 and 1, it indicates a chemisorption process [55].

$$q_e = K_F C_e^{1/n}$$ Eq. 2.8

A Temkin isotherm model is another mathematical equation that describes adsorption on a solid surface. The Temkin isotherm equation is described by Eq. 2.9 [55]:

$$q_e = \frac{RT}{b_T} \ln(K_T C_e)$$ Eq. 2.9

Where R is the universal gas constant (8.314 J/(mol K), T is the temperature (K), K_T is an equilibrium constant (L/μg), and b is a constant. In this model, nonlinear isotherms may result from heterogeneity in the adsorption site, interactions between the adsorbate and the adsorbate, and aggregation [56].

2.8.3. Adsorption fixed-bed models

As one of the most widely adopted methods for separation and purification, fixed-bed adsorption stands out due to its efficiency and simplicity. A critical aspect of fixed-bed adsorption is optimizing the design and operational parameters. Due to the challenges and costs associated with experimental investigations across various conditions, developed mathematical models are beneficial in predicting the performance of fixed-bed adsorption. An ideal model should be mathematically tractable and convenient to formulate in this context. Additionally, the model should be capable of accurately estimating breakthrough behaviour and assessing the impact of each variable on the adsorption process. Such models provide a better understanding of fixed-bed adsorption dynamics and more effective optimization of conditions for practical applications.

The dynamic changes in PFAS during the adsorption process within a fixed-bed column are usually studied using the Yan (Eq. 2.10) and Yoon-Nelson models (Eq. 2.11). A quantitative evaluation of the PFOA adsorption efficiency has been performed herein by identifying the breakthrough point (t_b), exhaustion point (t_e), and time to 50% breakthrough (τ). The t_b value indicates the point at which the effluent PFOA concentration reached 5% of the influent concentration, and the t_e value indicates the point at which the outlet PFOA concentration reached 95% of the influent concentration. Additionally, τ represents the time required to achieve a 50% breakthrough of the adsorbate [57].

The Yan model (Eq. 2.10) can describe adsorption in a fixed-bed column. In this model, adsorbent particles are assumed to be uniformly sized and shaped. The Yan model can be expressed as follows:

$$\frac{C_t}{C_0} = 1 - \frac{1}{1+(\frac{Vt}{b_Y})^{a_Y}} \quad \text{Eq. 2.10}$$

The Yoon-Nelson model is also widely used to describe the dynamics of fixed-bed adsorption processes (Eq. 2.11).

$$\frac{C_t}{C_0} = \frac{\exp(a_{YN}t - a_{YN}b_{YN})}{1+\exp(a_{YN}t - a_{YN}\, b_{YN})} \quad \text{Eq. 2.11}$$

In these models, t represents time (min), C_t indicates the effluent PFAS concentration at time t (µg/L), C_0 is the influent PFAS concentration (µg/L), V denotes flow rate (mL/min), a_Y and b_Y refer to the Yan model constants, and the Yoon- Nelson model constants are a_{YN} and b_{YN}.

2.8.4. Adsorption thermodynamics

Several thermodynamic factors can define the adsorption process, including Gibbs free energy change, adsorption enthalpy, and entropy changes. The Van't Hoff equation links the variation of enthalpy and entropy (Eq. 2.12) [58]. According to this equation, the slope and intercept of the linearized variation of ln K_c with T^{-1} can determine variations in enthalpy and entropy. In order to determine these parameters, the following thermodynamic equations can be used (Eqs. 2.12-2.14):

$$\Delta G^0 = -RT\ln K_c \quad \text{Eq. 2.12}$$

$$\ln K_c = -\frac{\Delta H^0}{RT} + \frac{\Delta S^0}{R} \quad \text{Eq. 2.13}$$

$$\Delta G^0 = \Delta H^0 - T\Delta S^0 \quad \text{Eq. 2.14}$$

The universal gas constant is R (8.314 J/mol K), T is the temperature (K), and K_c represents the thermodynamic equilibrium constant (dimensionless). As a result of Gibbs free energy change, the spontaneity of the process can be explained. A negative value indicates a spontaneous adsorption process, while a positive value shows that the adsorption process is not spontaneous [59]. Adsorption processes can be classified as exothermic or endothermic based on

the enthalpy change or heat of adsorption. For an adsorption process, a negative enthalpy change indicates that it is exothermic, and a positive change is endothermic.

Furthermore, this parameter can distinguish between chemical and physical adsorptions and provide information regarding the type of bond between the two molecules. Chemical bonds dominate chemical adsorption, while van der Waals forces dominate physical adsorption. Due to the weak bonding force, physical adsorption is fully reversible, whereas chemical adsorption is irreversible. Also, chemical adsorption usually induces monolayer coverage, while physical adsorption can also result in multilayer coverage. The entropy of a system is indicative of its randomness. In a solid-liquid system, an increase in this thermodynamic parameter indicates an increase in randomness.

2.8.5. Effects of environmental factors on adsorption

PFAS adsorption to biochar can be limited by competition for adsorption sites from different interferences, including organic matter, inter-PFAS competition, and PFAS solute-solute repulsion. Additionally, the environmental conditions within the solution affect adsorption mechanisms and, consequently, adsorption rate and capacity [60]. Several critical environmental factors, including temperature, pH, and ions, are critical in determining adsorbate-adsorbent interactions.

Temperature: Temperature affects the PFAS adsorption onto the biochar depending on the properties of both biochar and the compounds in water. Therefore, there is no clear relationship between temperature and PFAS adsorption, but higher temperatures result in increased PFAS solubility. In addition to increasing temperature, vibrational energy is also increased, which allows PFAS to have more contact with the surface of biochar [61].

pH: The pH of the solution influences adsorption behaviour by affecting the speciation of adsorbates. At lower pH values, adsorption occurs at a faster rate due to the presence of a positive or near-neutral charge on carbonaceous surfaces. Since the pH is closer to the PFAS pK_a, it causes the most significant degree of disassociation [62]. In the same way, adsorbent surface functional groups have higher adsorption capacities for PFAS at neutral and low pH levels. However, this phenomenon needs to be better understood and may involve

protonation/deprotonation and neutral ions existing within the sorbate molecules. PFAS will be more likely to repel negatively charged surfaces as pH increases [63].

Ions: Ions can influence adsorption processes in various ways, including electrical double-layer compression, neutralization of cationic bridges, surface charges, salting out, and competitive adsorption. Ion charge and valence determine the effects of ionic solution interferences, with cations often having a more significant effect than pH. As a result of electrical double-layer compression, cations in solution may reduce the net negative charge on the adsorbent surface, thereby aiding the adsorption of anionic PFASs. For example, seawater sediments containing calcium (Ca^{+2}) ions and magnesium (Mg^{+2}) ions showed higher adsorption capacities for PFAS than sediments in freshwater; specifically, higher Ca^{+2} concentrations correlated with higher PFAS adsorption capacities [63]. Higher pH and Ca^{+2} concentrations resulted in sorbents forming more basic sites for binding divalent cations onto carboxyl, phenolic, and hydroxyl groups in the negative charge regions. Consequently, more PFASs were bound through divalent cation bridging. It has been shown that increasing the number of ions in solution diminishes the electrostatic attraction and repulsion of PFAS by compressing their electrical double-layer [64].

Organic Matter: By retaining PFASs in the solution attached to organic matter, organic matter affects PFAS adsorption in the aqueous phase. Furthermore, it restricts the availability of adsorption sites through competition. The smaller organic molecules tend to have a greater affinity for PFASs for adsorption, while the larger molecules are more responsible for fouling and blocking pores. Organic matter bound to the surface of biochar usually delivers a net negative surface charge, causing PFAS to be repelled [65].

3. Knowledge gaps and research objectives

3.1. Knowledge gap

Although biochar has shown promise for PFAS adsorption, there are still significant research gaps preventing its use on a large scale:

- Optimization of pyrolysis conditions to produce biochar. More research needs to be conducted on optimal conditions to produce biochar adsorbents to increase their effectiveness in removing both long- and short-chain PFAS compounds.

- Study of modified and non-modified biochar for PFAS adsorption. This research gap highlights the need for more research to understand the difference in performance between modified and non-modified biochar in the adsorption of PFAS and how modifications may impact biochar effectiveness.
- Assessment of batch and continuous reactors to evaluate PFAS adsorption in contaminated waters. This research gap indicates a need for studies evaluating the real-world effectiveness of PFAS adsorption in contaminated water using batch and continuous reactor systems.
- Determination of the stability of biosorbents and regeneration-reuse cycles. This research gap highlights the need for further research on biochar's stability, regeneration, and reuse capabilities.
- Investigation of the effect of adsorption competitors in natural multi-contaminated waters on PFAS adsorption efficiency. It is essential to conduct more research to understand how other contaminants in water can affect the ability of PFAS to be absorbed by biochar.

3.2. Research objectives

This study aims to develop a method to produce modified biochar based on canola straw with a higher adsorption capacity for PFAS in water than untreated biochar. The effect of pyrolysis conditions and chemical treatment on PFAS adsorption efficiency was investigated. According to the main goal, the objectives of this study were as follows:

1. Synthesis and characterization of biochar activated by different activators to find the optimum biochar adsorbent for PFAS

   Hypothesis: Activator molarity, microwave heating time, and microwave power during the preparation of the microwave-activated biochar adsorbents from canola straw can be optimized by the design of the experiment to increase the PFOA adsorption capacity. H_3PO_4 was selected as an activator because phosphoric acid is a common and cost-effective acid that can introduce phosphorous functional groups to the surface of biochar. As a result of these functional groups, the biochar surface can interact more with PFAS. $ZnCl_2$ was an activator since it could form ZnO on the biochar surface, introducing new adsorption sites for PFAS adsorption.
2. Assessment of the PFAS adsorption process on different modified biochar adsorbents

Hypothesis: As a result of the modification of adsorbents by H_3PO_4 and $ZnCl_2$, the PFAS adsorption capacity is expected to depend on the surface chemistry, microporosity enhancement, and optimal modification conditions. Different chemical analyses and kinetic studies can confirm these differences.

3. Determination of the most important factors influencing the PFAS adsorption capacity
   Hypothesis: A temperature change is expected to affect kinetic energy and adsorption capacity. Furthermore, changes in pH and ions in water can affect the chemistry of the surface. This hypothesis contributes to a better understanding of how modified biochar performs under different environmental conditions by investigating the relationships between environmental factors and PFAS adsorption.

Chapter 3.

Research Methodology

This chapter describes the materials used during the chemical treatment of biochar and adsorption experiments. Furthermore, the preparation of adsorbents, experimental procedures, characterization techniques, and analytical methods are described in detail.

3.1. Materials

All chemicals and reagents were of analytical grade and used without further processing. Perfluorooctanoic acid (PFOA) (96%), zinc chloride powder ($ZnCl_2$, anhydrous, +98%), and o-phosphoric acid (85%) were purchased from Thermo Fisher Scientific Inc. (Ontario, Canada). Other chemicals and reagents were bought from Sigma-Aldrich (USA). Analytical-grade chemicals and Millipore deionized (DI) water were used to prepare all solutions (Q-H_2O, Millipore Corp). After collecting raw canola straw (RCS) from an agricultural field in Saskatoon (Canada), it was washed with water three times to remove dust and dried at 60 °C for 24 h. It was ground to obtain uniform particles and sieved in the size range between 400 and 840 µm (Figure 3.1).

3.2. Procedures

Experimental procedures involve the preparation of adsorbents, design of experiments, characterization techniques, and batch and continuous adsorption experiments, which are discussed in the following sections.

3.2.1. Preparation of biochar adsorbents (UBC, PBC, and ZnBC)

The preparation of modified biochar adsorbents involves two main steps: chemical treatment and pyrolysis (Figure 3.1). Two modified biochar adsorbents were synthesized, including H_3PO_4-treated biochar (PBC) and $ZnCl_2$-treated biochar (ZnBC). First, 5 g of RCS was mixed with 100 mL of different of H_3PO_4 and $ZnCl_2$ concentrations and stirred for 2h. The mixture was filtered and pyrolyzed by the MWP method at different microwave irradiation times and power levels. The final products were washed with hot water followed by cold water several times to remove residual H_3PO_4 and $ZnCl_2$, and impurities, and then dried at 70 °C for 12 h.

Untreated biochar (UBC) was synthesized without any activator under optimum MWP conditions.

Figure 3.1. Schematic of the procedure for preparing biochar adsorbents

3.2.2. Design of experiments

Response Surface Methodology (RSM) was utilized to examine the effects of several independent parameters and their combined effects on PBC and ZnBC adsorption capacity at equilibrium and 25 °C. A three-factor Central Composite Design (CCD) method based on RSM was applied to study and optimize the following parameters during the synthesis procedure: activator concentration (mol/L) (X_1), microwave irradiation time (min) (X_2), and microwave power (W) (X_3). The ranges of independent factors (X_1, X_2, and X_3) have been selected based on preliminary experiments (Table 3.1).

Table 3.1. The ranges of independent factors for synthesis of biochar (X_1: activator concentration (mol/L), X_2: microwave time (min), and X_3: microwave power (W))

Variables (Factors)	Unit		Minimum	Maximum
X_1	mol/L	H_3PO_4	1	5
	mol/L	$ZnCl_2$	0.1	1
X_2	min		3	9
X_3	W		300	900

3.2.3. Adsorbent characterization and analytical methods

The surface morphology and element distribution of adsorbents were studied by scanning electron microscopy (SEM, Hitachi SU8010, Japan) equipped with an energy dispersive spectrometer (EDS). Analyses were conducted under high vacuum conditions with an emission current of 10 µA and a voltage of 5 kV. In order to determine the specific surface area, total volume, and average pore diameter of adsorbents, a Brunauer-Emmett-Teller (BET) N_2 analyzer

(NOVAtouch; Quantachrome, USA) was used. The biomass and biochar samples were degassed at 60 and 160 °C, respectively. The effects of activators on the crystalline structure of the samples were investigated using a Bruker X-ray diffractometer with a scanning speed of 2°/min (Rigaku Americas Corp., USA). A Smith's Detection IlluminatIR FT-IR microscope (USA) was used to measure the Fourier-transform infrared (FT-IR) spectra to analyze chemical functional groups and surface chemistry of adsorbents. A Renishaw spectrometer (Gloucestershire, UK) provided the Raman spectra of the samples to investigate the pyrolysis effects on the biochar properties. X-ray photoelectron spectroscopy (XPS) (Kratos Analytical Ltd, UK) was employed to identify the functional states of carbon, oxygen, phosphorus, zinc, and fluorine on the surface of adsorbents. Minitab software version 19.0 (Minitab Inc., Pennsylvania, USA) was used to build the experimental design.

PFOA concentrations were determined by a 1290 Infinity II HPLC system in tandem with 6470A triple quadrupoles mass spectrometer. 80 µL of the PFOA samples were injected into the LC-MS/MS system equipped with a C18 column (150 mm × 2.1 mm, 3.5 µm) (Waters, Milford, MI) with a 0.5 mL/min flow rate. In the mobile phase, two solutions were used: 5 mM ammonium acetate in methanol and 5 mM ammonium acetate in water (50:50). For PFOA, the detection limit is 10 µg/L for the instrument. The samples were analyzed using HPLC-MS/MS after filtration by 0.45 µm syringe filters (PVDF Millex-HV, EMD Millipore).

3.2.4. PFOA adsorption experiments

3.2.4.1. Batch experiment

PFOA adsorption mechanisms on PBC and ZnBC adsorbents were studied by performing batch adsorption experiments in various conditions. The effects of PFOA concentration, adsorbent dosage, temperature, pH, ionic strength, and the presence of co-existing ions on PFAS adsorption were investigated in several adsorption experiments. The experiments were conducted in 100 mL glass bottles containing 80 mL water, PFOA, and the adsorbent dosage, continuously agitated at 200 rpm on a shaker table.

A batch adsorption kinetic study on PBC and ZnBC at 25 °C was carried out at a concentration of 200 µg/L PFOA and dosage of 0.5 g/L of modified adsorbents, and the obtained results were fitted to conventional kinetic models. Isotherm studies of modified adsorbents were evaluated in the PFOA concentration between 50-300 µg/L. The thermodynamics of PFOA

adsorption at different temperatures (281, 288, 298, and 308 K) were examined. Moreover, the pH drift method was used to determine the point of zero charge (pH_{pzc}). In the glass bottles, 40 mg of adsorbent and 80 mL of NaCl with a pH ranging from 2 to 13 were adjusted using NaOH and HCl solutions (1 and 0.1 M).

Additionally, the impact of the initial pH of the solution on PFOA adsorption capacity within the pH range of 3 to 12 was examined. The pH was adjusted by adding NaOH and HCl (0.1 and 1 M). PFOA adsorption capacity was investigated using solutions containing various salts (KCl, NaCl, $CaCl_2$, and $MgCl_2$ for cations and NaCl, Na_2CO_3, Na_2NO_3, Na_3PO_4, and Na_2SO_4 for anions). The effect of ionic strength was assessed by incorporating NaCl into the solution (as an electrolyte) at concentrations of 0, 0.001, 0.01, and 0.1 M. The batch experiments were duplicated for validation.

3.2.4.2. Fixed-bed experiment

A column with an internal diameter of 10 mm was used for the fixed bed adsorption experiments. Glass beads were packed at the top and bottom of the column, and 0.5 g of adsorbents were packed in the middle of the column (height of 5 cm) (Figure 3.2). A constant upward flow of 1.5 mL/min solution was pumped through the packed bed. A concentration of 200 µg/L of PFOA was set at the inlet of the system.

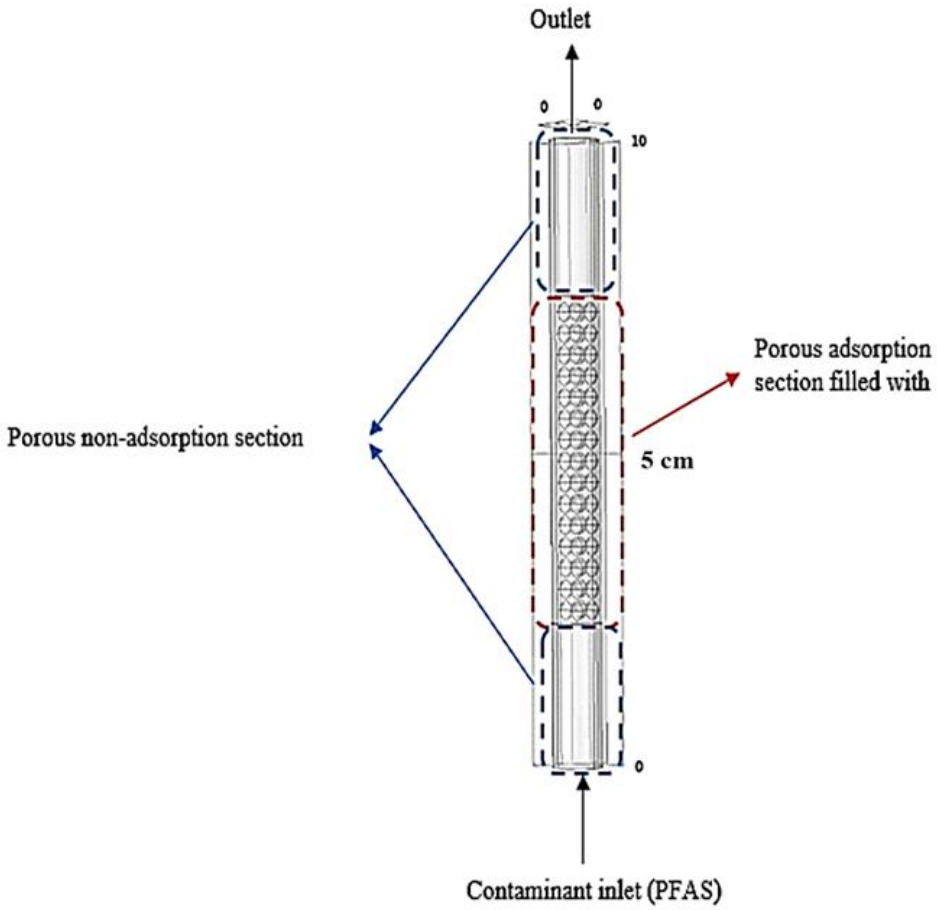

Figure 3.2. The scheme of fixed-bed adsorption column

Chapter 4.

Results and Discussion

This chapter describes the results obtained by the design of the experiment using the CCD method. The physicochemical properties of biochar adsorbents have been elucidated using the obtained results from various techniques. The following section examines the results of batch and continuous flow condition adsorption experiments conducted in water. Based on the results of the characterization and batch experiments, the final section investigates the adsorption mechanism.

4.1. CCD Optimization to prepare PBC and ZnBC

The CCD-RSM approach can facilitate the identification of optimal activation conditions, ensuring enhanced adsorption efficiency. In CCD, multiple parameters can be varied simultaneously to explore a wide range of synthesis parameters. This method allows researchers to evaluate each variable's significance and interaction. Therefore, this technique was used in this research to optimize the synthesis conditions of biochar. Adsorbents with the highest PFOA adsorption capacity were synthesized and characterized at the optimum X_1, X_2, and X_3 values. Table 4.1 provides the experimental design and comparisons of predicted and experimental PFOA adsorption efficiencies for PBC and ZnBC adsorbents.

The experiments yielded the highest adsorption removal of 368 µg/g (92%) and 336 µg/g (84%) for PBC and ZnBC at equilibrium, respectively (Table 4.1). In the case of PBC, the maximum adsorption removal percentage (92%) was achieved at microwave power settings of 600 W, 3 M of H_3PO_4, and a microwave irradiation time of 6 min. In comparison, for ZnBC, the maximum adsorption (84%) was obtained at 600 W, 0.55 M of $ZnCl_2$, and 6 min. As obtained by the standardized effects analysis, the three independent factors affected the PFOA adsorption on the PBC in the following order: X_1 (H_3PO_4 concentration, mol/L) > X_2 (Microwave time, min) > X_3 (Microwave power, W). This order for ZnBC is X_2 (Microwave time, min) > X_3 (Microwave power, W) > X_1 ($ZnCl_2$ concentration, mol/L).

It is imperative to determine the optimal synthesis conditions for biochar while considering the interdependencies of the three key parameters to maximize the PFOA adsorption capacity. When the concentration of the activation agent (X_1) is increased, more sites can be penetrated, improving the opening process of the pores. Nevertheless, excess activators can prevent the

release of volatile compounds and block the biochar pores, negatively impacting the biochar properties. Also, porosity can be enhanced by increasing the devolatilization rate of biomass by increasing the microwave heating time (X_2) [66]. It is important to note that there is a risk of widening or destroying pores when long-term exposure to microwave radiation occurs. As microwave power (X_3) increases, a stronger reaction between the biomass and activation agent can occur, improving the biochar porosity. However, high microwave power can damage the pores of the biochar [40].

Quadratic polynomial equations, tables of analysis of variance data (ANOVA), surface plots for the combined effect of independent factors on PFOA adsorption PBC and ZnBC adsorbents, and Pareto chart of standardized effects on the PFOA adsorption by PBC and ZnBC adsorbents have been presented as CCD Analysis Data in Appendix A. A quadratic polynomial equation represents the relationship between the independent variables (X_1, X_2, and X_3) and the model response (PFOA adsorption removal %) for PBC and ZnBC adsorbents. In Appendix A, Pareto charts and surface plots demonstrate how these variables interact to affect adsorption efficiency. Based on the F values and low p-values, the models are highly significant and accurately describe the relationships. As a result, the R^2 values of 0.94 for PBC and 0.97 for ZnBC indicate strong correlations, indicating that the models can accurately predict the percentages of PFOA removed. In addition to demonstrating the effectiveness of the CCD-RSM approach in optimizing synthesis conditions, these findings also guide optimizing biochar's capacity to adsorb PFOA, thus making a valuable contribution to environmental remediation.

Table 4.1. Central composite design (CCD) (X_1: H_3PO_4 concentration (mol/L), X_2: microwave time (min), and X_3: microwave power (W), η_e: experimental adsorption efficiency, η_p: predicted adsorption efficiency) and obtained experimental and predicted results for PFOA adsorption capacity at PFOA concentration of 200 µg/L, adsorbent dosage of 0.5 g/L, and temperature of 25 °C.

H_3PO_4						**$ZnCl_2$**					
Run	X_1	X_2	X_3	η_e%	η_p%	Run	X_1	X_2	X_3	η_e%	η_p%
1	3	6	600	92	90	1	0.55	6	600	84	82
2	3	6	600	90	90	2	0.55	6	600	81	82
3	6.4	6	600	75	69	3	0	6	600	3	17
4	3	6	600	87	90	4	0.55	6	1000	62	67
5	3	6	100	3	8	5	0.1	9	900	65	65
6	1	3	900	38	32	6	1	3	900	26	33
7	3	11	600	70	66	7	1.3	6	600	59	54
8	0	6	600	5	12	8	1	9	900	77	81
9	5	3	300	22	26	9	1	3	300	18	21
10	1	9	900	80	70	10	0.55	1	600	5	7
11	3	1	600	2	16	11	0.1	9	300	19	12
12	3	6	600	90	90	12	0.1	3	900	28	22
13	5	3	900	66	56	13	0.55	6	600	79	82
14	3	6	600	91	90	14	0.55	6	600	83	82
15	3	6	600	88	90	15	0.55	11	600	70	63
16	5	9	300	50	48	16	0.1	3	300	1	0
17	5	9	900	77	88	17	0.55	6	600	83	82
18	3	6	1000	72	78	18	1	9	300	35	44
19	1	3	300	3	0	19	0.55	6	600	80	82
20	1	9	300	12	15	20	0.55	6	100	8	11

4.2. Characterization of UBC, PBC, and ZnBC

4.2.1. SEM, elemental mapping, and EDX analysis

SEM images (Figure 4.1) illustrate the effect of chemical treatment and microwave-assisted pyrolysis on the structure of RCS. Moreover, these images show that the surface morphology of synthesized biochar has changed after modification by activators. As shown in Figure 4.1a, the RCS had a relatively smooth surface, and, as a result of pyrolysis, the fibres underwent expansion and opening, leading to the formation of micro-, mesopores fibres (Figure 4.1b) . The activation by H_3PO_4 facilitates the dehydration and release of volatile matter during

the pyrolysis process, resulting in more pores formation (Figure 4.1c). As a result of the interaction between H_3PO_4 and the biochar's chemical functional groups, phosphate links act as bridges between different carbon structures. Due to these interactions, more pores are created within the biochar structure. Additional bonding sites and connections are created by introducing phosphate groups into the carbon matrix, forming micropores and mesopores [67]. This abundant porous carbon material provided an excellent specific surface area and more adsorption sites to contact PFOA. It was also reported that H_3PO_4 activation could produce –C–P–C– linkages and pyrophosphate to improve the stability of the carbon structure [68].

$ZnCl_2$ can penetrate lignocellulosic biomass materials utilizing its chemical interaction with cellulose, allowing it to dissolve this organic compound and create microscopic pores. Due to its exceptionally high boiling point (732 °C), $ZnCl_2$ remains liquid throughout the carbonization process. As a result, it serves as a robust framework that provides crucial support for the subsequent carbon structure [44]. During this process, a significant percentage of fragments melt, and cell walls are destroyed, forming an extensive porous structure (Figure 4.1d).

Based on the elemental mapping analysis in Figure 4.2, the elements (C, O, P, and Zn) were distributed uniformly and evenly across the surface of the biochar, thereby improving its potential function as an adsorbent. The results of biochar molecular characteristics and composition show that chemical pretreatment and pyrolysis conditions can significantly influence the properties of biochar.

As seen from EDS peaks (Figure 4.3), UBC has a high H/C ratio, indicating a more significant presence of aromatic structures than other adsorbents [69]. Also, the presence of phosphorous and zinc elements in the PBC and ZnBC adsorbents was confirmed by EDS analysis (Figures 4.3c and 4.3d). A higher O/C ratio for PBC indicates more oxygen-containing chemical functional groups, enhancing the hydrophilicity and positively affecting the electrostatic attraction between an acid group of PFOA and these adsorbents [61,62]. PBC possesses a higher concentration of oxygen-containing functional groups than the ZnBC.

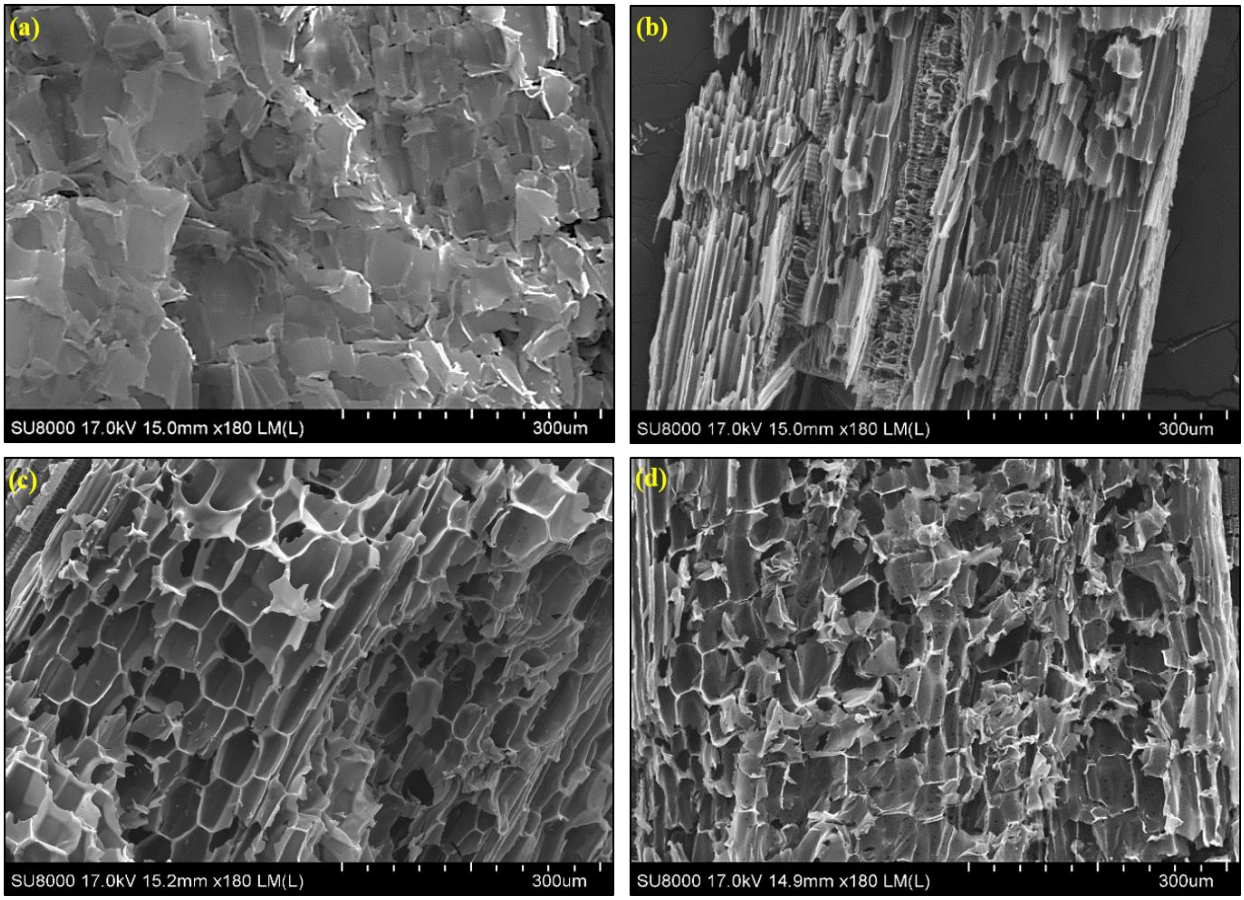

Figure 4.1. SEM images (300 μm) of (a) RCS, (b) UBC, (c) PBC, and (d) ZnBC

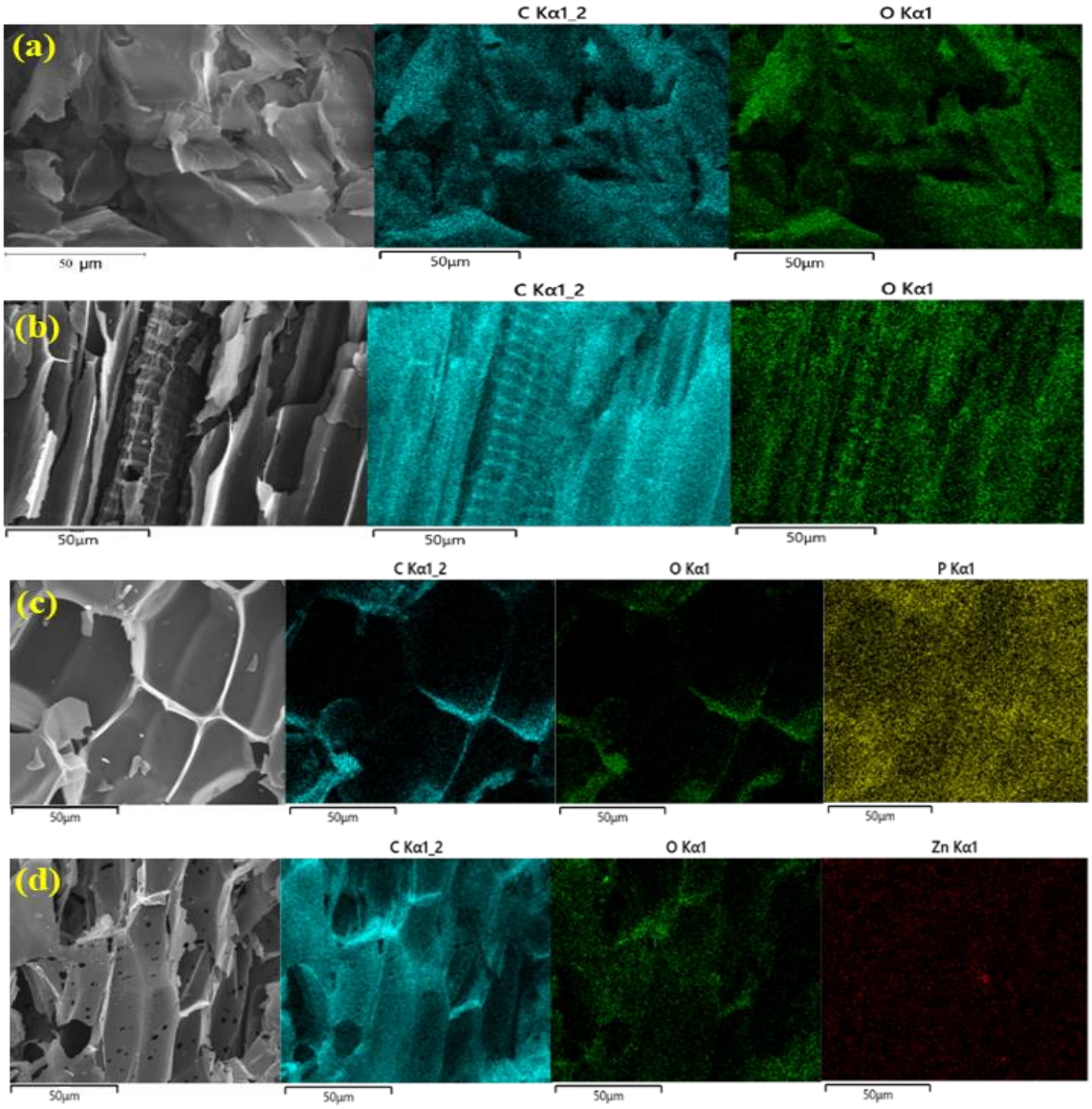

Figure 4.2. SEM images (50 µm) and elemental mapping analysis of (a) RCS, (b) UBC, (c) PBC, and (d) ZnBC.

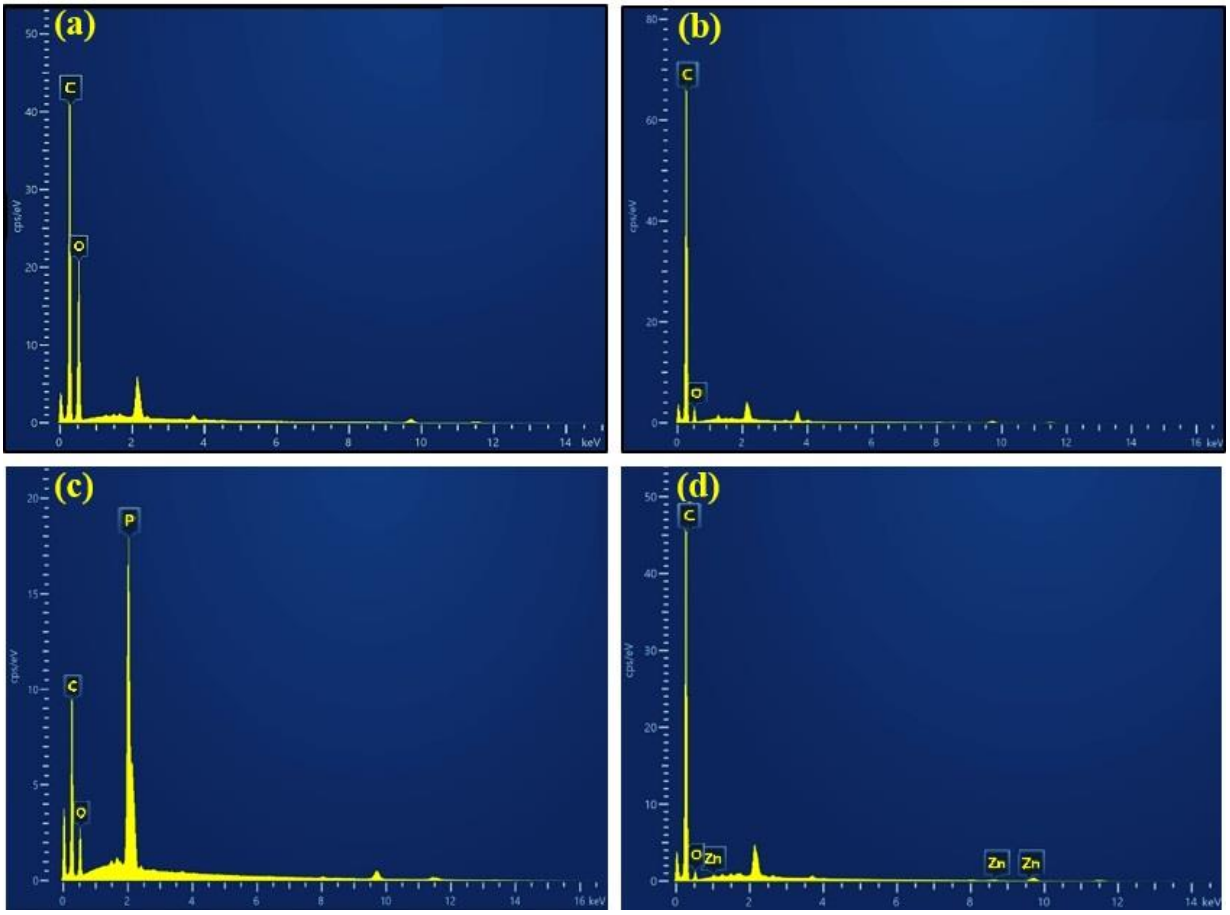

Figure 4.3. EDS analysis of (a) RCS, (b) UBC, (c) PBC, and (d) ZnBC.

4.2.2. BET analysis

The BET analysis also confirmed the effectiveness of the pyrolysis process in the presence of activators. The BET data demonstrated that PBC and ZnBC have 1,067 and 982 m^2/g of specific surface area, respectively, compared to UBC and RCS, with 17 and 3 m^2/g. The activation with H_3PO_4 and $ZnCl_2$ resulted in a notable increase in the total pore volume of the biochar. A total pore volume of 0.003 cm^3/g for the RCS and 0.031 cm^3/g for the UBC increased significantly to 0.553 cm^3/g and 0.481 cm^3/g for the PBC and ZnBC, respectively. Furthermore, the average pore size of biochar reduced after activation and pyrolysis. The average pore size for RCS, UBC, PBC and ZnBC are 14, 12, 2.23 and 2.39 nm, respectively. As a result of the chemical activation process, new pores form and existing pores are modified, resulting in pore size and volume changes.

As discussed in the evolution of SEM images, H_3PO_4 acts as a dehydration agent during crosslinking reactions, including condensation and cyclization, which result in the formation of pores [72]. In the case of ZnBC, $ZnCl_2$ is responsible for swelling and catalytic hydrolysis of cellulose, playing an important role in the activation process, resulting in a higher specific surface area and porosity. Moreover, as mentioned in Section 4.2.1, $ZnCl_2$ penetrates lignocellulosic biomass due to its dissolving action on cellulose [44]. Overall, volatile compounds are released during the activation and heating processes, causing shrinkage and compaction of the biochar, resulting in a reduction in the average size of the pores. Therefore, not only can activation of biochar result in higher specific surface areas and, consequently, more adsorption sites, but it can also increase porosity, facilitating the adsorption process.

4.2.3. XRD analysis

The XRD patterns of RCS and modified biochar adsorbents have been presented in Figure 4.4. The XRD analysis of RCS confirmed the presence of cellulose, hemicellulose, and lignin, indicated by three broad peaks observed at approximately 15.6, 22.1, and 34.5 degrees [73]. The peaks at approximately 15.6° (101 plane) and 22.1° (10-10 plane) are characteristic of cellulose I, the main crystalline component of plant cell walls. Furthermore, the appearance of a peak at around 34.5° (2θ) suggests the possible presence of cellulose II, another crystalline form of cellulose, in the canola straw sample. This XRD pattern indicates a combination of both crystalline and amorphous cellulose structures in the canola straw. The sharp peaks at approximately 15.6° and 22.1° suggest the presence of crystalline cellulose. At the same time, the amorphous regions contributed by hemicellulose and lignin are expected to appear as a broader amorphous hump around 16.5°. However, due to its low intensity and overlap with other peaks, the amorphous hump might not be clearly distinguishable in the XRD pattern [65,66]. After the carbonization during pyrolysis, the XRD analysis of PBC and ZnBC reveals only a broad peak in the 17° to 27°, which is associated with the graphite crystal face and reflects the degree of graphitization during the reaction process. The activation of biochar using $ZnCl_2$ under pyrolysis conditions via microwave treatment leads to the formation of ZnO as following reactions [76]:

$$ZnCl_2 + H_2O \rightarrow Zn(OH)Cl + HCl \qquad \text{Eq. 4.1}$$

$$Zn(OH)Cl \rightarrow ZnO + HCl \qquad \text{Eq. 4.2}$$

As seen in Figure 4.4, ZnO related peaks were observed at 31.6° (1 0 0), 34.3° (0 0 2), 36.1° (1 0 1), 47.3° (1 0 2), 56.4° (1 1 0), 62.7° (1 0 3), 66.2° (2 0 0), 67.8° (1 1 2), and 68.9° (2 0 1), according to the Joint Committee on Powder Diffraction Standard (JCPDS - n° 01-075-0576) [77].

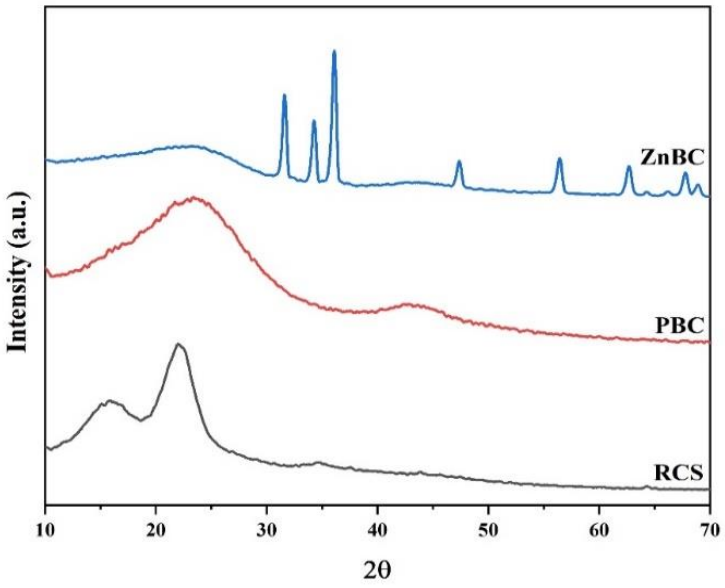

Figure 4.4. XRD analysis of RCS, PBC, and ZnBC.

4.2.4. FT-IR and Raman spectra

The FT-IR spectra of RCS, PBC, and ZnBC adsorbents are presented in Figure 4.5. These spectra illustrate the changes in chemical functional groups occurring during pyrolysis and activation. In the spectrum of RCS, a broad peak is observed at approximately 3300-3500 cm^{-1} associated with the O-H stretching vibrations of the hydroxyl group (-OH of carboxyl, alcohol or phenol), and a band at approximately 2900 cm^{-1} is related to the C-H stretching vibrations of the methyl group. The bands situated around 1600-1700 cm^{-1} are linked to aromatic C=C or conjugated C=O and 1380–1400 cm^{-1} (C–O stretching of carboxylate anion or aliphatic C–H or phenolic –OH). The spectrum also contains a peak at approximately 1050-1100 cm^{-1}, which corresponds to C-OH stretching [78].

In the PBC spectrum (Figure 4.5), a broad band between 1000 and 1400 cm^{-1} has a maximum of 1217 cm^{-1}, related to the carbons activated with phosphoric acid and oxidized carbons. Additionally, phosphorus and phosphocarbonaceous compounds exhibit absorption in

this region. Phosphoric acid ester formation caused the appearance of a band at 1203 cm^{-1}. As a result of the overlap of absorption bands from several oxygen and phosphorus compounds in this region, it is difficult to make a clear assignment. Based on the available data, subsequent phosphorus species could explain the absorption within the 1000-1300 cm^{-1} range. This signal may be related to the stretching mode of P=O in a phosphate ester, vibrations resulting from the stretching of O–C in P–O–C (aromatic) connections, and the presence of P=O(OH) groups in the phosphates or polyphosphates [70,71]. There is a difference between the FT-IR spectrum of ZnBC and PBC, which is attributed to the presence of phosphorus functional groups in PBC (1000–1300 cm^{-1}) (Figure 4.5).

As a result of FT-IR analysis of RCS, PBC, and ZnBC biochar adsorbents, significant chemical transformations were observed during the activation and pyrolysis processes. Changes in functional groups were evident in the FT-IR spectra reflected in distinct peaks and shifts, which indicated alterations in the surface chemistry of the compounds. Chemical bonds in the raw material broke, resulting in the decrease or disappearance of their related bands in the FT-IR spectra, especially the peaks associated with the O–H, C-H, C=O, C–C, and C-O groups. For example, following activation, the band at 2900 cm^{-1} disappears, indicating that hydrogen has been removed [81]. It was evident that phosphorus had been incorporated into activated samples through the presence of bands associated with phosphoric acid esters and phosphates. Therefore, the FT-IR analysis confirmed the initial hypotheses while providing specific chemical signatures contributing to a deeper understanding of biochar structural changes. Thus, variations in the adsorption capacities of adsorbents are related to the differences in surface chemistry and their distinct interactions with PFOA during the adsorption process.

By precisely engineering the graphitization process during pyrolysis, biochar characteristics can be improved to increase its adsorption efficiency. The graphitization and carbon structure of biochar can be fine-tuned using Raman spectroscopy. Displayed in Figure 4.6, the Raman spectra of PBC and ZnBC reveal noticeable peaks at 1358 cm^{-1}(D band) and 1590 cm^{-1} (G band), respectively. The occurrence of D-bands and G-bands signifies the presence of graphite and disordered carbon, respectively, indicating the process of graphitization during pyrolysis [82].

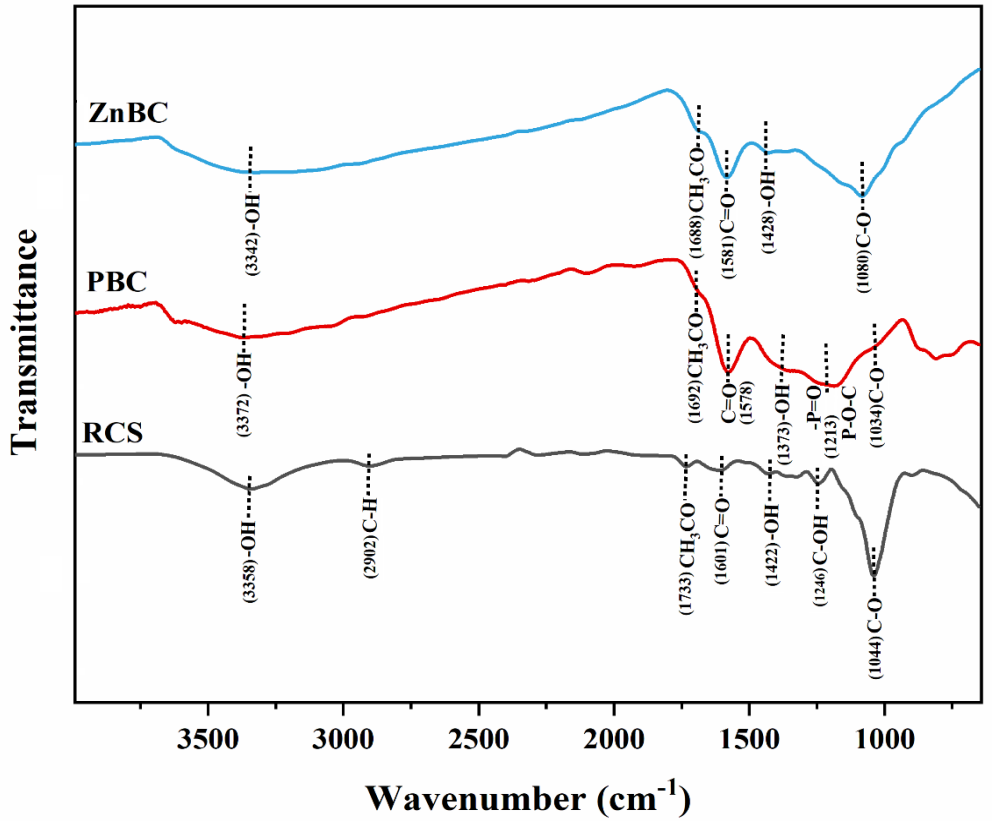

Figure 4.5. FTIR spectra of RCS, PBC and ZnBC

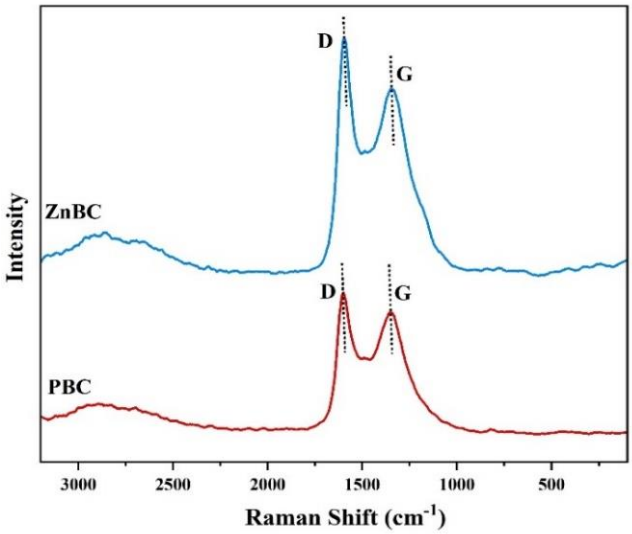

Figure 4.6. Raman spectra of PBC and ZnBC

4.2.5. XPS spectra

An XPS analysis was performed on the biochar adsorbents to determine the surface elemental bonding and composition (Figure 4.7). C, O, P, and Zn elements were identified in the spectrum of all biochar adsorbents (Figure 4.7a). The peak of F1s related to the PFOA adsorbent on the PBC and ZnBC appeared around 688 eV in Figure 4.7b.

Using the deconvolution of C1s peaks in UBC spectra (Figure 4.8a), four sub-peaks were found around 282.12, 282.60, 284.20, and 285.72 eV, related to C-C, C=C, C-O, and C=O, respectively [71]. Similar peaks for PBC (Figure 4.8b) were observed at 284.20 eV, 284.39 eV, 285.76 eV, and 287.78 eV, assigned to C-C, C=C, C-O, and C=O, respectively. A portion of the C1s spectrum of PBC contains C–P (284.80 Ev), indicating that H_3PO_4 activation allowed the P element to be incorporated onto the carbon surface. These peaks for ZnBC were about 284.52, 284.70, 285.99, and 288.70 eV, corresponding to C-C, C=C, C-O, and C=O, respectively (Figure 4.8c).

Two major peaks can be distinguished in the O1s peak of the UBC, including 528.82 and 529.80 eV, corresponding to C=O and C-O, respectively (Figure 4.9a). These peaks appear at 530.61 (C=O) and 532.31 (C-O) eV for PBC and at 530.50 (C=O) and 531.70 (C-O) for ZnBC (Figures 4.9b and 4.9c). There are three sub-peaks in the P2p spectra of PBC, including C-P=O (131.94 eV), C-P–O (133.20 eV), and C–O–P (133.89 eV) (Figure 4.10 a).

Zn2p of ZnBC shows spin orbitals of $Zn2p_{3/2}$ and $Zn2p_{1/2}$ at 1022.06 and 1045.17 eV, respectively (Figure 4.10 b) [71]. After PFOA adsorption on PBC and ZnBC, the peak of F1s appears at 688.36 and 690.21 eV, respectively (Figure 4.7b) [28]. When H_3PO_4 is used as an activator, element P on PBC is doped, and the number of acidic functional groups increases. As a result of the H_3PO_4 treatment of biochar, the proportion of C=O functional groups increased from 4.33% in UBC to 16.91% in PBC in C1s spectra (Figures 4.8a and b) and from 13.97% in UBC to 33.17% in PBC in O1s spectra (Figures 4.9a and b). Furthermore, $ZnCl_2$ modification increased the proportion of C=O functional groups in C1s spectra from 4.33% in UBC to 11.83% in ZnBC (Figures 4.8a and c) and in O1s spectra from 13.97% in UBC to 26.78% in ZnBC (Figures 4.9a and c).

Based on the observed changes in functional groups and elemental composition, activation and modification processes impact the surface chemistry of biochar adsorbents and, consequently, improve their PFOA adsorption capacities.

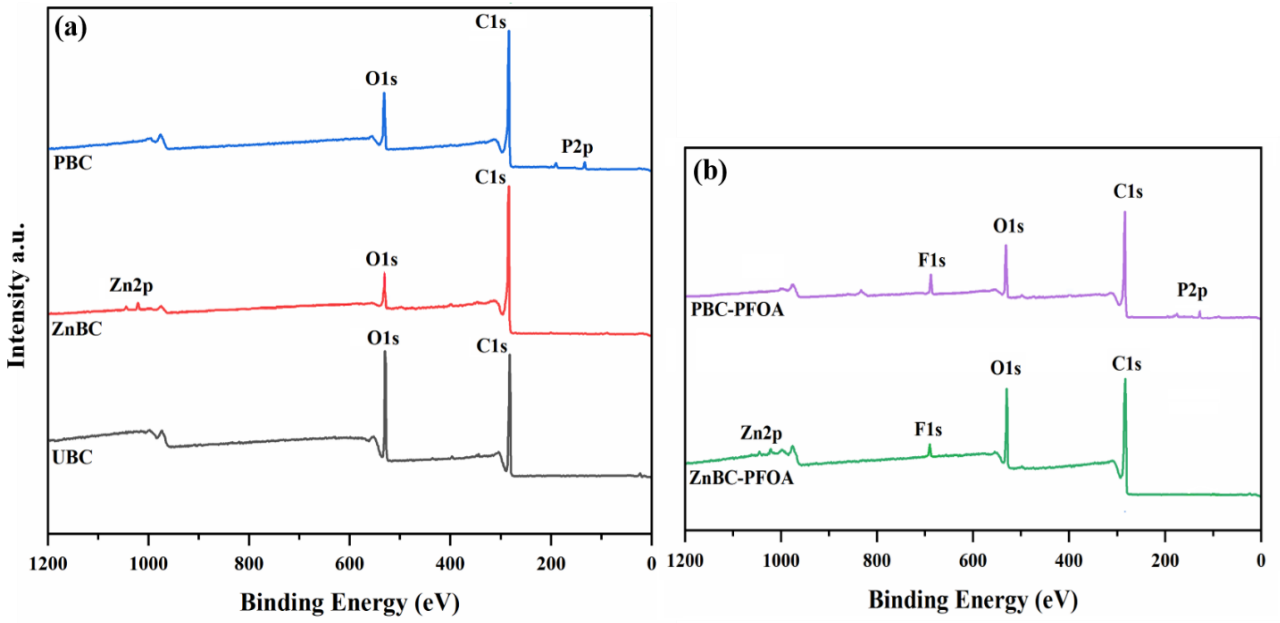

Figure 4.7. XPS spectra of (a) UBC, ZnBC, and PBC before PFOA adsorption and, (b) PBC and ZnBC after PFOA adsorption

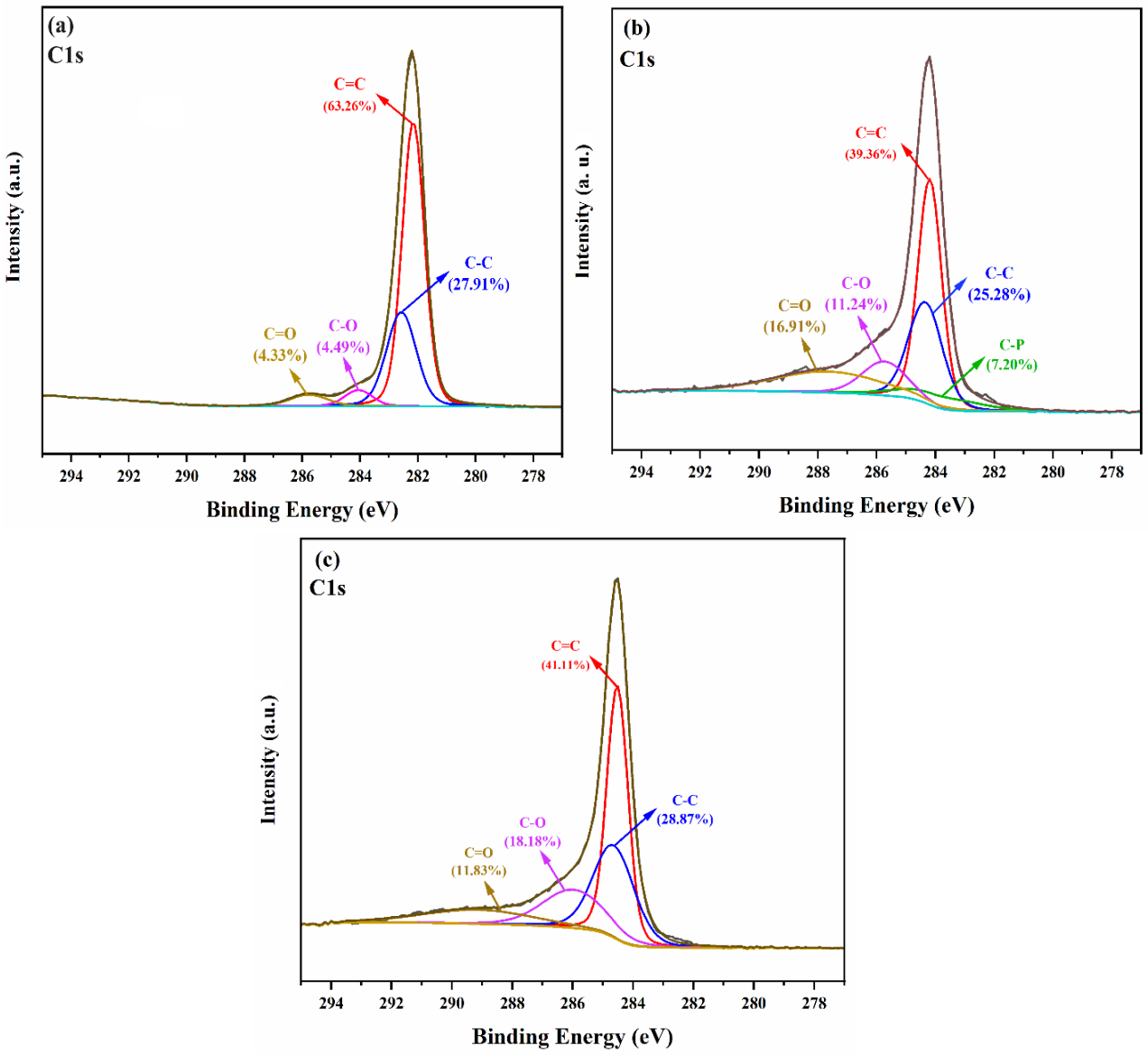

Figure 4.8. High resolution C1s XPS of (a) UBC, (b) PBC, and (c) ZnBC

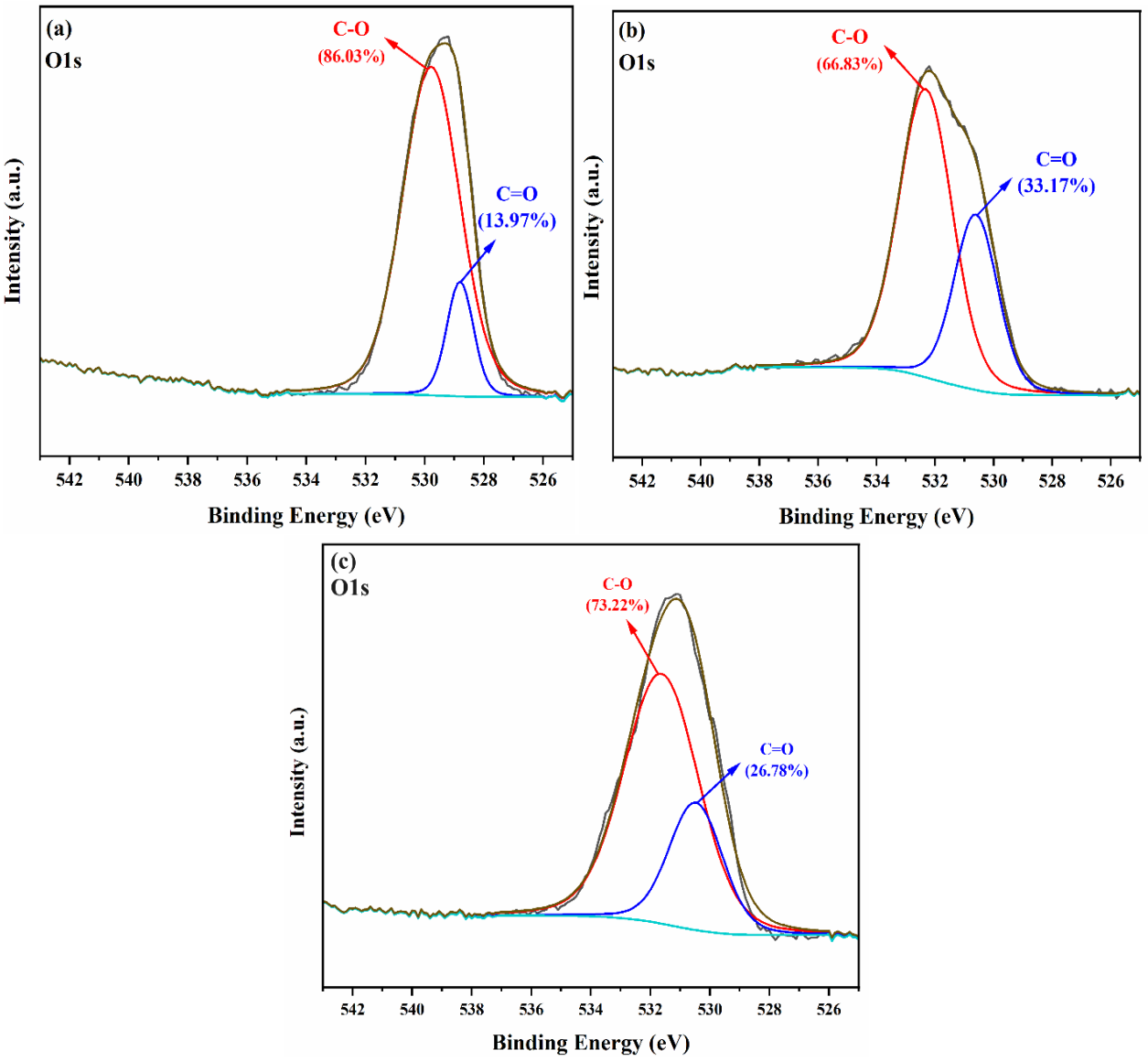

Figure 4.9. High resolution O1s XPS of (a) UBC, (b) PBC, and (c) ZnBC

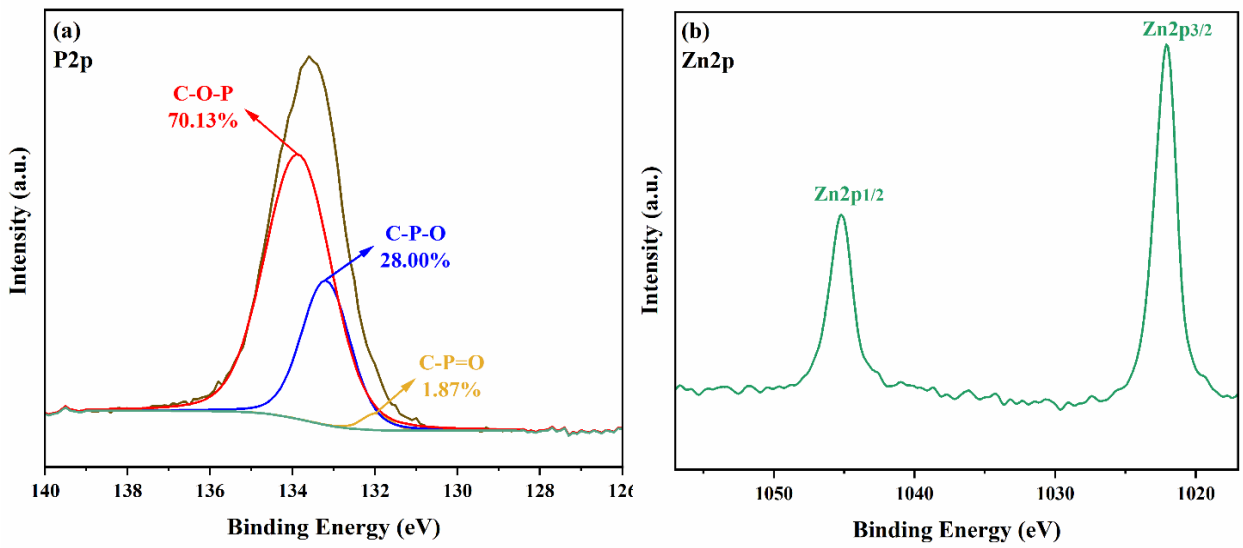

Figure 4.10. High resolution XPS of (a) PBC: P2p, and (b) ZnBC: Zn2p

4.3. Adsorption experiments

4.3.1. Adsorbent dosage and PFOA concentration

Firstly, batch experiments were conducted to find the most effective dosage of the adsorbent. The samples were prepared with different adsorbent dosages (0.25, 0.50, 1.00, and 1.25 g/L) and then exposed to various concentrations of PFOA (100, 200, 500, 1,000, and 10,000 µg/L) for 24 h at 25 °C (Figure 4.11a). PFOA adsorption efficiency for PBC decreases at higher PFOA concentrations because of the limited capacity of adsorbents to remove contaminants.

The performance of chemically treated biochar adsorbents (PBC and ZnBC) was compared with that of AC (as the most common adsorbent for PFOA), UBC, and RCS adsorbents (Figure 4.11b) at 200 µg/L of PFOA. This concentration was determined based on the limitation of LC-MS/MS to detect PFOA (10 g/L) and the MAC of PFOA. Adsorbents reached equilibrium in the absorption of PFOA within 10 h, with a PFOA adsorption efficiency exceeding 90% (see section 4.3.2). Thus, all subsequent adsorption experiments were conducted over 10 h. Batch testing results indicate that PFOA removal efficiencies for PBC and ZnBC were 92% and 84%, respectively, compared to 5% for UBC and 1% for RCS for 10 h at 25 °C. In similar conditions, AC exhibits an adsorption efficiency of 94%.

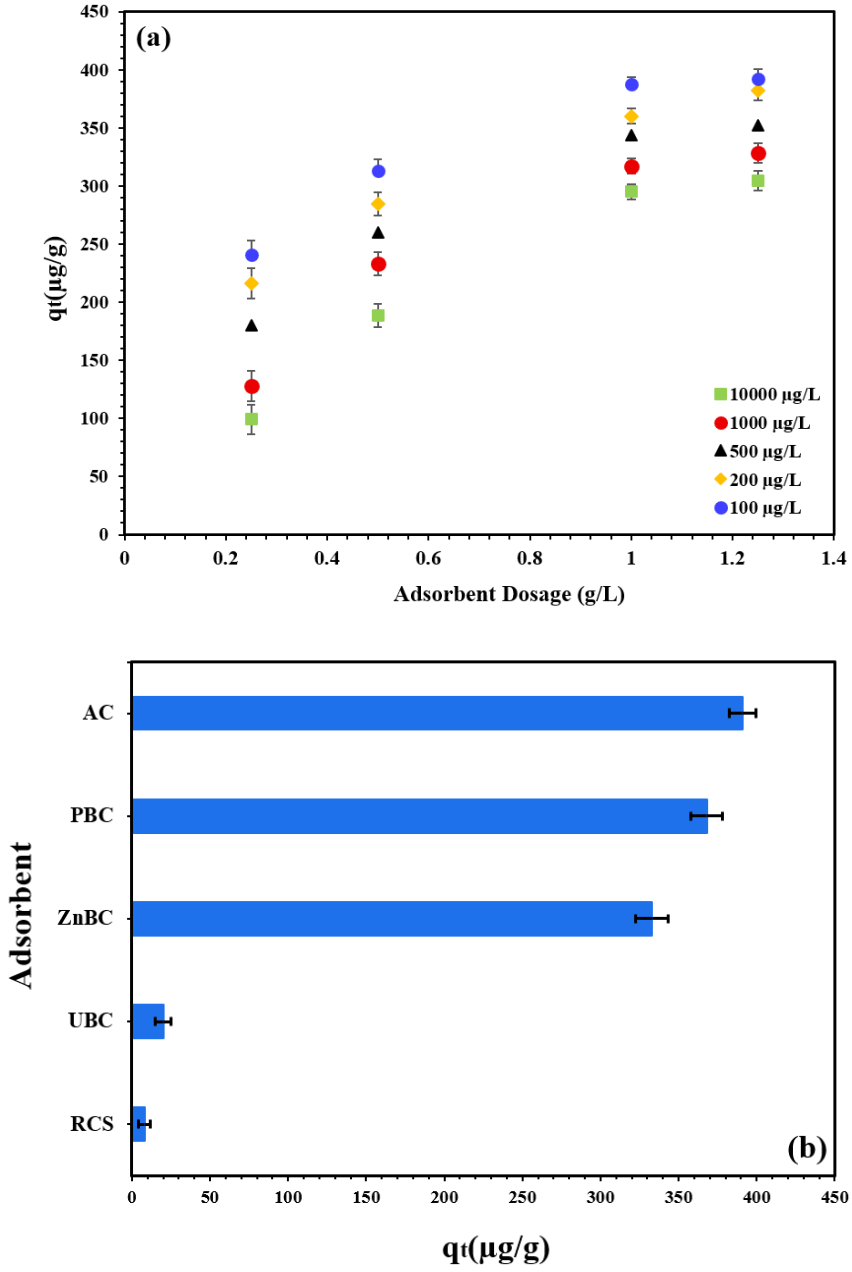

Figure 4.11. (a) Effect of adsorbent dosage on PFOA adsorption in different concentration of PFOA, and (b) PFOA removal efficiencies of different adsorbents with contact time of 10 h at 25 °C. Note error bars are standard deviations with n=3.

4.3.2. Determination of equilibrium time and adsorption kinetic

As shown in Figure 4.12, the PBC and ZnBC absorbed PFOA rapidly within the first five hours (PFOA adsorption efficiency >70 %), followed by equilibrium within 10 h (PFOA adsorption efficiency >90 %). An initial fast adsorption stage indicates that PFOA molecules from the liquid phase are rapidly moving and binding to the surface of the adsorbent material. The pseudo-first-order and pseudo-second-order models were more accurate in modelling PFOA adsorption data onto PBC and ZnBC adsorbents as indicated by higher correlation coefficients of R^2_{PFO}=0.922 and R^2_{PSO}=0.995 for PBC, R^2_{PFO}=0.929 and R^2_{PSO}=0.998 for ZnBC (Table 4.2). The pseudo-second order model best fits with data given higher R^2 values. In this model, chemical adsorption or chemisorption is assumed as the rate-limiting step. Therefore, based on the obtained kinetic results, the chemisorption of PFOA is the most important step in the adsorption process because of electron exchange and sharing between PFOA and chemical functional groups on the adsorbent [75,76]. Several chemical processes are involved in the PFOA adsorption process: electron sharing, electron exchange, and surface complexation [84]. Similar results have been reported by Lei et al. (2022), indicating that the pseudo-second-order kinetic model provided a better fit to the experimental data for PFOA adsorption on mesoporous carbon [85]. In addition, Militao et al. demonstrated that PFOS adsorption on a rice straw-derived biochar had the best fit with the pseudo-second-order kinetic model (R^2 of 0.999) [86].

Kinetic and characterization results indicate that chemical activators significantly increased the number of active sites on the biochar surface by increasing surface area, porosity and chemical functional groups, enhancing the chemical interaction between the surface heteroatoms and PFOA molecules involving the chemisorption. This, in turn, leads to improved adsorption capacity and facilitates the overall adsorption process [75,5].

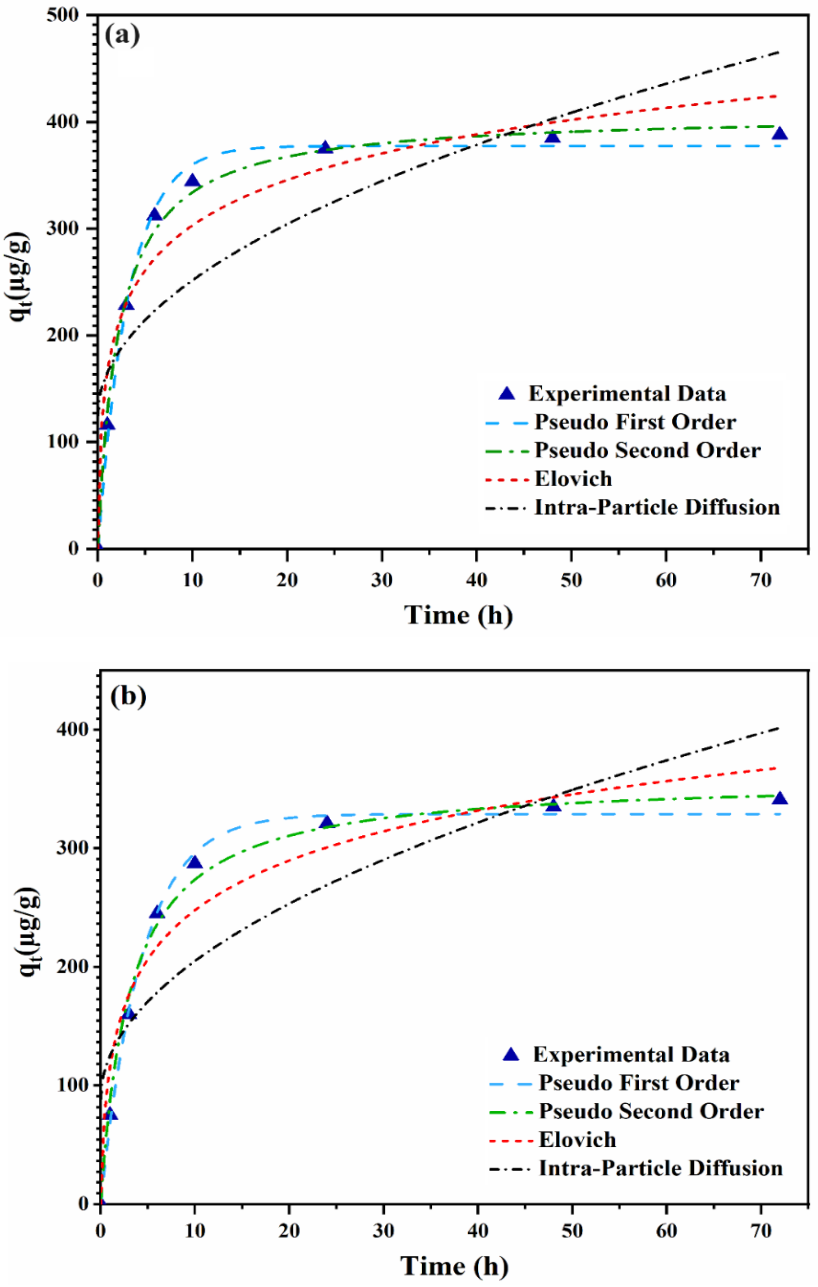

Figure 4.12. Adsorption kinetics of PFOA on PBC (a) and ZnBC (b) (adsorbent dosage=0.5 g/L; PFOA initial concentration=200 μg/L; temperature=25 °C)

Table 4.2. Kinetic models, equations, and calculated parameters

Model	PBC	ZnBC
Pseudo-first order	k_{pfo}= 0.307 (1/h)	k_{pfo}= 0.230 (1/h)
$q_t = q_e\ (1-exp(-k_{pfo}t))$	q_e=378 (µg/g)	q_e=329 (µg/g)
	R^2=0.922	R^2=0.929
	RSS=722	RSS=1129
Pseudo- second order	k_{pso}=0.0011 (g/µg.h)	k_{pso}=8.87×10^{-4} (g/µg.h)
$\frac{t}{q_t} = \frac{1}{k_{pso}q_e^2} + \left(\frac{1}{q_e}\right)$	q_e = 408 (µg/g)	q_e = 359 (µg/g)
	R^2=0.995	R^2=0.998
	RSS=548	RSS=445
Elovich	a=833 (µg/g.h)	a=342 (µg/g.h)
$q_t = \frac{1}{b} ln(1 + abt)$	b= 0.0162 (g/µg)	b= 0.0163 (g/µg)
	R^2=0.851	R^2=0.838
	RSS=7558	RSS=6900
Intra- particle diffusion	k_p=40.191(µg/g.$h^{0.5}$)	k_p=36.932(µg/g.$h^{0.5}$)
$q_t = k_p t^{0.5} + C$	C = 124.55 (µg/g)	C = 88.08 (µg/g)
	R^2=0.637	R^2=0.684
	RSS=44695	RSS=31036

4.3.3. Adsorption isotherms

Adsorption isotherms were studied to understand the adsorption mechanisms and the interaction between PFOA and adsorbents at equilibrium (Figure 4.13). Freundlich, Langmuir, and Temkin isotherm models were used to fit the PFAS adsorption isotherm data. These models are commonly used in studying PFAS adsorption on carbon-based materials. In the Langmuir model, PFOA adsorption is assumed to occur on homogeneous active sites on the biochar adsorbents. This leads to monolayer adsorption because each site can accommodate only one molecule. Alternatively, the Freundlich isotherm model predicts a heterogeneous adsorbent surface with a non-uniform energy distribution, resulting in multilayer adsorption. A Temkin model differs from a Langmuir or Freundlich model; it considers that the adsorption energy decreases linearly as surface coverage increases. This model is suitable for chemisorption, which is characterized by electrostatic interactions [54].

As a result of isotherm adsorption experiments performed on PBC, the adsorption capacity of PFOA increased from 99 to 340 µg/g when the PFOA concentration was varied between 50 and 300 µg/L, and the adsorption capacity of ZnBC increased from 96 to 322 µg/g. The Freundlich model performs well in modelling experimental data for both PBC and ZnBC adsorbents with R^2 = 0.990 and 0.965, respectively, in contrast to the Langmuir model with R^2 = 0.932 for PBC and R^2 = 0.921 for ZnBC. According to Lei et al., PFOA anions can form micelles on the surface of a mesoporous carbon adsorbent via hydrophobic interactions, which could lead to a multilayer adsorption process [87].

Based on the calculated results in Table 4.3, a multilayer (Freundlich) adsorption mechanism resembles the adsorption behaviour of modified biochar adsorbents. PFOA can be bound more diversely by PBC due to its more significant number of acid groups. Because of the heterogeneity of the adsorption sites, the adsorbent is capable of accommodating multilayer adsorption, which Freundlich model can adequately describe. Hydrophobic interactions between PFOA and PFOA have also characterized multilayer adsorption of PFAS through the formation of micelles and hemi-micelles (self-assembly of the hydrophobic part of PFOA) [89]. PFOA anions can form micelles on the surface of a mesoporous carbon adsorbent via hydrophobic interactions, which could lead to a multilayer adsorption process [87]. In a similar study by Militao, Freundlich model was shown to fit the experimental data better with the PFOA adsorption on rice straw-derived biochar [31]. Further, Hassan et al. demonstrated in 2022 that the isothermal data of PFOA adsorption on magnetic biochar had a better fit using Freundlich model, demonstrating a multilayer adsorption process [88].

Based on the obtained R^2, the data was also well fitted to the Temkin equilibrium model for both modified biochar adsorbents, indicating that the electrostatic interaction is the dominant mechanism involved in the adsorption of PFAS onto PBC and ZnBC [90]. Zhang et al. explained that PFOS adsorption on hydrous ferric oxide is related to the Temkin model, in which a chemical adsorption process occurs due to electrostatic interactions [91]. Chemisorption primarily occurs between the chemical functional groups in PFAS and modified adsorbents (Figure 4.14a). Then, owing to PFAS amphiphilic nature, it forms complex aggregated structures, such as micelles and bilayers (Figure 4.14b). Through strategic modifications involving the introduction of phosphorus, zinc, and additional functional groups into biochar, its

ability to interact with PFOA is enhanced. This intentional improvement results in the formation of more chemical bonds, leading to a more extensive aggregation of PFOA.

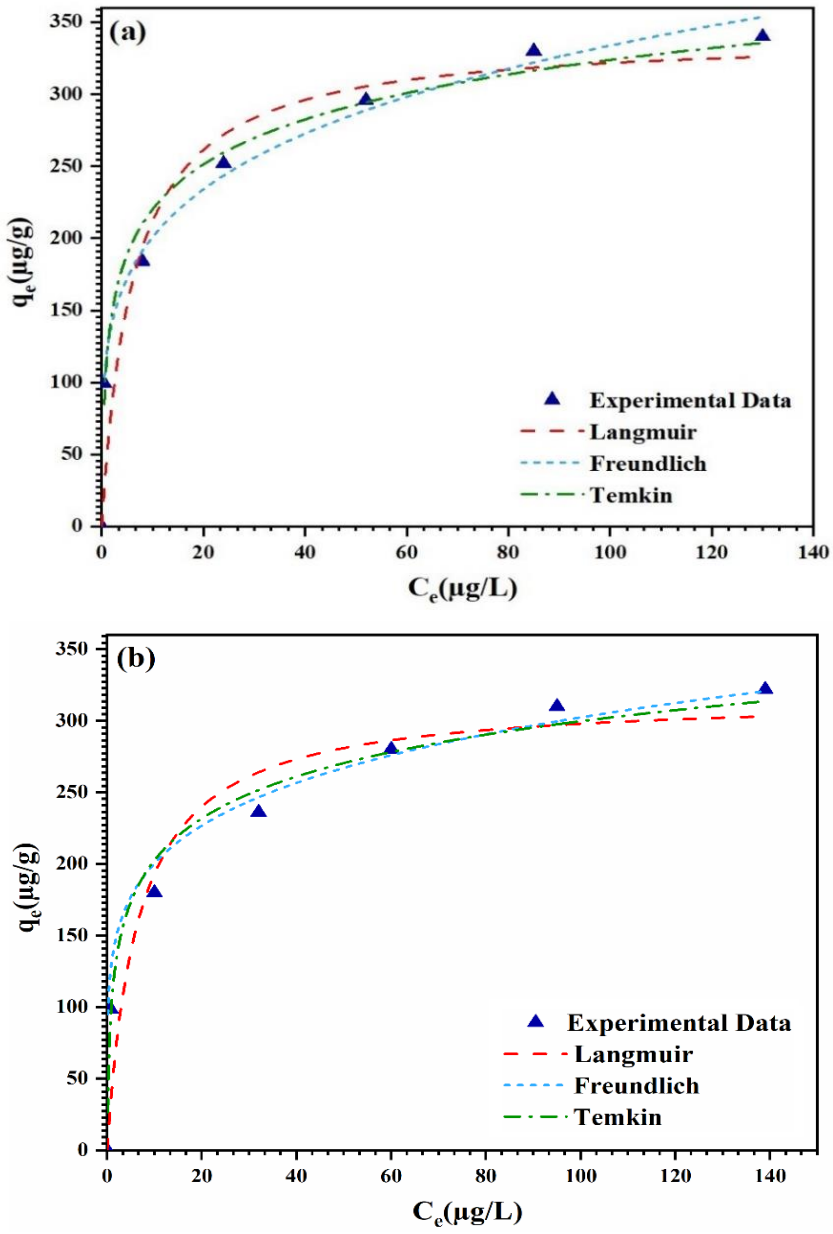

Figure 4.13. Adsorption isotherms of PFOA on PBC (a) and ZnBC (b) (adsorbent dosage=0.5 g/L; temperature=25 °C; contact time=10h)

Table 4.3. Isotherm models, equations, and calculated parameters

Model	PBC	ZnBC
Langmuir $q_e = \frac{K_L q_{max} C_e}{1 + K_L C_e}$	q_{max}=341 (µg/g)	q_{max}=317 (µg/g)
	K_L=0.1635 (L/µg)	K_L=0.1555 (L/µg)
	R^2=0.932	R^2=0.921
	RSS=	RSS=
Freundlich $q_e = K_F C_e^{1/n}$	K_F=120.75(µg/g)(L/µg)$^{1/n}$	K_F=132.56 (µg/g)(L/µg)$^{1/n}$
	n = 4.525	n = 5.587
	R^2=0.990	R^2=0.965
	RSS=	RSS=6075
Temkin $q_e = \frac{RT}{b_T} ln(K_T C_e)$	K_T=13.180 (L/µg)	K_T=12.08 (L/µg)
	b_T= 54.99	b_T= 58.70
	R^2=0.988	R^2=0.981
	RSS=	RSS=32391

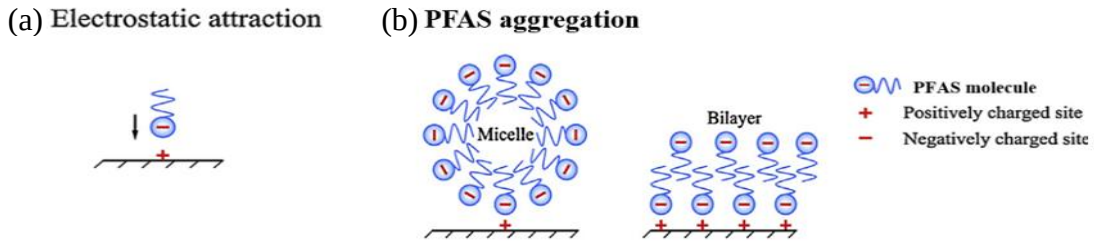

Figure 4.14. Electrostatic attraction (chemisorption) (a) and PFAS aggregation (b) on the biochar (adapted from Du et al. [29])

4.3.4. Adsorption thermodynamic

The PFOA adsorption mechanism on PBC and ZnBC was also examined at different temperatures (281, 288, 298 and 308 K) through batch adsorption experiments. Figure 4.15 illustrates the temperature-dependent adsorption capacities of PBC and ZnBC adsorbents to remove PFOA. Additionally, Figure 4.16 includes the thermodynamic values (ΔH°, ΔG°, and ΔS°) which were calculated using the van't Hoff equation [58].

When the temperature decreased from 308 K to 298 K, the adsorption capacity of PBC for PFOA reduced from 384 µg/g to 242 µg/g. A reduction from 366 µg/g to 214 µg/g was also

observed for ZnBC when the temperature was changed similarly. Since the calculated ΔG° is negative, it indicates that PFOA adsorption onto the PBC surface is spontaneous and thermodynamically favourable. As the adsorption capacity of PFOA on PBC and ZnBC reduces with decreasing temperature, it is apparent that the adsorption process is endothermic. Additionally, enthalpy determines adsorption mechanisms. The enthalpy values of 72.20 kJ/mol for PBC and 74.22 kJ/mol for ZnBC are acceptable for chemisorption in adsorption. Positive values for ΔH° confirmed that the process is endothermic in nature, which supports that the process is chemisorption and provides the driving force for governing the ΔG° for the process. Wu et al. studied the removal of PFAS from water using biochar made from switchgrass and water oak leaves. The authors described an endothermic process based on the enthalpy value [28].

PFOA has chemical interactions with PBC or ZnBC by breaking existing weak intermolecular bonds (hydrogen bonds, van der Waals forces, or other non-covalent interactions) between biochar and PFOA and forming some new stronger chemical bonds (electrostatic attraction like ionic and dative bonds). This process requires energy input, leading to an endothermic process. A chemisorption reaction involves strong chemical bonds and is endothermic due to heat absorption. A positive ΔS° value indicates an increase in system randomness during adsorption. A disordered state results from molecules reorienting and becoming more mobile on the adsorbent surface. The biochar has an affinity for adsorbing PFOA during the adsorption process. So, PFOA adsorption on PBC and ZnBC surfaces can disrupt the reorientation of water molecules, increasing the randomness at the surface. Entropy also increases because of the rearrangement of solvent molecules at the interface between PFOA and modified biochar. Furthermore, the formation of hydration shells or changes in the solvation structure impacts the entropy during PFOA adsorption.

A study conducted by Salawu in 2022 found that the adsorption of ciprofloxacin and long-chain PFAS on porous carbon has a positive ΔS. This is attributed to an escalation in randomness and increased freedom at the interface between the adsorbent and adsorbate molecules [92]. Additionally, Jian et al. reported an increase in entropy following the adsorption of PFOS on nanosized alumina. As a result of replacing adsorbed water molecules with PFOS, randomness increased. The authors mentioned that this process would increase the translational entropy of the displaced water molecules, allowing a greater degree of randomness in the system [64].

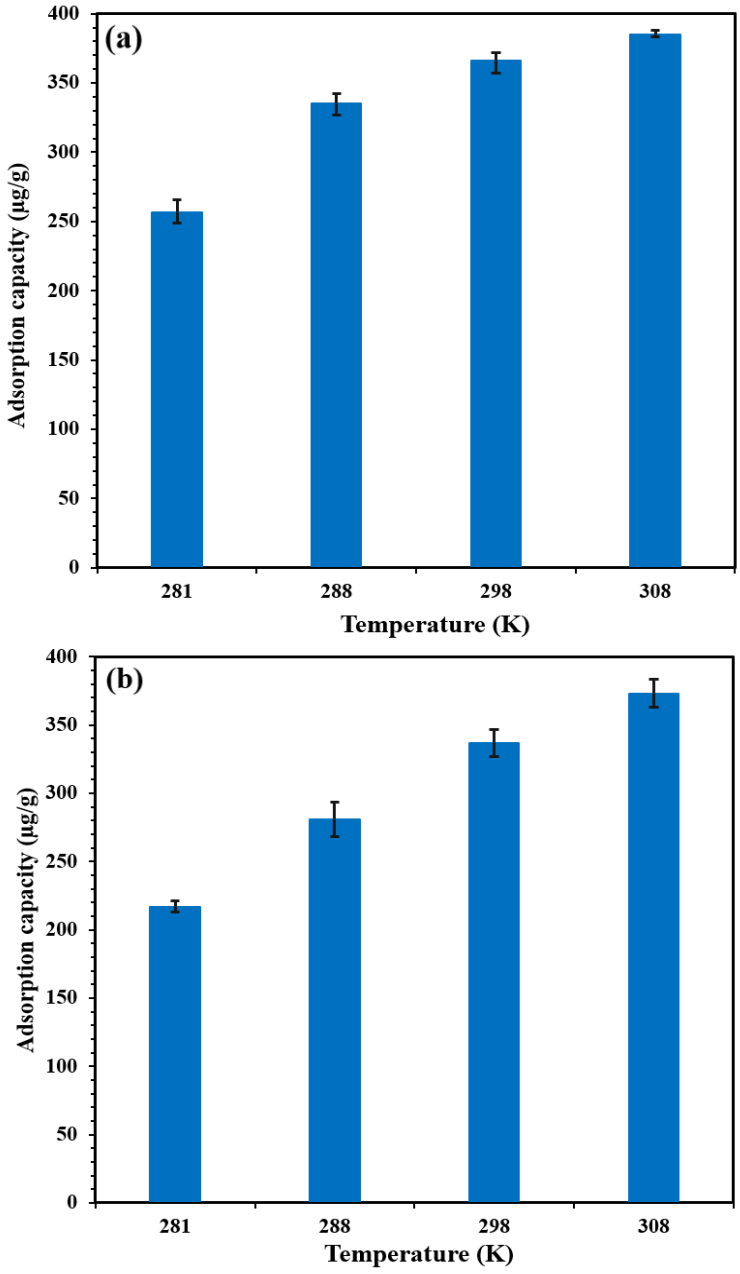

Figure 4.15. The effect of temperature on PFOA adsorption capacity for PBC (a) and ZnBC (b) (adsorbent dosage=0.5 g/L; PFOA initial concentration=200 µg/L; contact time=10h). Note error bars are standard deviations with n=3.

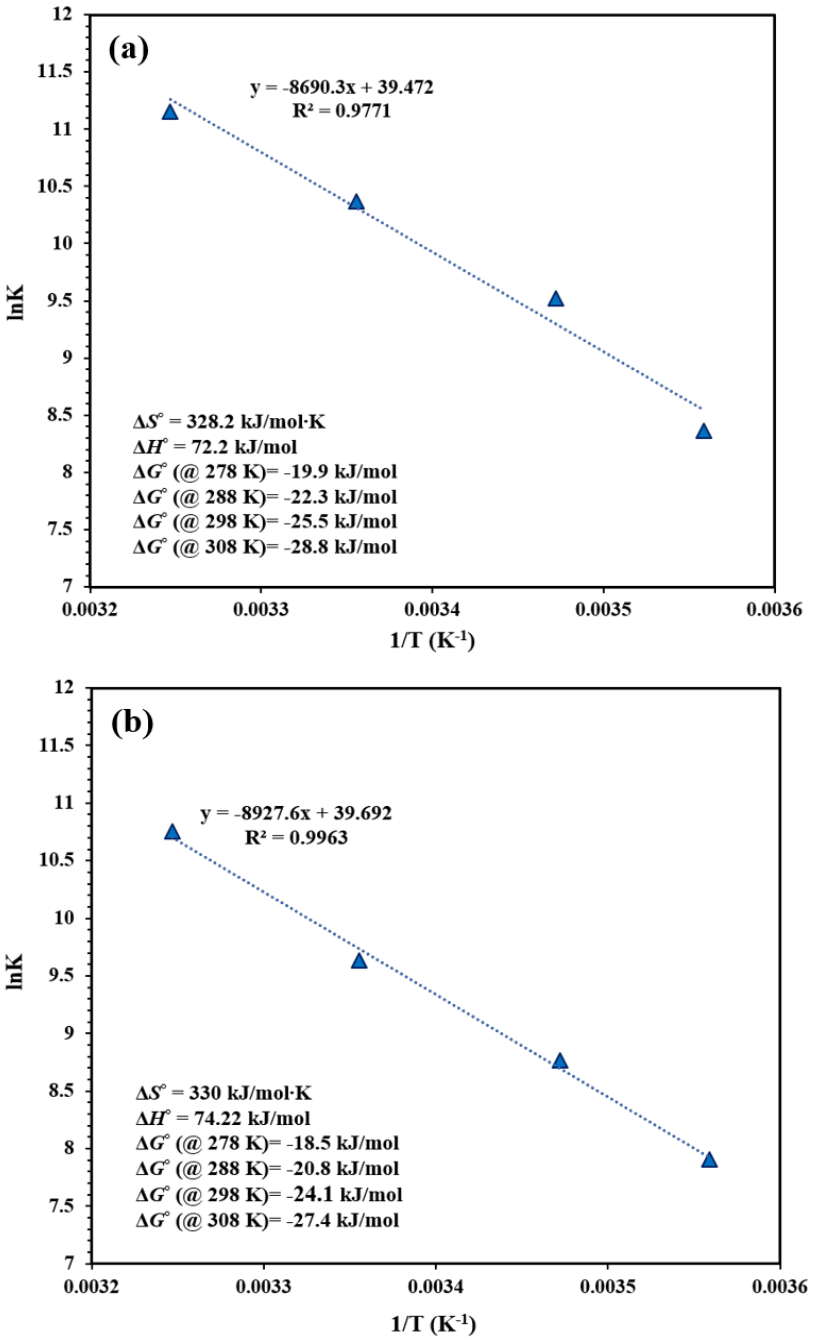

Figure 4.16. Plot of lnK vs. 1/T (K^{-1}) for calculation of thermodynamic parameters for the adsorption of PFOA onto PBC (a) and ZnBC (b) (adsorbent dosage=0.5 g/L; PFOA initial concentration=200 µg/L; contact time=10h)

4.3.5. Evaluating the influence of pH

PFOA molecules are generally found in deprotonated form (anions) in aqueous solutions due to pK_a of 2.8 [93]. ZnBC contains fewer oxygen-containing groups than PBC, especially acid groups, so, its pH_{pzc} is higher than PBC, meaning they have different surface chemistry at various pH levels to remove PFOA in water. pH_{pzc} values are 3.65 and 6.08 for PBC and ZnBC, respectively (Figure 4.17a). The adsorbent surface carries a positive charge when the pH of the solution is less than pH_{pzc}. This facilitates the removal of anions from the solution by electrostatic attraction forces. Adsorbent surfaces become negatively charged in pH regions above pH_{pzc}, resulting in electrostatic repulsion between adsorbent and PFOA anions. In this case, PFOA molecules (with no charge) and positively charged PFOA molecules (resulting from dissociating of a hydrogen ion) will be more likely to be attracted to the adsorbent surface. Additionally, the hydrophobic interactions between the alkyl branches or/and aromatic parts of biochar and the alkyl tails of PFAS may also contribute to the adsorption of PFOA under this condition [94].

Figure 4.17b illustrates the effect of pH on the PFOA adsorption capacity of modified biochar adsorbents. For ZnBC, PFOA adsorption decreased continuously as pH increased from 7 to 12, whereas this reduction occurred when pH increased from 8 to 13 for PBC. PBC has more positive charges because of more acid functional groups (based on the FT-IR analysis) than ZnBC. PBC shows a higher adsorption capacity at lower pH values (between 3 and 9) because of more electrostatic attraction between PBC and PFOA anions. As the pH of the solution increases, the surface charge of the biochar changes. When pH levels rise, the biochar surface becomes negatively charged, resulting in electrostatic repulsion between the anion form of PFOA in water and the negatively charged surface of biochar. PFOA anions are pushed away from the surface of adsorbents by this electrostatic repulsion, reducing the PFOA adsorption capacity. PBC exhibits this effect more strongly than ZnBC in higher pH conditions because its positive surface can attract more hydroxide ions [87].

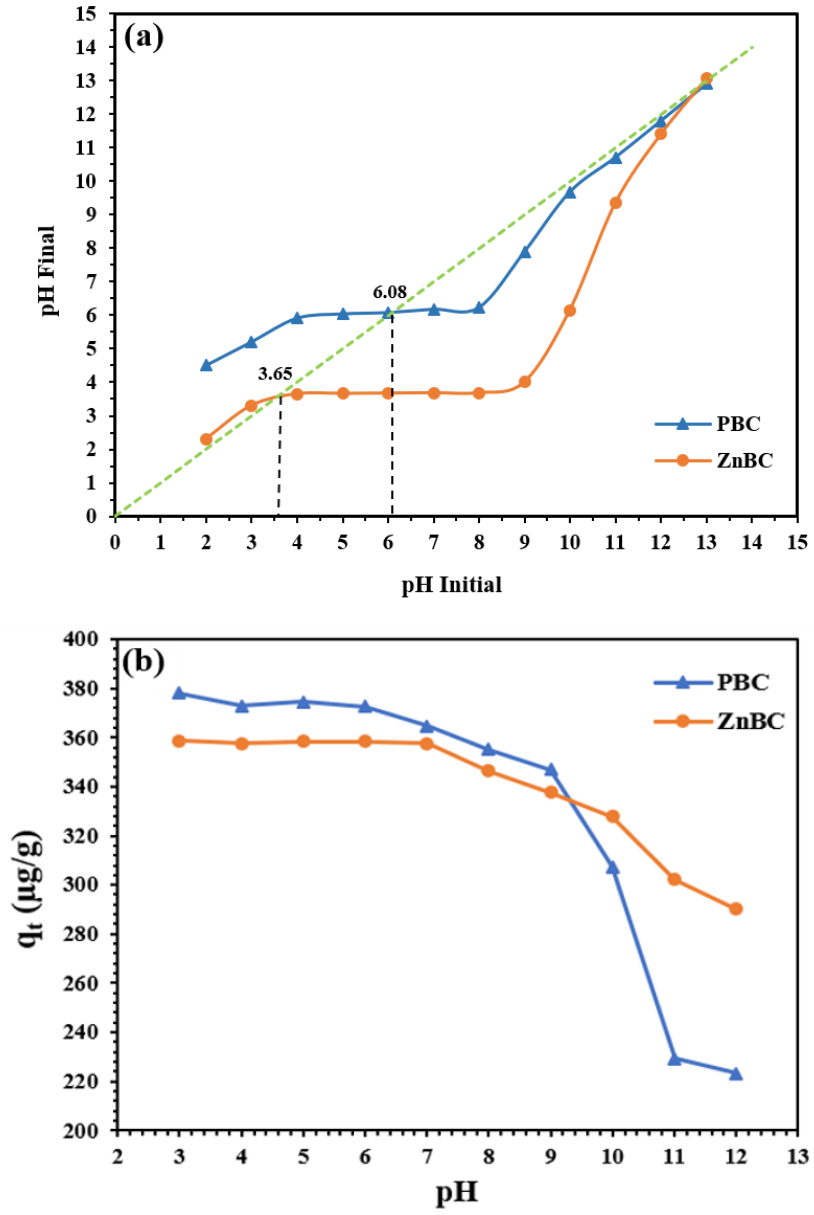

Figure 4.17. pH of point of zero charge (pH_{pzc}) of PBC and ZnBC adsorbents (a), and effect of pH on PFOA adsorption capacity for PBC and ZnBC (b) (adsorbent dosage=0.5 g/L; PFOA initial concentration=200 µg/L; temperature=25 °C)

4.3.6. Effect of ionic strength

The ionic strength of the solution can influence electrostatic interactions between ions in water. As shown in Figure 4.18, the PFOA adsorption capacity of modified biochar adsorbents can be affected by ionic strength and various ions in the solution. Ionic strength was investigated using NaCl at different concentrations (0, 0.001, 0.01, and 0.1 M). The results demonstrated that

as the ionic strength increased from 0.001 M to 0.1 M, the PFOA adsorption capacity was enhanced due to the salting-out effect and thereby, the hydrophobic interactions between the salting-out PFOA and the surface of the biochar [53,83]. On the other hand, by introducing chloride ions (Cl^-) into the solution, NaCl can affect the electrostatic interactions between the biochar surface and the PFOA molecules during the adsorption process. PBC and ZnBC have different surface chemistry, which means that their PFOA adsorption capacities are affected by ionic strength differently. There are more acid groups (containing O and P atoms) and positive active sites in PBC so that chloride ions can compete with PFOA anions on the active sites on the biochar surface. This can lead to reducing the attractive forces between PFOA and biochar. PBC exhibits a lower improvement in the capacity to adsorb PFOA at higher ionic strengths (0.1 M NaCl) than ZnBC because the presence of chloride anions has a more negative impact on PBC's ability to adsorb PFOA.

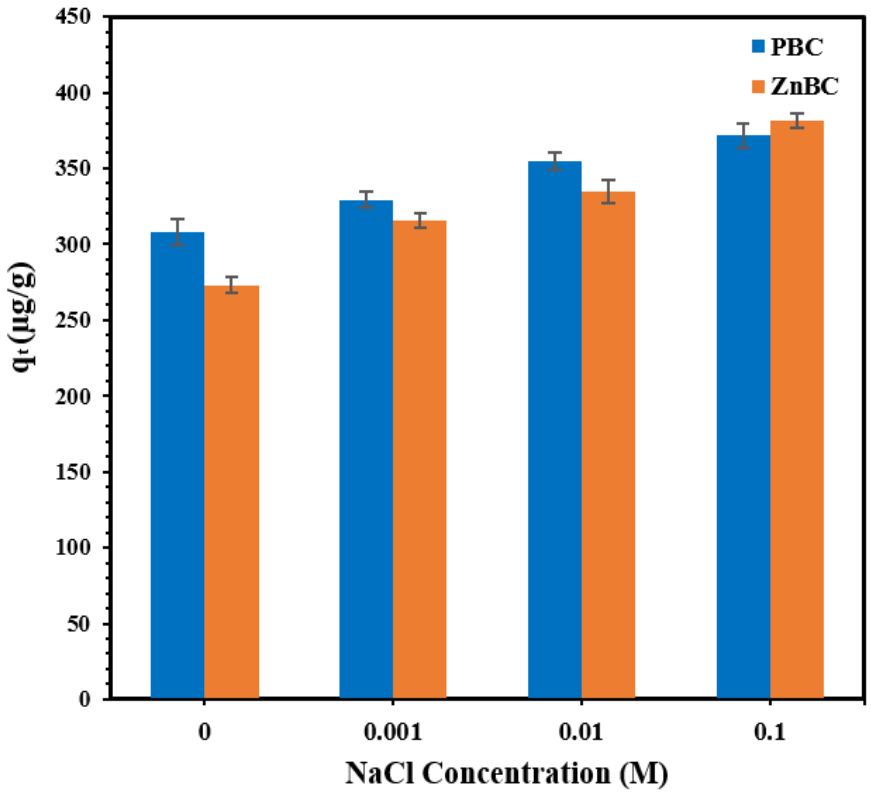

Figure 4.18. Effect of ionic strength at on PFOA adsorption capacity for PBC and ZnBC (adsorbent dosage=0.5 g/L; PFOA initial concentration=200 µg/L; temperature=25 °C). Note error bars are standard deviations with n=3.

4.3.7. Effect of co-existing ions

Figure 4.19 depicts the effect of different ions in water on the PFOA adsorption process on the PBC and ZnBC. Based on Figure 4.19a, divalent cations (Ca^{2+} and Mg^{2+}) enhance the PFOA adsorption capacity of both modified biochar adsorbents. Divalent cations can neutralize the negative surface charges of adsorbents, as evidenced by the increase in zeta potential when added to the solution. They form a bridge between the PFOA anions and the negatively charged functional groups on the biochar surface. This mechanism was confirmed by Wang et al. during studying of PFOS and PFOA adsorption on alumina in the presence of Ca^{2+} and Mg^{2+} ions [94]. PBC has more oxygen-containing functional groups than ZnBC, resulting in higher improvement through the divalent bridge effect in water-containing divalent cations like Ca^{2+} and Mg^{2+}. K^{+} and Na^{+} cannot create divalent bridges in water. They have less impact on PFOA adsorption by biochar. However, they can have electrostatic interactions with negatively charged groups on the biochar surface (functional groups containing free electron pairs on atoms like oxygen). These show decreased electrostatic repulsion between biochar and PFOA anions, facilitating the PFOA adsorption.

Anions can enhance the PFOA adsorption on the biochar through the salting-out effect (Figure 4.19b). Smaller anions have a stronger ability to salting-out the PFOA than larger anions [82,85]. So, as shown in Figure 4.17b, Cl^{-} can lead to higher enhancement in the PFOA adsorption capacity of biochar compared to CO_3^{2-}, NO_3^{-}, PO_4^{3-}, and SO_4^{2-}. However, there is competition between PFOA and anions to attach the positively charged sites on the biochar surface, which can decrease PFOA adsorption. As a result, salting-out the PFOA can increase adsorption efficiency, whereas the competition between anions and the PFOA can decrease it.

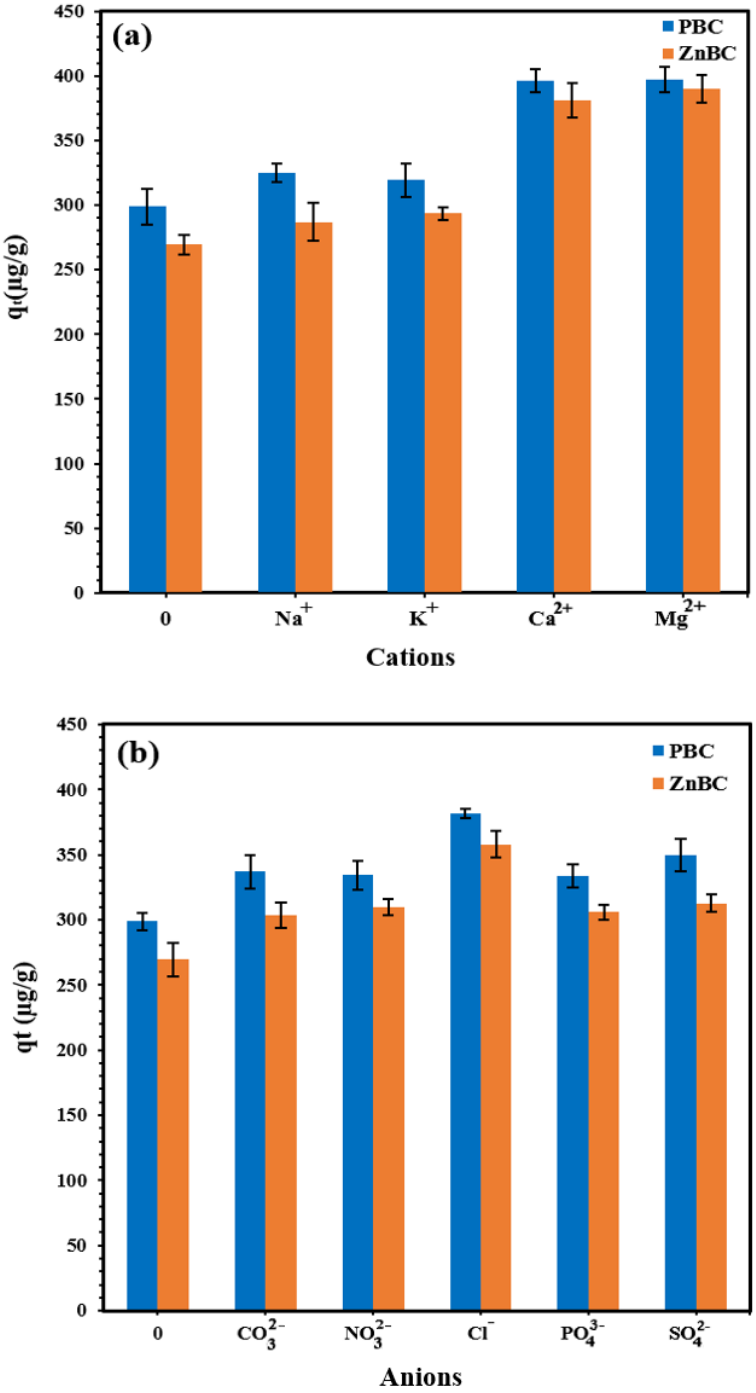

Figure 4.19. The effect of presence of cations (a) and anions (b) on the PFOA adsorption capacity for PBC and ZnBC adsorbents (adsorbent dosage=0.5 g/L; PFOA initial concentration=200 µg/L; temperature=25 °C). Note error bars are standard deviations with n=3.

4.3.8. Modeling of PFOA adsorption by PBC and ZnBC in fixed-bed column

In order to effectively utilize fixed-bed columns to treat PFOA-contaminated water in real-world applications, it is imperative to assess the effectiveness of adsorbents in continuous flow scenarios. In this research, the adsorption of PFOA on modified biochar adsorbents was studied using Yan and Yoon-Nelson models (Figure 4.20). PBC had a t_b and t_e of 60 min and 400 min, whereas ZnBC had a t_b and t_e of 54.5 min and 336.5 min, respectively. According to Yan's model, t_b is 123 min for PBC and 87 min for ZnBC. Consequently, PBC and ZnBC reach breakthrough relatively quickly in the experimental setup, while the Yan model predicts slightly longer times, especially for PBC. The models also indicate that t_e for PBC is 480 min for the Yan model and 433 min for the Yoon-Nelson model, while ZnBC, t_e is 378 and 335 min for the Yan and Yoon-Nelson models, respectively. Accordingly, PBC continues to remove PFOA for a longer duration than ZnBC. In experimental testing, τ is 257 min for PBC, whereas in the Yan model, it is 244 min, and in the Yoon-Nelson model, it is 250 min. In the case of ZnBC, τ is 178 min in the experimental test, 182 min for the Yan model and 190 min for the Yoon-Nelson model.

It should be noted that although both adsorbents exhibit reasonable performance, PBC achieved a 50% breakthrough for more extended periods. These results suggest that PBC and ZnBC are effective adsorbents for removing PFOA in continuous flow situations. Despite some variations in the breakthrough and exhaustion times predicted by the Yan and Yoon-Nelson models, the experimental results agree reasonably well with those of the Yan and Yoon-Nelson models (R^2>0.98). A longer t_e indicates that a large volume of water can be treated. Chularueangaksorn et al. studied the removal of PFOS from water using anion exchange resins and activated carbon in a fixed-bed column [97]. In this research, a Yoon-Nelson model was used to predict the half-saturation time of the adsorbent.

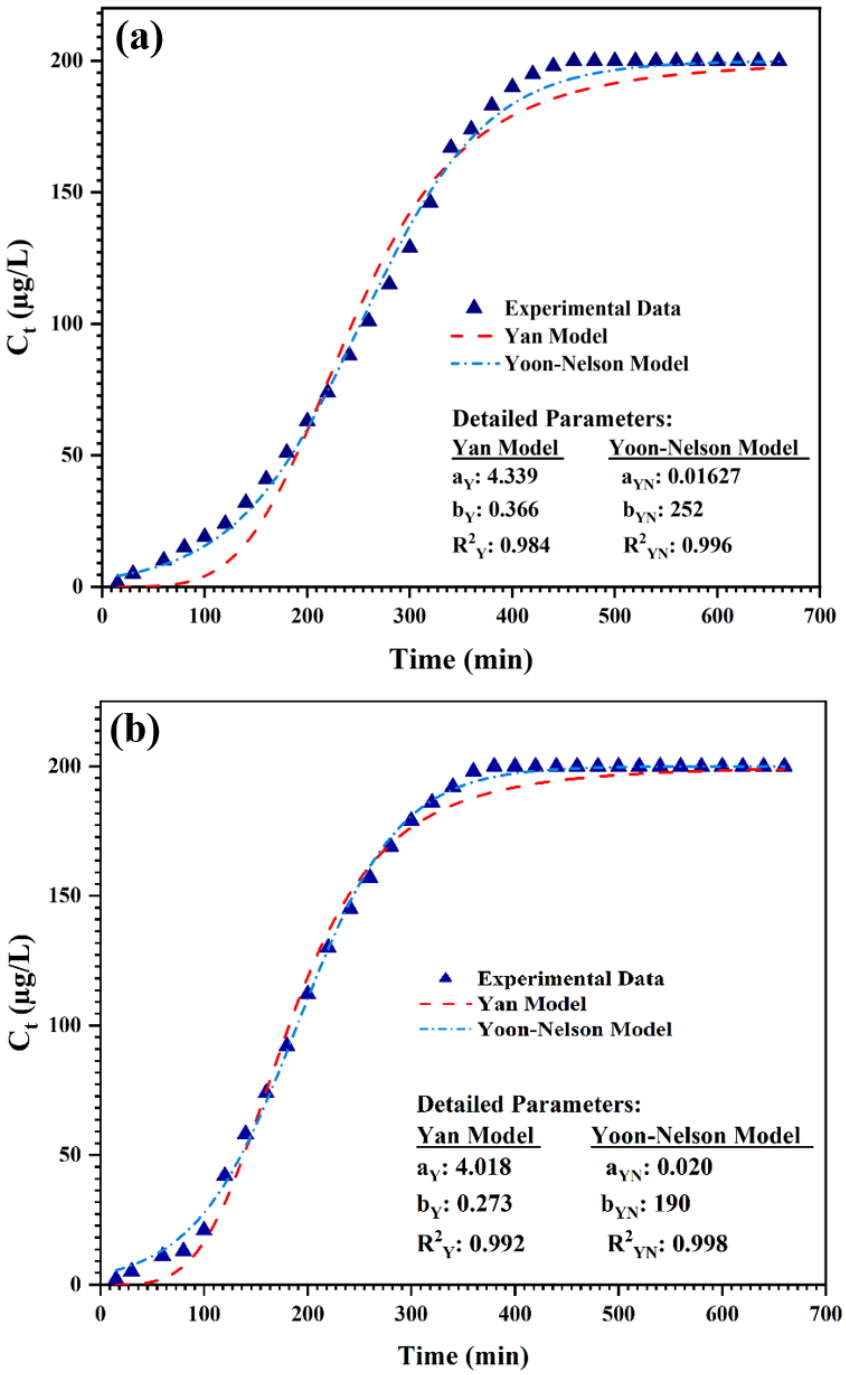

Figure 4.20. Modeling of the breakthrough curve for adsorption of PFOA onto (a) PBC and (b) ZnBC using Yan and Yoon-Nelson models

The ZnBC column becomes saturated with PFOA more quickly than the PBC column. Due to the different chemical and physical properties of each adsorbent, this difference can be explained. This study analyzes the relationship between experimentally observed and model-predicted breakthrough and exhaustion times. According to various analyses, including FT-IR, SEM, BET, and XPS, PBC serves better as an adsorbent for PFOA than ZnBC, mainly because of its surface chemistry and larger surface area. Therefore, the characteristics of PBC influence t_b, t_e, and τ. Experimental data shows these values are 60, 400, and 257 min for PBC, respectively, whereas they are 54, 336, and 178 min for ZnBC, respectively. The findings show that PBC outperforms in removing sustained PFOA.

Although there are some slight differences between experimental results and predictions, both Yan and Yoon-Nelson models can accurately capture the dynamic behaviour of PFOA adsorption in fixed-bed columns. As indicated by both experimental and model predictions, the longer t_e of PBC indicates that PBC can treat a larger volume of water before exhaustion. This information has considerable practical significance for situations in which extended treatment is required. A comparison of experimental and model-predicted values reveals valuable insight into the complexities of real-world systems, emphasizing the importance of considering various factors that influence adsorption behaviour.

4.4. Adsorption mechanism of PFOA on PBC and ZnBC

As part of the presented research, various analytical methods, including SEM, EDS, FTIR, and XPS, were employed to explore the structural modifications of adsorbents. The results of these analyses have contributed substantially to understanding the adsorption of PFOA on the PBC and ZnBC adsorbents. The results provide insight into the complex interplay of chemical interactions in adsorption. A comprehensive investigation of significant factors affecting the adsorption process and fixed-bed experiments were conducted to gain a deeper understanding of the adsorption chemical mechanism. Generally, biochar adsorbs PFAS compounds through electrostatic attraction, hydrogen bonds, hydrophobic interactions, van der Waals forces and pore filling (Figures 2.3 and 2.4). As a result of the release of water and volatile compounds during pyrolysis with H3PO4, the structure of biochar changed in terms of porosity, surface area, and type and number of the chemical functional groups. When phosphoric acid reacts with hydroxyl groups in cellulose, hemicellulose, and lignin, phosphorus-containing functional groups are

introduced onto the organic structure of canola straw. These chemical functional groups are more likely in the form of C-O-P and C-P groups and can induce a positive charge on the biochar structure (Figure 4.21). Rosas et al. observed the release of CO from phosphoric acid-activated carbons at high temperatures attributed to the decomposition of C-O-PO_3 groups on the carbon surface, leading to the formation of C-PO_3 groups [99]. As these phosphorus functional groups can bond to the PFOA during adsorption, the nature and concentration of these groups have a significant impact on the adsorbent performance [100]. EDS, FT-IR, and XPS results confirmed the presence of chemical functional groups containing phosphorus atoms.

Besides, during the activation of H_3PO_4, more -OH and -COOH groups can be introduced to the biochar structure, forming more covalent and hydrogen bonds with PFOA. As a result, these new chemical functional groups function as active sites to interact with PFOA. Higher porosity leads to a larger internal surface area and more active sites. The SEM images and BET data revealed a higher surface area and greater porosity. Consequently, PFOA can interact more readily with biochar with more active sites, leading to a higher adsorption capacity.

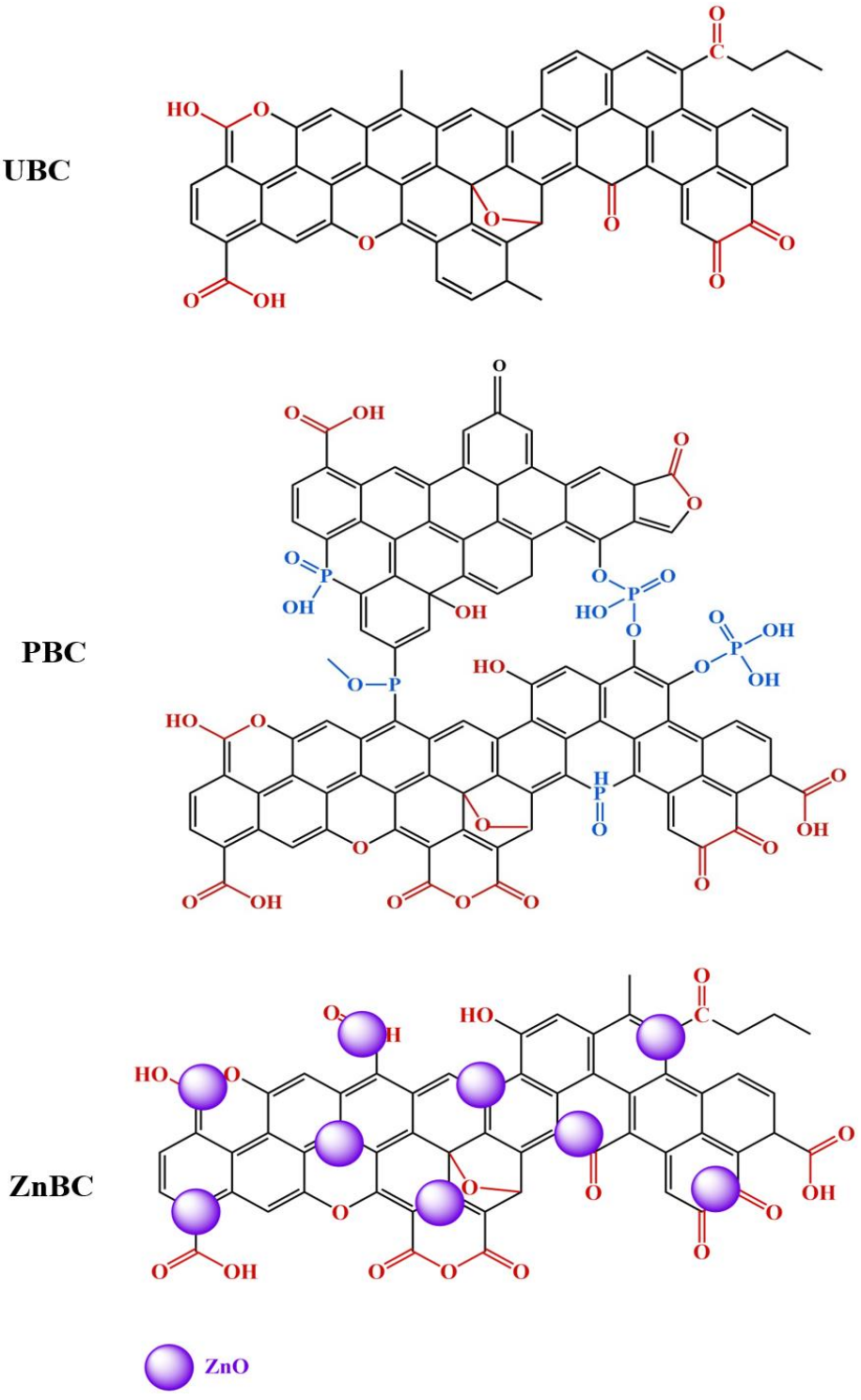

Figure 4.21. Chemical structure of UBC, PBC, and ZnBC

PFAS molecules and their anion form are also more likely to be adsorbed on PBC surfaces due to the positive charge they place on the phosphorus atom in chemical functional groups containing phosphorus. The positive charge is caused by the empty *d* orbital of phosphorous. As an electron acceptor, this orbital can accept an electron pair in the carboxylic acid group of PFOA or the carboxylate in PFOA anion and form a dative bond (Figure 4.22a). A dative bond is a covalent bond between an electron acceptor (an atom with an empty orbital) and an electron donor (an atom with a free electron pair).

$ZnCl_2$ has two significant effects on cellulose: swelling and catalytic hydrolysis. As a result of these actions, surface area and porosity are increased during the activation process. $ZnCl_2$ can permeate lignocellulosic biomass by dissolving cellulose, thereby creating pores within the biomass. Moreover, treatment with $ZnCl_2$ can create Lewis acid sites closely related to Zn. As a result of $ZnCl_2$ treatment, ZnO is formed on the surface of biochar, and zinc now has an empty orbital that can accept electrons (Figure 4.21). A dative bond can be formed between zinc, as an electron acceptor, and PFOA as an electron donor, particularly in the anion form of PFOA (Figure 4.22a) [100]. A chemisorption mechanism is observed during adsorption since dative bonds and electrostatic interactions are strong.

Also, there are other chemical interactions (hydrogen bonding, esterification, etc.) that occur between chemical functional groups containing oxygen (carboxylic acid, carboxylate, hydroxyl, ester, aldehyde, ketone, and epoxide) in PBC and ZnBC and acid group in PFOA (Figure 4.22b). PBC and ZnBC contain aliphatic and aromatic groups which can adsorb PFOA due to hydrophobic interactions. In addition, hydrophobic aggregates of PFOA quickly form hemi-micelles, micelles, and bilayers. Additionally, the C–F chains of PFOA have an entropic tendency to self-aggregate through hydrophobic interactions. As a result of isotherm studies and the observation of multilayer adsorption on modified adsorbents, this phenomenon has been demonstrated.

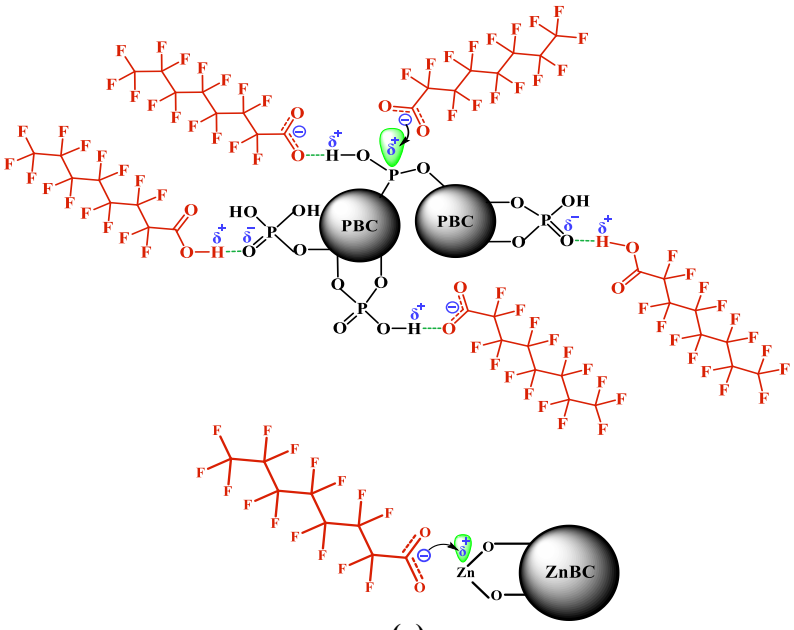

(a)

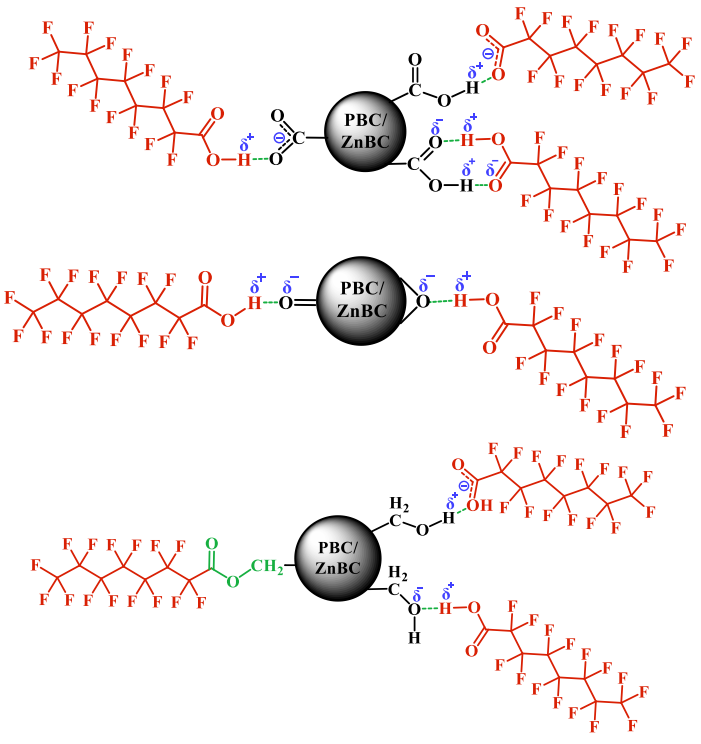

(b)

Figure 4.22. (a) Formation of dative bonds between phosphorus in PBC, zinc in ZnBC, and oxygen atoms in PFOA, and (b) different chemical interactions between chemical functional groups containing oxygen of PBC and ZnBC, and PFOA.

Chapter 5.

Conclusions and Recommendations for Future Work

The following chapter summarizes the findings of this study and offers valuable insights into potential avenues for future research.

5.1. Conclusions

- Chemical treatment and microwave-assisted pyrolysis methods significantly enhance the adsorption capacity of biochar. H_3PO_4-treated biochar (PBC) has a greater PFOA adsorption capacity than $ZnCl_2$-treated biochar (ZnBC).
- The pseudo-second-order model was more accurate in modelling PFOA adsorption data onto PBC and ZnBC adsorbents, as indicated by higher correlation coefficients (R^2 values). Therefore, a chemical interaction occurs between PFOA and chemical functional groups of modified adsorbents.
- Adsorption data were modelled using Langmuir, Freundlich, and Temkin isotherms. PBC and ZnBC adsorption data best fit the Freundlich model, indicating that a heterogeneous multilayer adsorption mechanism resembles the adsorption behaviour of modified biochar adsorbents. Furthermore, the data were well-fitted to the Temkin equilibrium model for both biochar adsorbents, suggesting that electrostatic interactions were likely to play a role in PFAS adsorption onto PBC and ZnBC.
- Chemically treated biochar adsorbents have a temperature-dependent adsorption capacity toward PFOA. PBC and ZnBC adsorb more PFOA at higher temperatures, suggesting that this process is endothermic.
- Modified biochar adsorbents demonstrated good performance across a wide pH range, with maximum PFOA adsorption occurring at lower pH levels.
- The results of this study indicate that the composition of the solution also affected the PFOA adsorption behavior; therefore, consideration should be given to the potential bridging effect initiated by particular cations and functional groups in biochar.
- Fixed-bed column experiments were conducted to evaluate the treated adsorbents performances under continuous flow conditions. It is found that both modified adsorbents can be helpful for PFOA.

5.2. Recommendations for future works

As a result of the studies conducted in this research, biochar has the potential to be used as a suitable and sustainable sorbent for the removal of PFAS from water. Some intriguing concepts emerged that are worth exploring in more detail as following:

Using various biomass resources: To optimize biochar adsorbents for PFAS removal, it is essential to research a variety of feedstock varieties for biochar production. The composition of the feedstock contributes to variations in the properties of biochar, making it possible for researchers to identify materials that enhance biochar's adsorption capacity and kinetics. This approach can be used to develop a biochar adsorption process that is cost-effective, efficient, and adaptable to various contaminants containing PFAS.

Design a multifunctional modified biochar: A thorough evaluation of the performance and effectiveness of the developed methods for adsorbing different types of chemicals can provide valuable insight into their versatility and application to water treatment. Expanding the research to remove contaminants from wastewater, including other contaminant compounds, is valuable, especially for those with different chemical structures. This will enhance the applicability of the findings and contribute to a better understanding of the performance of modified biochar adsorbents

Exploring the applicability of both long-chain and short-chain PFAS compounds: Combining different modification agents to create a multifunctional modified biochar offers a promising approach for efficiently adsorbing PFAS, short-chain and long-chain. In order to enhance the adsorption capacity of biochar for PFAS compounds over a wide range of concentrations, researchers should optimize parameters such as temperature, concentration, and duration during the modification process. Modified biochar needs to be validated using authentic water samples containing PFAS and assessments of regeneration potential and environmental impact to confirm its practical application and sustainability as a water treatment tool.

Regeneration and reusability of adsorbents: It is vital to explore the potential for regeneration to reduce the overall costs of the treatment process. Adsorbents must be examined and optimized for reusability and longevity to ensure they retain their adsorption capacity and effectiveness throughout their lifetime.

Studying lifecycle assessment: The modified biochar production and application process should be subjected to a life cycle assessment (LCA). The environmental impact and energy

consumption associated with the entire life cycle should be evaluated to provide an overall picture of the product's sustainability.

Application for real water samples: In the future, studies can be conducted to evaluate the performance of modified biochar for actual water samples. These practical scenarios can provide researchers with an insight into the effectiveness of modified biochar when treating water with diverse compositions and complex matrixes, providing a more realistic assessment of its applicability to water treatment processes. As a result, the findings are scientifically robust and directly applicable to addressing water quality challenges in a practical, field-based setting.

References

[1] R. C. Buck *et al.*, "Perfluoroalkyl and polyfluoroalkyl substances in the environment: Terminology, classification, and origins," *Integr. Environ. Assess. Manag.*, vol. 7, no. 4, pp. 513–541, 2011, doi: 10.1002/ieam.258.

[2] S. Yadav *et al.*, "Updated review on emerging technologies for PFAS contaminated water treatment," *Chem. Eng. Res. Des.*, vol. 182, pp. 667–700, 2022, doi: 10.1016/j.cherd.2022.04.009.

[3] S. K. Kim and K. Kannan, "Perfluorinated acids in air, rain, snow, surface runoff, and lakes: Relative importance of pathways to contamination of urban lakes," *Environ. Sci. Technol.*, vol. 41, no. 24, pp. 8328–8334, 2007, doi: 10.1021/es072107t.

[4] I. M. Militao, F. A. Roddick, R. Bergamasco, and L. Fan, "Removing PFAS from aquatic systems using natural and renewable material-based adsorbents: A review," *J. Environ. Chem. Eng.*, vol. 9, no. 4, 2021, doi: 10.1016/j.jece.2021.105271.

[5] D. Q. Zhang, W. L. Zhang, and Y. N. Liang, "Adsorption of perfluoroalkyl and polyfluoroalkyl substances (PFASs) from aqueous solution - A review," *Sci. Total Environ.*, vol. 694, 2019, doi: 10.1016/j.scitotenv.2019.133606.

[6] V. Boiteux *et al.*, "Concentrations and patterns of perfluoroalkyl and polyfluoroalkyl substances in a river and three drinking water treatment plants near and far from a major production source," *Sci. Total Environ.*, vol. 583, pp. 393–400, 2017, doi: 10.1016/j.scitotenv.2017.01.079.

[7] D. Longpré, L. Lorusso, C. Levicki, R. Carrier, and P. Cureton, "PFOS, PFOA, LC-PFCAS, and certain other PFAS: A focus on Canadian guidelines and guidance for contaminated sites management," *Environ. Technol. Innov.*, vol. 18, p. 100752, 2020, doi: 10.1016/j.eti.2020.100752.

[8] E. Panieri, K. Baralic, D. Djukic-Cosic, A. B. Djordjevic, and L. Saso, "PFAS Molecules: A Major Concern for the Human Health and the Environment," *Toxics*, vol. 10, no. 2, pp. 1–55, 2022, doi: 10.3390/toxics10020044.

[9] I. T. Cousins *et al.*, "Strategies for grouping per-and polyfluoroalkyl substances (PFAS) to protect human and environmental health," *Environ. Sci. Process. Impacts*, vol. 22, no. 7, pp. 1444–1460, 2020, doi: 10.1039/d0em00147c.

[10] K. H. Kucharzyk, R. Darlington, M. Benotti, R. Deeb, and E. Hawley, "Novel treatment technologies for PFAS compounds: A critical review," *J. Environ. Manage.*, vol. 204, pp. 757–764, 2017, doi: 10.1016/j.jenvman.2017.08.016.

[11] Z. Wang *et al.*, "A New OECD Definition for Per- And Polyfluoroalkyl Substances," *Environ. Sci. Technol.*, vol. 55, no. 23, pp. 15575–15578, 2021, doi: 10.1021/acs.est.1c06896.

[12] I. Ross *et al.*, "A review of emerging technologies for remediation of PFASs," *Remediation*, vol. 28, no. 2, pp. 101–126, 2018, doi: 10.1002/rem.21553.

[13] V. A. Arias Espana, M. Mallavarapu, and R. Naidu, "Treatment technologies for aqueous perfluorooctanesulfonate (PFOS) and perfluorooctanoate (PFOA): A critical review with an emphasis on field testing," *Environ. Technol. Innov.*, vol. 4, pp. 168–181, 2015, doi: 10.1016/j.eti.2015.06.001.

[14] R. Loos *et al.*, "Pan-European survey on the occurrence of selected polar organic persistent pollutants in ground water," *Water Res.*, vol. 44, no. 14, pp. 4115–4126, 2010, doi: 10.1016/j.watres.2010.05.032.

[15] D. M. Wanninayake, "Comparison of currently available PFAS remediation technologies in water: A review," *J. Environ. Manage.*, vol. 283, no. January, p. 111977, 2021, doi: 10.1016/j.jenvman.2021.111977.
[16] J. Horst *et al.*, "Water treatment technologies for PFAS: the next generation," *Groundw. Monit. Remediat.*, vol. 38, no. 2, pp. 13–23, 2018, doi: 10.1111/gwmr.12281.
[17] T. Teymourian, T. Teymoorian, E. Kowsari, and S. Ramakrishna, "A review of emerging PFAS contaminants: sources, fate, health risks, and a comprehensive assortment of recent sorbents for PFAS treatment by evaluating their mechanism", *Res. Chem. Intermed.,* vol. 47, no. 12. 2021. doi: 10.1007/s11164-021-04603-7.
[18] T. Liu, Y. Gu, D. Y. Xing, W. Dong, and X. Wu, "Rapid and high-capacity adsorption of PFOS and PFOA by regenerable ammoniated magnetic particle," *Environ. Sci. Pollut. Res.*, vol. 25, no. 14, pp. 13813–13822, 2018, doi: 10.1007/s11356-018-1578-1.
[19] N. B. Saleh *et al.*, "Removal of poly- and per-fluoroalkyl substances from aqueous systems by nano-enabled water treatment strategies," *Environ. Sci. Water Res. Technol.*, vol. 5, no. 2, pp. 198–208, 2019, doi: 10.1039/c8ew00621k.
[20] P. S. Pauletto and T. J. Bandosz, "Activated carbon versus metal-organic frameworks: A review of their PFAS adsorption performance," *J. Hazard. Mater.*, vol. 425, no. November 2021, p. 127810, 2022, doi: 10.1016/j.jhazmat.2021.127810.
[21] O. Das, A. K. Sarmah, and D. Bhattacharyya, "Biocomposites from waste derived biochars: Mechanical, thermal, chemical, and morphological properties," *Waste Manag.*, vol. 49, pp. 560–570, 2016, doi: 10.1016/j.wasman.2015.12.007.
[22] H. A. Alhashimi and C. B. Aktas, "Life cycle environmental and economic performance of biochar compared with activated carbon: a meta-analysis," *Resour. Conserv. Recycl.*, vol. 118, pp. 13–26, 2017.
[23] B. R. Patra, A. Mukherjee, S. Nanda, and A. K. Dalai, "Biochar production, activation and adsorptive applications: a review," *Environ. Chem. Lett.*, vol. 19, no. 3, pp. 2237–2259, 2021, doi: 10.1007/s10311-020-01165-9.
[24] T. M. Abdel-Fattah, M. E. Mahmoud, S. B. Ahmed, M. D. Huff, J. W. Lee, and S. Kumar, "Biochar from woody biomass for removing metal contaminants and carbon sequestration," *J. Ind. Eng. Chem.*, vol. 22, pp. 103–109, 2015, doi: 10.1016/j.jiec.2014.06.030.
[25] A. Dechene, I. Rosendahl, V. Laabs, and W. Amelung, "Sorption of polar herbicides and herbicide metabolites by biochar-amended soil," *Chemosphere*, vol. 109, pp. 180–186, 2014, doi: 10.1016/j.chemosphere.2014.02.010.
[26] D. Kupryianchyk, S. E. Hale, G. D. Breedveld, and G. Cornelissen, "Treatment of sites contaminated with perfluorinated compounds using biochar amendment," *Chemosphere*, vol. 142, pp. 35–40, 2016, doi: 10.1016/j.chemosphere.2015.04.085.
[27] M. Aboughaly and ; I M R Fattah, "Production of biochar from biomass pyrolysis for removal of PFAS from wastewater and biosolids: a critical review," *Preprint*, vol. 1, no. 1, pp. 1–11, 2023, doi: 10.20944/preprints202304.0309.v1.
[28] Y. Wu, L. Qi, and G. Chen, "A mechanical investigation of perfluorooctane acid adsorption by engineered biochar," *J. Clean. Prod.*, vol. 340, no. February, p. 130742, 2022, doi: 10.1016/j.jclepro.2022.130742.
[29] Z. Du *et al.*, "Adsorption behavior and mechanism of perfluorinated compounds on various adsorbents-A review," *J. Hazard. Mater.*, vol. 274, pp. 443–454, 2014, doi: 10.1016/j.jhazmat.2014.04.038.

[30] Y. Zhi and J. Liu, “Sorption and desorption of anionic, cationic and zwitterionic polyfluoroalkyl substances by soil organic matter and pyrogenic carbonaceous materials,” *Chem. Eng. J.*, vol. 346, no. December 2017, pp. 682–691, 2018, doi: 10.1016/j.cej.2018.04.042.
[31] I. M. Militao, F. Roddick, L. Fan, L. C. Zepeda, R. Parthasarathy, and R. Bergamasco, “PFAS removal from water by adsorption with alginate-encapsulated plant albumin and rice straw-derived biochar,” *J. Water Process Eng.*, vol. 53, no. December 2022, 2023, doi: 10.1016/j.jwpe.2023.103616.
[32] M. D. Nguyen *et al.*, “Investigation on removal of perfluorooctanoic acid (PFOA), perfluorooctane sulfonate (PFOS), perfluorohexane sulfonate (PFH_xS) using water treatment sludge and biochar,” *Chemosphere*, vol. 338, no. March, p. 139412, 2023, doi: 10.1016/j.chemosphere.2023.139412.
[33] K. M. Krahn *et al.*, “Sewage sludge biochars as effective PFAS-sorbents,” *J. Hazard. Mater.*, vol. 445, no. September 2022, 2023, doi: 10.1016/j.jhazmat.2022.130449.
[34] D. Saha, S. Khan, and S. E. Van Bramer, “Can porous carbons be a remedy for PFAS pollution in water? A perspective,” *J. Environ. Chem. Eng.*, vol. 9, no. 6, p. 106665, 2021, doi: 10.1016/j.jece.2021.106665.
[35] S. C. E. Leung, D. Wanninayake, D. Chen, N. T. Nguyen, and Q. Li, “Physicochemical properties and interactions of perfluoroalkyl substances (PFAS) - Challenges and opportunities in sensing and remediation,” *Sci. Total Environ.*, vol. 905, no. September, 2023, doi: 10.1016/j.scitotenv.2023.166764.
[36] D. Chandler, “Interfaces and the driving force of hydrophobic assembly,” *Nature*, vol. 437, no. 7059, pp. 640–647, 2005, doi: 10.1038/nature04162.
[37] P. Zareitalabad, J. Siemens, M. Hamer, and W. Amelung, “Perfluorooctanoic acid (PFOA) and perfluorooctanesulfonic acid (PFOS) in surface waters, sediments, soils and wastewater - A review on concentrations and distribution coefficients,” *Chemosphere*, vol. 91, no. 6, pp. 725–732, 2013, doi: 10.1016/j.chemosphere.2013.02.024.
[38] H. Chen, C. Zhang, Y. Yu, and J. Han, “Sorption of perfluorooctane sulfonate (PFOS) on marine sediments,” *Mar. Pollut. Bull.*, vol. 64, no. 5, pp. 902–906, 2012, doi: 10.1016/j.marpolbul.2012.03.012.
[39] S. Xin *et al.*, “Chemical structure evolution of char during the pyrolysis of cellulose,” *J. Anal. Appl. Pyrolysis*, vol. 116, pp. 263–271, 2015, doi: 10.1016/j.jaap.2015.09.002.
[40] R. Wahi, N. F. Q. ain Zuhaidi, Y. Yusof, J. Jamel, D. Kanakaraju, and Z. Ngaini, “Chemically treated microwave-derived biochar: An overview,” *Biomass and Bioenergy*, vol. 107, pp. 411–421, 2017, doi: 10.1016/j.biombioe.2017.08.007.
[41] F. Mushtaq, R. Mat, and F. N. Ani, “A review on microwave assisted pyrolysis of coal and biomass for fuel production,” *Renew. Sustain. Energy Rev.*, vol. 39, pp. 555–574, 2014.
[42] G. Yang *et al.*, “Effects of pyrolysis temperature on the physicochemical properties of biochar derived from vermicompost and its potential use as an environmental amendment,” *RSC Adv.*, vol. 5, no. 50, pp. 40117–40125, 2015, doi: 10.1039/c5ra02836a.
[43] D. Akhil, D. Lakshmi, A. Kartik, D. V. N. Vo, J. Arun, and K. P. Gopinath, “Production, characterization, activation and environmental applications of engineered biochar: A review”, *Processes*, vol. 19, no. 3. pp. 1–20, 2021. doi: 10.1007/s10311-020-01167-7.
[44] L. Leng *et al.*, “An overview on engineering the surface area and porosity of biochar,” *Sci. Total Environ.*, vol. 763, p. 144204, 2021, doi: 10.1016/j.scitotenv.2020.144204.
[45] H. Zeghioud, L. Fryda, H. Djelal, A. Assadi, and A. Kane, “A comprehensive review of

biochar in removal of organic pollutants from wastewater: Characterization, toxicity, activation/functionalization and influencing treatment factors," *J. Water Process Eng.*, vol. 47, no. January, p. 102801, 2022, doi: 10.1016/j.jwpe.2022.102801.
[46] G. Chu *et al.*, "Phosphoric acid pretreatment enhances the specific surface areas of biochars by generation of micropores," *Environ. Pollut.*, vol. 240, pp. 1–9, 2018, doi: 10.1016/j.envpol.2018.04.003.
[47] C. Wang and T. Liu, "Nori-based N, O, S, Cl co-doped carbon materials by chemical activation of $ZnCl_2$ for supercapacitor," *J. Alloys Compd.*, vol. 696, pp. 42–50, 2017, doi: 10.1016/j.jallcom.2016.11.206.
[48] W. Tian, Q. Gao, Y. Tan, and Z. Li, "Unusual interconnected graphitized carbon nanosheets as the electrode of high-rate ionic liquid-based supercapacitor," *Carbon N. Y.*, vol. 119, pp. 287–295, 2017, doi: 10.1016/j.carbon.2017.04.050.
[49] H. Qiu, L. Lv, B. C. Pan, Q. J. Zhang, W. M. Zhang, and Q. X. Zhang, "Critical review in adsorption kinetic models," *J. Zhejiang Univ. Sci. A*, vol. 10, no. 5, pp. 716–724, 2009, doi: 10.1631/jzus.A0820524.
[50] J. P. Vareda, "On validity, physical meaning, mechanism insights and regression of adsorption kinetic models," *J. Mol. Liq.*, vol. 376, p. 121416, 2023, doi: 10.1016/j.molliq.2023.121416.
[51] J. Wang and X. Guo, "Adsorption kinetic models: Physical meanings, applications, and solving methods," *J. Hazard. Mater.*, vol. 390, no. January, p. 122156, 2020, doi: 10.1016/j.jhazmat.2020.122156.
[52] D. Tian *et al.*, "Removal of perfluorooctanoic acid (PFOA) from aqueous solution by amino-functionalized graphene oxide (AGO) aerogels: Influencing factors, kinetics, isotherms, and thermodynamic studies," *Sci. Total Environ.*, vol. 783, p. 147041, 2021, doi: 10.1016/j.scitotenv.2021.147041.
[53] R. Liu, J. Zhang, H. Fu, L. Yin, Y. Song, and G. He, "A comparative study of methylene blue adsorption and removal mechanisms by calcium carbonate from different sources," *Bioresour. Technol.*, vol. 387, no. August, p. 129603, 2023, doi: 10.1016/j.biortech.2023.129603.
[54] K. Y. Foo and B. H. Hameed, "Insights into the modeling of adsorption isotherm systems," *Chem. Eng. J.*, vol. 156, no. 1, pp. 2–10, 2010, doi: 10.1016/j.cej.2009.09.013.
[55] M. Musah, Y. Azeh, J. Mathew, M. Umar, Z. Abdulhamid, and A. Muhammad, "Adsorption kinetics and isotherm models: A review," *Caliphate J. Sci. Technol.*, vol. 4, no. 1, pp. 20–26, 2022, doi: 10.4314/cajost.v4i1.3.
[56] F. Batool, J. Akbar, S. Iqbal, S. Noreen, and S. N. A. Bukhari, "Study of isothermal, kinetic, and thermodynamic parameters for adsorption of cadmium: An overview of Linear and Nonlinear Approach and Error Analysis," *Bioinorg. Chem. Appl.*, vol. 2018, 2018, doi: 10.1155/2018/3463724.
[57] Z. Aksu and F. Gönen, "Biosorption of phenol by immobilized activated sludge in a continuous packed bed: Prediction of breakthrough curves," *Process Biochem.*, vol. 39, no. 5, pp. 599–613, 2004, doi: 10.1016/S0032-9592(03)00132-8.
[58] E. C. Lima, A. A. Gomes, and H. N. Tran, "Comparison of the nonlinear and linear forms of the van't Hoff equation for calculation of adsorption thermodynamic parameters ($\Delta S°$ and $\Delta H°$)," *J. Mol. Liq.*, vol. 311, p. 113315, 2020, doi: 10.1016/j.molliq.2020.113315.
[59] Y. Liu, "Is the free energy change of adsorption correctly calculated?," *J. Chem. Eng. Data*, vol. 54, no. 7, pp. 1981–1985, 2009, doi: 10.1021/je800661q.

[60] C. P. Higgins and R. G. Luthy, “Sorption of perfluorinated surfactants on sediments,” *Environ. Sci. Technol.*, vol. 40, no. 23, pp. 7251–7256, 2006, doi: 10.1021/es061000n.
[61] Y. Qu, C. Zhang, F. Li, X. Bo, G. Liu, and Q. Zhou, “Equilibrium and kinetics study on the adsorption of perfluorooctanoic acid from aqueous solution onto powdered activated carbon,” *J. Hazard. Mater.*, vol. 169, no. 1–3, pp. 146–152, 2009, doi: 10.1016/j.jhazmat.2009.03.063.
[62] Q. Yu, R. Zhang, S. Deng, J. Huang, and G. Yu, “Sorption of perfluorooctane sulfonate and perfluorooctanoate on activated carbons and resin: Kinetic and isotherm study,” *Water Res.*, vol. 43, no. 4, pp. 1150–1158, 2009, doi: 10.1016/j.watres.2008.12.001.
[63] X. Lei *et al.*, “A review of PFAS adsorption from aqueous solutions: Current approaches, engineering applications, challenges, and opportunities,” *Environ. Pollut.*, vol. 321, no. January, p. 121138, 2023, doi: 10.1016/j.envpol.2023.121138.
[64] J. M. Jian, C. Zhang, F. Wang, X. Lu, F. Wang, and E. Y. Zeng, “Effect of solution chemistry and aggregation on adsorption of perfluorooctanesulphonate (PFOS)to nano-sized alumina,” *Environ. Pollut.*, vol. 251, pp. 425–433, 2019, doi: 10.1016/j.envpol.2019.05.025.
[65] E. Gagliano, M. Sgroi, P. P. Falciglia, F. G. A. Vagliasindi, and P. Roccaro, “Removal of poly- and perfluoroalkyl substances (PFAS) from water by adsorption: Role of PFAS chain length, effect of organic matter and challenges in adsorbent regeneration,” *Water Res.*, vol. 171, p. 115381, 2020, doi: 10.1016/j.watres.2019.115381.
[66] Y. Zhang, S. Fan, T. Liu, W. Fu, and B. Li, “A review of biochar prepared by microwave-assisted pyrolysis of organic wastes,” *Sustain. Energy Technol. Assessments*, vol. 50, no. January 2021, p. 101873, 2022, doi: 10.1016/j.seta.2021.101873.
[67] A. Ateş, “The effect of microwave and ultrasound activation on the characteristics of biochar produced from tea waste in the presence of H_3PO_4 and KOH,” *Biomass Convers. Biorefinery*, pp. 9075–9094, 2021, doi: 10.1007/s13399-021-01838-7.
[68] O. Oginni, K. Singh, G. Oporto, B. Dawson-Andoh, L. McDonald, and E. Sabolsky, “Effect of one-step and two-step H_3PO_4 activation on activated carbon characteristics,” *Bioresour. Technol. Reports*, vol. 8, no. July, p. 100307, 2019, doi: 10.1016/j.biteb.2019.100307.
[69] W. A. W. A. K. Ghani *et al.*, “Biochar production from waste rubber-wood-sawdust and its potential use in C sequestration: Chemical and physical characterization,” *Ind. Crops Prod.*, vol. 44, pp. 18–24, 2013, doi: 10.1016/j.indcrop.2012.10.017.
[70] M. Hassan *et al.*, “Influences of feedstock sources and pyrolysis temperature on the properties of biochar and functionality as adsorbents: A meta-analysis,” *Sci. Total Environ.*, vol. 744, p. 140714, 2020, doi: 10.1016/j.scitotenv.2020.140714.
[71] Y. Zhang *et al.*, “A three-dimensional active biochar for sintering in steel industry and remove methylene blue by synergistic activation of H_3PO_4 and $ZnCl_2$,” *Fuel*, vol. 336, no. November 2022, p. 127079, 2023, doi: 10.1016/j.fuel.2022.127079.
[72] J. Xu, L. Chen, H. Qu, Y. Jiao, J. Xie, and G. Xing, “Preparation and characterization of activated carbon from reedy grass leaves by chemical activation with H_3PO_4,” *Appl. Surf. Sci.*, vol. 320, pp. 674–680, 2014, doi: 10.1016/j.apsusc.2014.08.178.
[73] A. El Oudiani, Y. Chaabouni, S. Msahli, and F. Sakli, “Crystal transition from cellulose i to cellulose II in NaOH treated Agave americana L. fibre,” *Carbohydr. Polym.*, vol. 86, no. 3, pp. 1221–1229, 2011, doi: 10.1016/j.carbpol.2011.06.037.
[74] A. D. French, “Idealized powder diffraction patterns for cellulose polymorphs,” *Cellulose*,

vol. 21, no. 2, pp. 885–896, 2014, doi: 10.1007/s10570-013-0030-4.
[75] S. Nomura, Y. Kugo, and T. Erata, "^{13}C NMR and XRD studies on the enhancement of cellulose II crystallinity with low concentration NaOH post-treatments," *Cellulose*, vol. 27, no. 7, pp. 3553–3563, 2020, doi: 10.1007/s10570-020-03036-6.
[76] F. Zhao, R. Shan, W. Li, Y. Zhang, H. Yuan, and Y. Chen, "Synthesis, characterization, and dye removal of $ZnCl_2$-modified biochar derived from pulp and paper sludge," *ACS Omega*, vol. 6, no. 50, pp. 34712–34723, 2021, doi: 10.1021/acsomega.1c05142.
[77] M. S. Alam, B. Nahar, M. A. Gafur, G. Seong, and M. Z. Hossain, "Forced convective heat transfer coefficient measurement of low concentration nanorods ZnO–ethylene glycol nanofluids in laminar flow," *Nanomaterials*, vol. 12, no. 9, 2022, doi: 10.3390/nano12091568.
[78] O. Pezoti Junior *et al.*, "Synthesis of $ZnCl_2$-activated carbon from macadamia nut endocarp (Macadamia integrifolia) by microwave-assisted pyrolysis: Optimization using RSM and methylene blue adsorption," *J. Anal. Appl. Pyrolysis*, vol. 105, pp. 166–176, 2014, doi: 10.1016/j.jaap.2013.10.015.
[79] A. M. Puziy, O. I. Poddubnaya, A. Martínez-Alonso, F. Suárez-García, and J. M. D. Tascón, "Synthetic carbons activated with phosphoric - Acid I. Surface chemistry and ion binding properties," *Carbon N. Y.*, vol. 40, no. 9, pp. 1493–1505, 2002, doi: 10.1016/S0008-6223(01)00317-7.
[80] S. M. Yakout and G. Sharaf El-Deen, "Characterization of activated carbon prepared by phosphoric acid activation of olive stones," *Arab. J. Chem.*, vol. 9, pp. S1155–S1162, 2016, doi: 10.1016/j.arabjc.2011.12.002.
[81] E. Yagmur, I. I. G. Inal, Y. Gokce, T. G. Ulusoy Ghobadi, T. Aktar, and Z. Aktas, "Examination of gas and solid products during the preparation of activated carbon using phosphoric acid," *J. Environ. Manage.*, vol. 228, no. September, pp. 328–335, 2018, doi: 10.1016/j.jenvman.2018.09.046.
[82] C. Guo *et al.*, "Protein-enriched fish 'biowaste' converted to three-dimensional porous carbon nano-network for advanced oxygen reduction electrocatalysis," *Electrochim. Acta*, vol. 236, pp. 228–238, 2017, doi: 10.1016/j.electacta.2017.03.169.
[83] Z. Li *et al.*, "Adsorption behaviors of near-critical carbon dioxide on organic-rich shales: Modeling, multifractality, and kinetics," *Chem. Eng. J.*, vol. 428, no. July 2021, p. 132526, 2022, doi: 10.1016/j.cej.2021.132526.
[84] K. L. Tan and B. H. Hameed, "Insight into the adsorption kinetics models for the removal of contaminants from aqueous solutions," *J. Taiwan Inst. Chem. Eng.*, vol. 74, pp. 25–48, 2017, doi: 10.1016/j.jtice.2017.01.024.
[85] X. Lei *et al.*, "Enhanced adsorption of perfluorooctanoate (PFOA) onto low oxygen content ordered mesoporous carbon (OMC): Adsorption behaviors and mechanisms," *J. Hazard. Mater.*, vol. 421, no. August 2021, 2022, doi: 10.1016/j.jhazmat.2021.126810.
[86] I. M. Militao, F. Roddick, L. Fan, L. C. Zepeda, R. Parthasarathy, and R. Bergamasco, "PFAS removal from water by adsorption with alginate-encapsulated plant albumin and rice straw-derived biochar," *J. Water Process Eng.*, vol. 53, no. March, 2023, doi: 10.1016/j.jwpe.2023.103616.
[87] X. Lei *et al.*, "Enhanced adsorption of perfluorooctanoate (PFOA) onto low oxygen content ordered mesoporous carbon (OMC): Adsorption behaviors and mechanisms," *J. Hazard. Mater.*, vol. 421, no. July 2021, 2022, doi: 10.1016/j.jhazmat.2021.126810.
[88] M. Hassan *et al.*, "Magnetic biochar for removal of perfluorooctane sulphonate (PFOS):

Interfacial interaction and adsorption mechanism," *Environ. Technol. Innov.*, vol. 28, p. 102593, 2022, doi: 10.1016/j.eti.2022.102593.
[89] W. Chen, X. Zhang, M. Mamadiev, and Z. Wang, "Sorption of perfluorooctane sulfonate and perfluorooctanoate on polyacrylonitrile fiber-derived activated carbon fibers: In comparison with activated carbon," *RSC Adv.*, vol. 7, no. 2, pp. 927–938, 2017, doi: 10.1039/c6ra25230c.
[90] S. Chen *et al.*, "Study on the adsorption of dyestuffs with different properties by sludge-rice husk biochar: Adsorption capacity, isotherm, kinetic, thermodynamics and mechanism," *J. Mol. Liq.*, vol. 285, pp. 62–74, 2019, doi: 10.1016/j.molliq.2019.04.035.
[91] J. Zang, T. Wu, J. Yang, Z. Xie, S. Fan, and J. Tang, "Sorption behavior of perfluorooctane sulfonate on hydrous ferric oxide from aqueous solution," *Desalin. Water Treat.*, vol. 226, pp. 197–207, 2021, doi: 10.5004/dwt.2021.27270.
[92] O. A. Salawu, Z. Han, and A. S. Adeleye, "Shrimp waste-derived porous carbon adsorbent: Performance, mechanism, and application of machine learning," *J. Hazard. Mater.*, vol. 437, no. February, p. 129266, 2022, doi: 10.1016/j.jhazmat.2022.129266.
[93] K.-U. Goss, " The pK_a values of PFOA and other highly fluorinated carboxylic acids ," *Environ. Sci. Technol.*, vol. 42, no. 13, pp. 5032–5032, 2008, doi: 10.1021/es8011904.
[94] F. Wang and K. Shih, "Adsorption of perfluorooctanesulfonate (PFOS) and perfluorooctanoate (PFOA) on alumina: Influence of solution pH and cations," *Water Res.*, vol. 45, no. 9, pp. 2925–2930, 2011, doi: 10.1016/j.watres.2011.03.007.
[95] J. Jeon, K. Kannan, H. K. Lim, H. B. Moon, J. S. Ra, and S. D. Kim, "Bioaccumulation of perfluorochemicals in pacific oyster under different salinity gradients," *Environ. Sci. Technol.*, vol. 44, no. 7, pp. 2695–2701, 2010, doi: 10.1021/es100151r.
[96] C. You, C. Jia, and G. Pan, "Effect of salinity and sediment characteristics on the sorption and desorption of perfluorooctane sulfonate at sediment-water interface," *Environ. Pollut.*, vol. 158, no. 5, pp. 1343–1347, 2010, doi: 10.1016/j.envpol.2010.01.009.
[97] P. Chularueangaksorn, S. Tanaka, S. Fujii, and C. Kunacheva, "Batch and column adsorption of perfluorooctane sulfonate on anion exchange resins and granular activated carbon," *J. Appl. Polym. Sci.*, vol. 131, no. 3, pp. 1–7, 2014, doi: 10.1002/app.39782.
[98] N. M. R. S.G. Oh, "In-situ electron-microscopy studies of the inhibition of graphite oxidation by phosphorus," *J. Mater. Res*, vol. 8, pp. 2879–2888, 1993.
[99] J. M. Rosas, J. Bedia, J. Rodríguez-Mirasol, and T. Cordero, "Preparation of hemp-derived activated carbon monoliths. Adsorption of water vapor," *Ind. Eng. Chem. Res.*, vol. 47, no. 4, pp. 1288–1296, 2008, doi: 10.1021/ie070924w.
[100] M. J. Valero-Romero, F. J. García-Mateos, J. Rodríguez-Mirasol, and T. Cordero, "Role of surface phosphorus complexes on the oxidation of porous carbons," *Fuel Process. Technol.*, vol. 157, pp. 116–126, 2017, doi: 10.1016/j.fuproc.2016.11.014.

Appendix A: CCD Analysis Data

Quadratic polynomial equations were derived from experimental data (Eqs. A1 and A2 for PBC and ZnBC, respectively) that describe the relationship between the independent variables (X_1, X_2 and X_3) and the model response (PFOA adsorption removal (%)):

$$\text{Removal (\%)} = -174.4X_1 + 34.82X_1 + 26.27X_2 + 0.2891X_3 - 3.906X_1^2 - 1.893X_2^2 - 0.000183X_3^2 - 0.146X_1X_2 - 0.00562X_1X_3 + 0.00292X_2X_3 \quad \text{(A1)}$$

$$\text{Removal (\%)} = -124.2X_1 + 123.2X_1 + 20.93X_2 + 0.2349X_3 - 86.67X_1^2 - 1.695X_2^2 - 0.000179X_3^2 + 1.20X_1X_2 - 0.0212X_1X_3 0.007362X_2X_3 \quad \text{(A2)}$$

Based on the independent variables given in Table 4.1, the PFOA removal percentages were calculated by using the ANOVA method (Tables A1 and A2). The prediction of the PFOA removal percentages was close to the experimental results. For PBC, based on the F value of 17.15 and the p-value of < 0.0001, the model is highly significant. In the developed model for estimating the PFOA adsorption capacity on PBC, an R^2 value of 0.94 was obtained. F value, p-value and R^2 for ZnBC are 39.32, < 0.0001 and 0.97, respectively. This indicates that the model accurately describes the relationship between the independent variables and the PFOA removal percentage, providing reliable predictions. In Figures A1 and A2, additional insights into the response nature of the design are provided by surface plots of the combined effects of the independent variables.

Table A1. Analysis of variance data of the CCD for PFOA adsorption removal of PBC

Source	DF	Adj SS	Adj MS	F-Value	P-Value
Model	9	21496.3	2388.48	17.15	0.000
Linear	3	11636.1	3878.71	27.85	0.000
Concentration of H_3PO_4 (mol/L)	1	2776.5	2776.48	19.94	0.001
Microwave time (min)	1	2910.3	2910.27	20.90	0.001
Microwave power (W)	1	5949.4	5949.39	42.72	0.000
Square	3	9707.8	3235.93	23.24	0.000
Concentration of H_3PO_4 (mol/L)*Concentration of H_3PO_4 (mol/L)	1	3518.6	3518.57	25.27	0.001
Microwave time (min)*Microwave time (min)	1	4184.3	4184.30	30.05	0.000
Microwave power (W)*Microwave power (W)	1	3927.9	3927.90	28.20	0.000
2-Way Interaction	3	152.4	50.79	0.36	0.780
Concentration of H_3PO_4 (mol/L)*Microwave time (min)	1	6.1	6.12	0.04	0.838
Concentration of H_3PO_4 (mol/L)*Microwave power (W)	1	91.1	91.13	0.65	0.437
Microwave time (min)*Microwave power (W)	1	55.1	55.13	0.40	0.543
Error	10	1392.7	139.27		
Lack-of-Fit	5	1383.8	276.76	156.66	0.000
Pure Error	9	21496.3	2388.48	17.15	0.000
Total	3	11636.1	3878.71	27.85	0.000

Table A2. Analysis of variance data of the CCD for PFOA adsorption removal of ZnBC

Source	DF	Adj SS	Adj MS	F-Value	P-Value
Model	9	18758.5	2084.27	39.32	0.000
Linear	3	8677.5	2892.49	54.57	0.000
Concentration of $ZnCl_2$ (mol/L)	1	1377.9	1377.95	26.00	0.000
Microwave Time (min)	1	3951.9	3951.93	74.55	0.000
Microwave Power (W)	1	3347.6	3347.60	63.15	0.000
Square	3	9642.6	3214.20	60.64	0.000
Concentration of $ZnCl_2$ (mol/L)*Concentration of $ZnCl_2$ (mol/L)	1	4439.2	4439.24	83.75	0.000
Microwave Time (min)*Microwave Time (min)	1	3352.8	3352.82	63.25	0.000
Microwave Power (W)*Microwave Power (W)	1	3752.7	3752.66	70.79	0.000
2-Way Interaction	3	438.4	146.13	2.76	0.098
Concentration of $ZnCl_2$ (mol/L)*Microwave Time (min)	1	21.1	21.13	0.40	0.542
Concentration of $ZnCl_2$ (mol/L)*Microwave Power (W)	1	66.1	66.13	1.25	0.290
Microwave Time (min)*Microwave Power (W)	1	351.1	351.13	6.62	0.028
Error	10	530.1	53.01		
Lack-of-Fit	5	515.2	103.05	34.74	0.001
Model	9	18758.5	2084.27	39.32	0.000
Linear	3	8677.5	2892.49	54.57	0.000

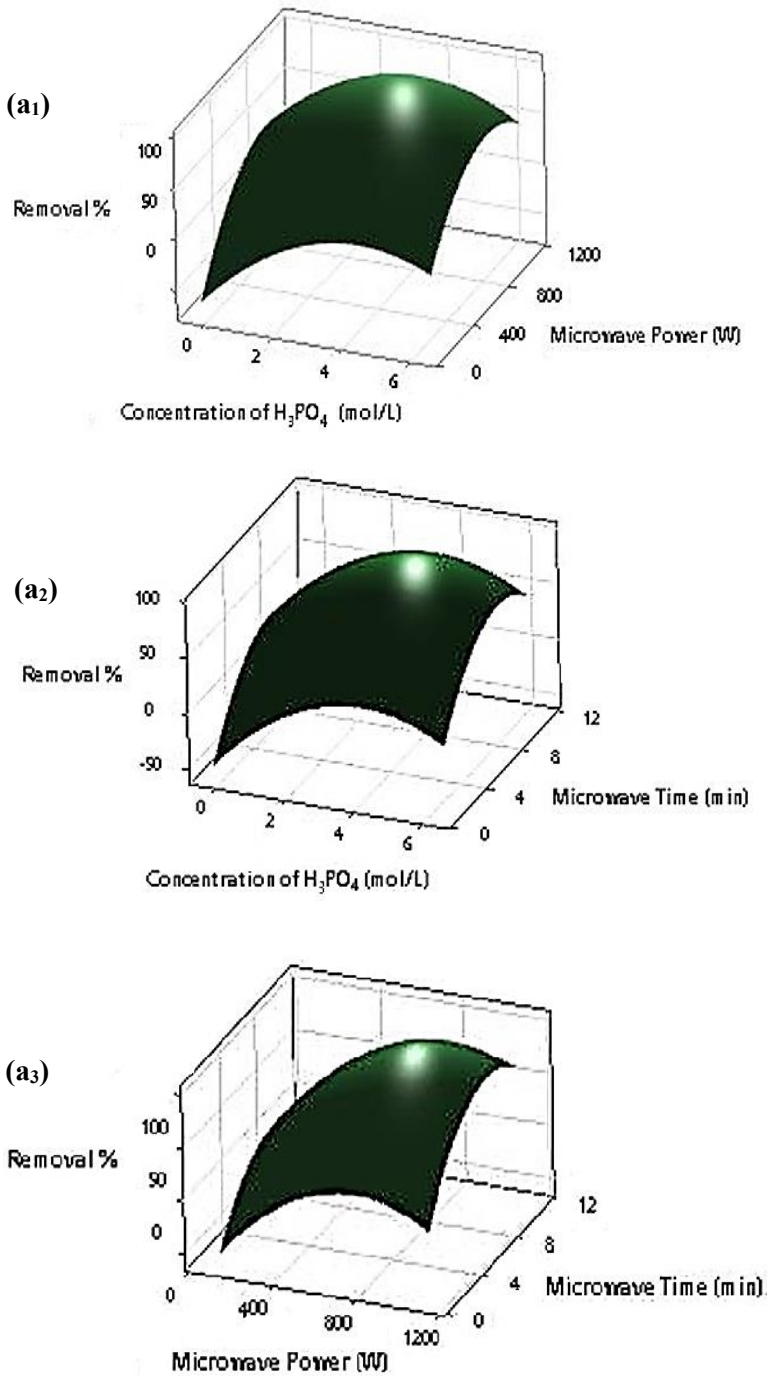

Figure A1. Surface plots for the combined effect of independent factors on PFOA adsorption removal percentage: (a_1) H_3PO_4 concentration and microwave time (microwave power of 600 W), (a_2) H_3PO_4 concentration and microwave power (microwave time of 6 min), and (a_3) microwave power and microwave time

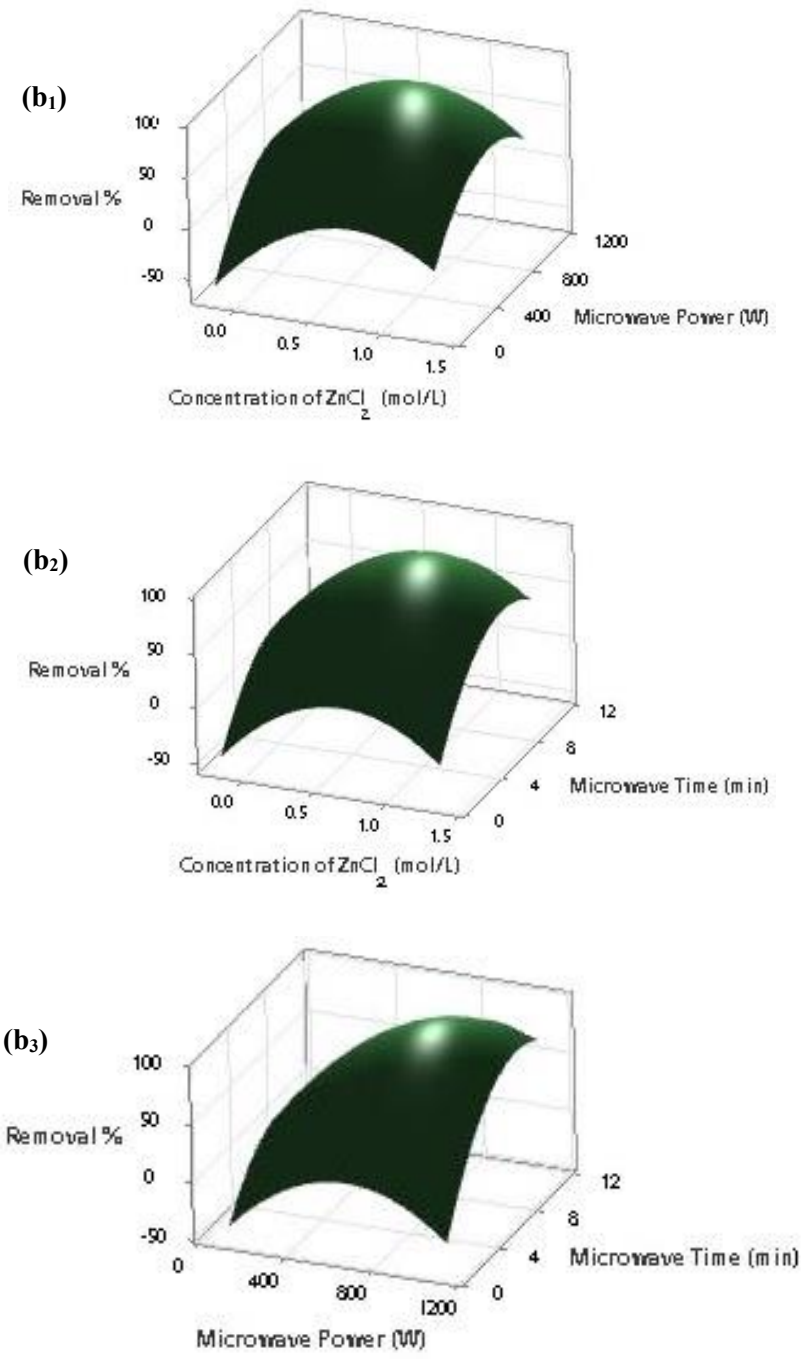

Figure A2. Surface plots for the combined effect of independent factors on PFOA adsorption removal percentage: (a_1) $ZnCl_2$ concentration and microwave time (microwave power of 600 W), (a_2) $ZnCl_2$ concentration and microwave power (microwave time of 6 min), and (a_3) microwave power and microwave time

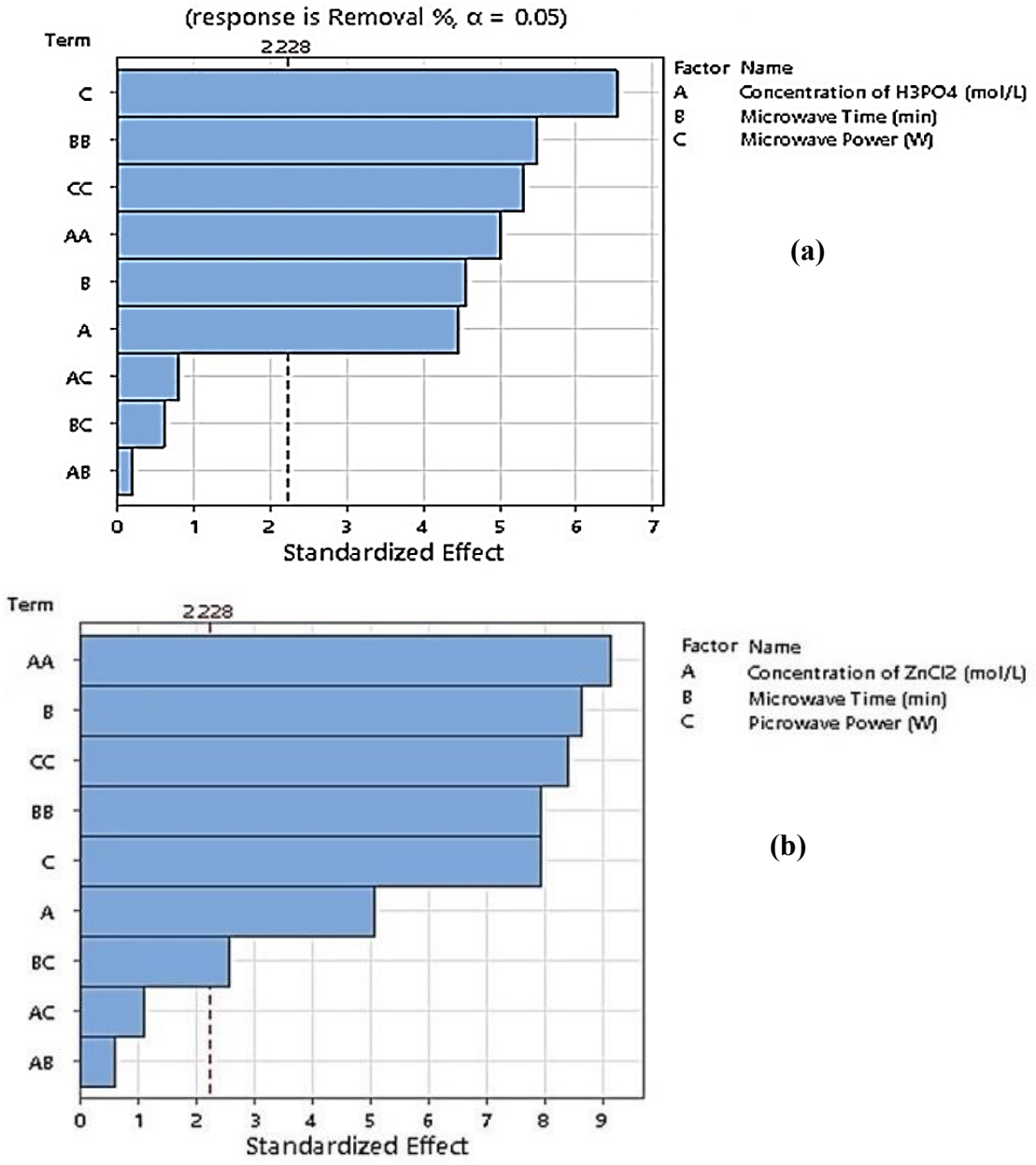

Figure A3. Pareto chart of standardized effects on the PFOA adsorption by PBC (a) and ZnBC (b)